COMPUTER AIDED ANALYSIS OF FRICTION DAMPED BRACED FRAMES

Xiao Ming Zhao

A Thesis

in

The Centre for

Building Studies

Presented in Partial Fullfillments of the Requirements
for the Degree of Master of Applied Science at
Concordia University

March 1994

ISBN 0-315-90901-3

Canada

ABSTRACT

COMPUTER AIDED ANALYSIS OF FRICTION DAMPED BRACED FRAMES

Xiao Ming Zhao

A computer aided design system was developed to provide engineers with a practical and efficient approach to determine the optimum slip-load and to design buildings equipped with friction dampers. It implements the current NBC design procedure consisting of the elastic limit state design and an inelastic dynamic analysis of the final design. The second phase employs an optimization procedure which allows the designer to place relative importance on the two objective functions: minimum deflection and permanent damage expressed in terms of the number of plastic hinges.

The designer also has the option to include soil-structure interaction in the analysis. The soil mass is assumed to be linear elastic while the superstructure may exhibit non-linear behaviours. Three different earthquake input mechanisms are available for the non-linear time domain analysis of FDBF-Soil system. The dynamic responses of FDBF-Soil system under different earthquake input mechanisms were evaluated, and some conclusions were drawn for the design of FDBF when the soil condition and the soil-structure interaction need be considered. A 20-storey all-steel office building and a 10-storey reinforced concrete office building were used as application examples to evaluate the effectiveness of the computer program as a tool for assisting engineers in seismic design of FDBF.

ACKNOWLEDGEMENTS

I am most grateful to Professor K.H. Ha, for his valuable guidance and help throughout my graduate studies.

With respect and love, I sincerely thank my wife for her patience, understanding, encouragement and moral support.

CONTENTS

List of Figures

List of Tables

CHAPTER 1 INTRODUCTION

1.1 General

The aim of building code's provisions on seismic resistant design is to prevent significant damage in moderate earthquakes, and structural collapse in major earthquakes. However, it is being increasingly recognized that for modern buildings or some crucial buildings such as hospital, military stations, computer or communication centre etc., the mere avoidance of structural collapse is not enough.

Learning from the lessons of the 1985 Mexican earthquake, the State of California passed a legislative resolution that all new and existing important buildings must incorporate new seismic resistant technology. The National Building Code of Canada 1990[1] also allows the use of new earthquake resistant systems.

In recent years, many researchers have directed their attention to the development of new aseismic structural systems which are intended to minimize the dynamic responses and permanent damages in structures. In 1982, Pall and Marsh[2] introduced a novel structural system which incorporates a friction device at the intersection of the diagonal brace elements (Fig.1.1a). Tests performed at the University of British Columbia and at the Earthquake Engineering Research Centre of the University of California at Berkeley have demonstrated the superior

performance of this new system. The friction devices may be used in new constructions (Concordia University new library)[3] or for retrofitting of existing buildings (school buildings at Sorel, Quebec)[4].

1.2 Friction damped braced frame system

The Friction Damped Braced Frame(FDBF) system basically consists of an inexpensive mechanism containing friction brake lining pads introduced at the intersection of the frame's cross braces. Schematic details of the device are shown in Fig.1.1. Fig.1.2 illustrates the five stages in a typical load cycle for a simple friction damped frame.

Stage (1): To begin the cycle, assume that brace 1 is in tension and brace 2 in compression. Both of them remain linear elastic until the compression force in brace 2 reaches the buckling load.

Stage (2): After buckling of the compression brace, the axial tension load in brace 1 continues to increase elastically until it reaches the slip-load which was set to slip before yielding occurs in the tension brace.

Stage (3): When the tension brace slips, it activates the four links which force the other diagonal within the mechanism to slip simultaneously, and straighten brace 2.

Stage (4): In the reversed loading, brace 2 becomes tension member, acting as brace 1 in the first half loading cycle as illustrated in stage (1) and (2).

Stage (5): After the completion of one cycle, energy is dissipated in both

braces in each half cycle.

During severe earthquake excitations, the friction devices slip at a predetermined load and a large portion of the input energy is dissipated mechanically. Properly designed, the system will protect the main structural components(beams and columns) from inelastic yielding or cracking. The device is designed not to slip under the action of wind forces or minor earthquakes.

1.3 Current state of research

Research on FDBF system may be classified into four aspects:

(1) Experimental studies

(2) Comparative studies

(3) Parametric studies

(4) Methods for analysis and design of the FDBF system

A brief review is presented in the following.

1.3.1 Experimental studies

Two large scale model tests have been performed on shaking tables. The first test was at the University of British Columbia.[5] The model frame, shown in Fig.1.3 is a 1/3 scale model of a 3- storey FDBF. The second test was a 1/4 scale 9-storey steel moment resisting frame(MRF) at the Earthquake Engineering Research Centre of the University of California at Berkeley.[6] The model frame is shown in Fig.1.4.

These tests have shown that the seismic performance of the frames are considerably enhanced by the inclusion of the friction damping devices in the frame. The energy dissipation characteristics of the friction damping mechanisms are reliable and because of the large portion of the input energy was dissipated by the friction dampers, the main structural elements are able to remain elastic.

1.3.2 Comparative studies

By computer simulation, Baktash[7] has analyzed a series of single bay steel frames. The results show the superior performance of the FDBF when compared with the Moment Resistant Frame (MFR), Braced Moment Resistant Frame (X-braced,K-braced), and Eccentric Braced Frame (EBF).

Filiatrault and Cherry[8] have also compared the performance of FDBF system to that of base isolation system. Their comparative study is made of the seismic responses of an existing braced frame structure when retrofitted in one case with friction damping devices, and in another with lead-rubber base isolators. The FDBF system and the base-isolation system were both subjected to three earthquake excitations (1940 El Centro,N S, 1977 Romania, Bucharest, N-S and 1985 Mexcico, SCT, E-W). Their study showed that, while both systems reduce similarly the response of conventional structures to the El Centro earthquake, the friction damped structure exhibits superior performance under low frequency excitations.

1.3.3 Parametric studies

The amount of energy dissipation in a friction damper is the product of the slip load to the slip travel. For a very high slip load, there will be no energy dissipation because no slippage occurs. If the slip load is very small, the amount of energy dissipation will also be negligible. Between these extremes, there is an intermediate value which gives maximum energy dissipation and thereby minimizes the dynamic response of the structure. This value is known as the optimum slip-load.

Factors which are believed to affect the optimum slip-load are:[9][10]

1. The earthquake ground motion anticipated for the construction site (peak value, focal depth, attenuation characteristics, frequency content, duration, etc.).

2. The soil condition of the construction site (the layer profile of the soil, the dynamic properties of the soil such as zonal velocity ratio, viscous damping etc.).

3. The stiffness and buckling load of the diagonal cross-braces etc.

Previous parametric studies have indicated that the optimum slip-load is mainly a function of the type and intensity of the earthquake and the relative stiffness of the braced frame to the un-braced frame.

1.3.4 Methods for analysis and design of FDBF system

Baktash[7] proposed a simple expression for the optimum slip-load based on the plastic moment capacity of the floor beams:

$$P_s = \frac{2M_p}{h\cos\beta} \qquad (1.1)$$

where P_s is the optimum slip force in brace, M_p is the limiting moment in the beam, h is the story height, β is the angle between the brace and the beam as shown in Fig. 1.5. This equation is based on quasi-static monotonic loading applied to a single bay frame.

Filiatrault and Cherry[11] developed a Friction Damped Braced Frame Analysis Program(FDBFAP). This computer program can give the optimum slip-load by performing a series of dynamic-response analysis. It takes into account the inelastic behaviour of the friction dampers, but assumes that the beams and columns remain elastic at all times. By using FDBFAP, Filiatrault and Cherry[12] also proposed a design slip-load spectrum for the evaluation of the optimum slip-load distribution.

By using the TABS77[13] program to carry out the spectrum analysis for the unbraced moment resisting frames, and to compare the maximum deflections with those obtained from non-linear step-by-step analyses, Tan proposed a response acceleration spectrum for modal response analysis of the FDBF system.[10]

1.4 Objectives of the present study

According to the present provisions in the NBCC for the design of buildings equipped with friction dampers, engineers have to design the building frames for

dead, live, wind and quasi-static seismic loads to the requirements of the codes, and then conduct the non-linear analysis to assess the seismic responses of the frames during earthquakes. This two-stage analysis is complex and time consuming. Thus, the first purpose of the present study is to develop an efficient computer-aided design system which can determine the optimum slip-load based on a multiobjective function optimization procedure and design buildings equipped with friction dampers.

Since past analytical and experimental works were based on the assumption of rigid foundation, the second objective of the present work is to study the influence of the soil conditions and the soil-structure interaction in FDBF under severe earthquake excitations.

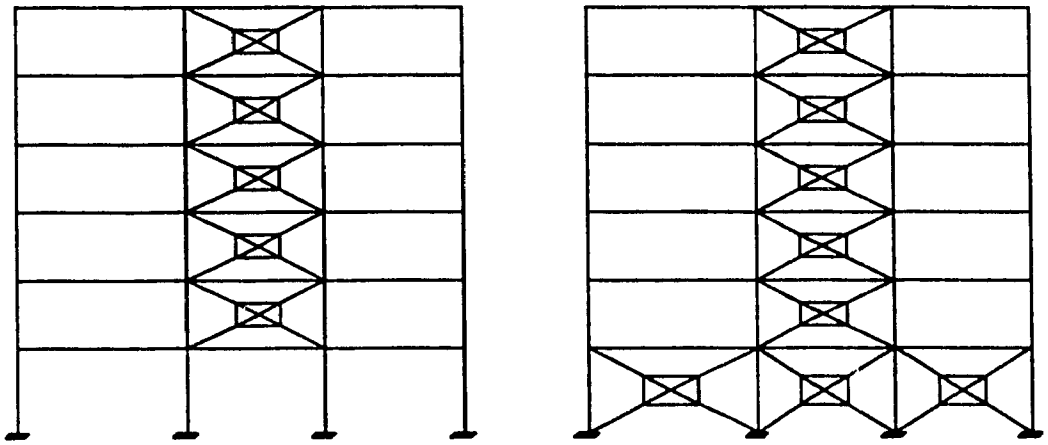

a. Location of Devices

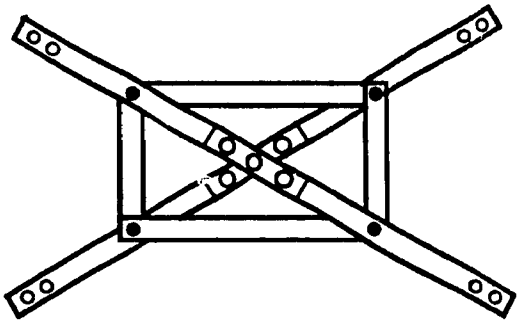

b. Schematic Description of a Friction Device

Fig.1.1 Friction Damped Braced Frames

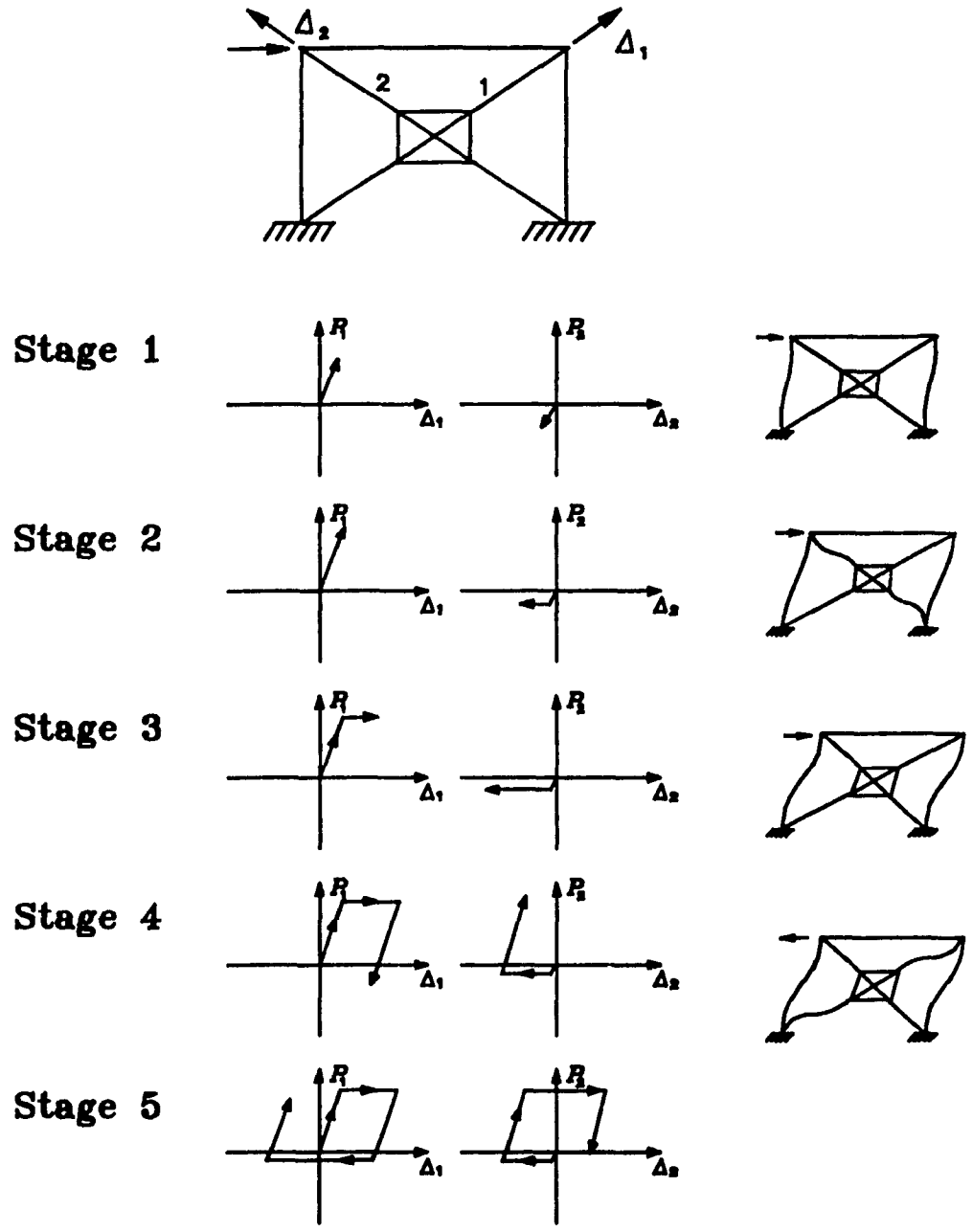

Fig.1.2 Hysteretic behaviour of a simple friction damped braced frame[8]

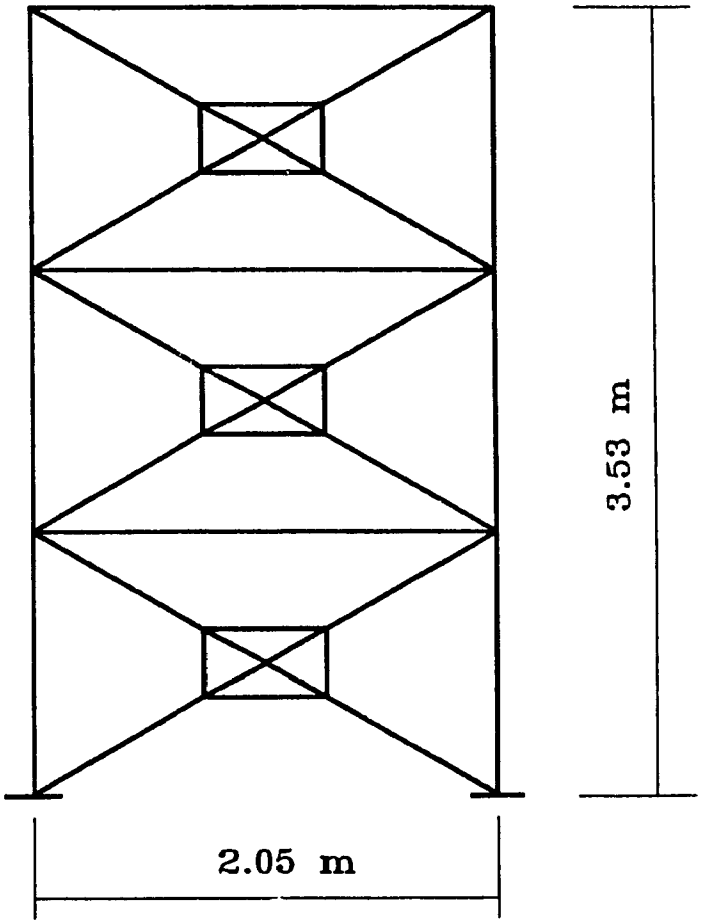

Fig.1.3 1/3 scale 3-storey FDBF tested at the University of British Columbia[5]

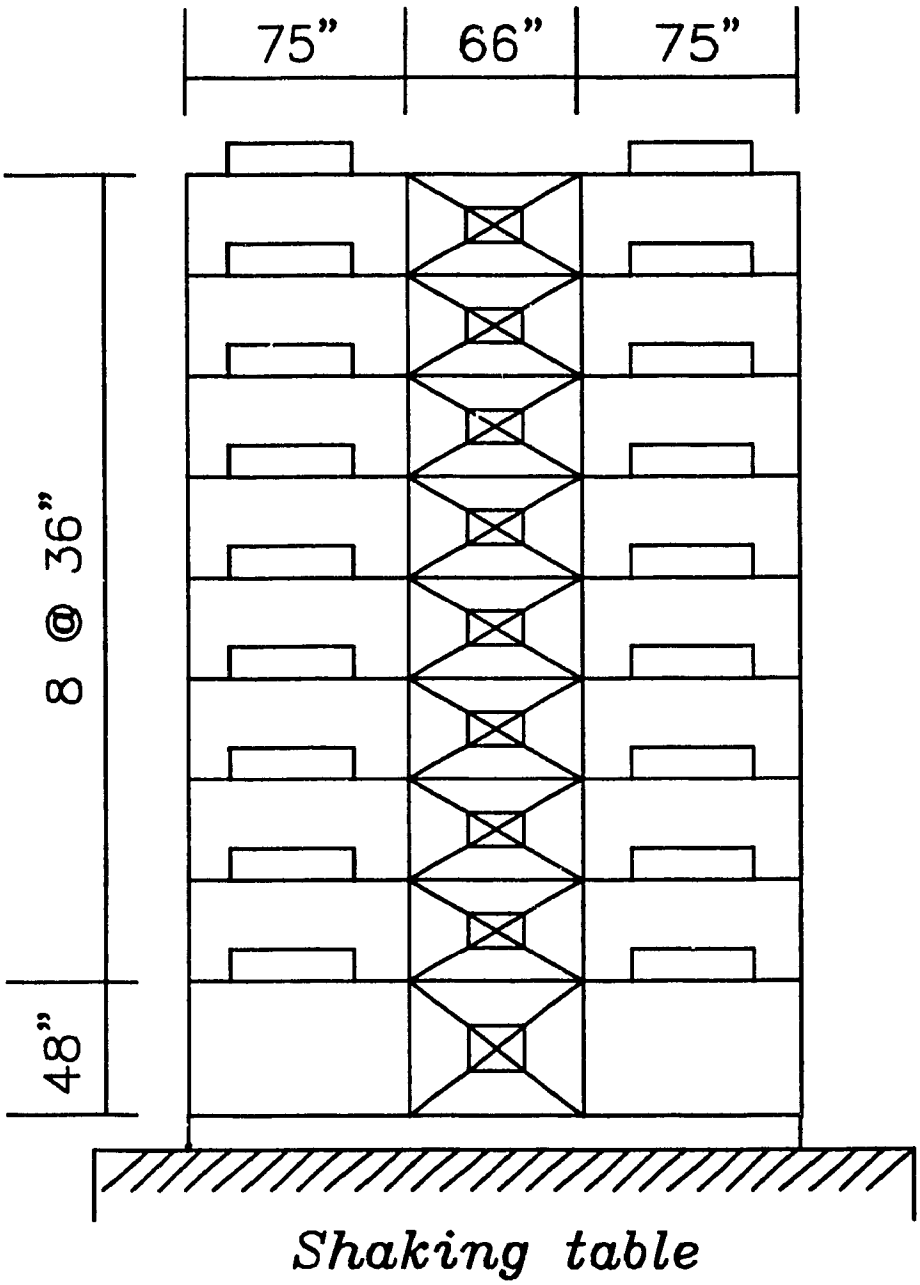

Fig.1.4 1/4 scale 9-storey FDBF tested at the University of California at Berkeley[6]

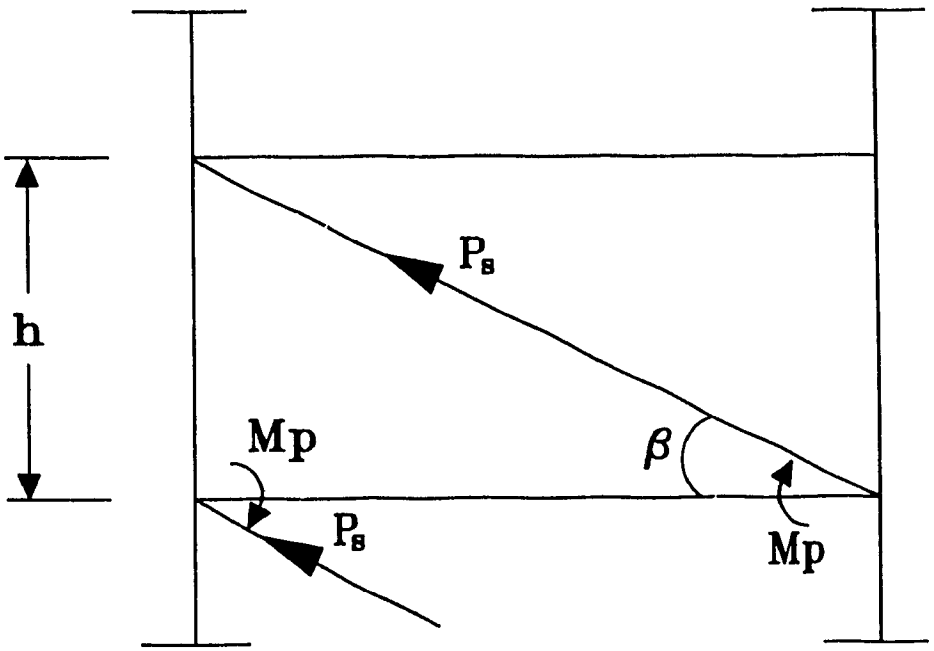

$$Ps = \frac{2Mp}{h\cos\beta}$$

Fig.1.5 Brace force for optimum slip load

Chapter 2 Multi-bay multi-story friction damped braced frames

In the literature, single bay FDBF systems are often used for the purpose of comparison and parametric studies. Since this study is concerned with the design and assessing damages in practical, real buildings, multi-bay multi-story frames will be employed. In addition, previous optimum slip load studies were based on minimization of the maximum deflection while damage in terms of plastic hinges in beams and columns was only a by-product. In this chapter, a series of multi-bay multi-story frames equipped with the friction devices will be analyzed to assess the findings of previous studies, and the dynamic responses in terms of damage versus slip load will also be investigated.

2.1 Superior performance of friction damped braced frames

A family of four 10 storey 3 bay frames were chosen for the non-linear time-history dynamic analysis. They are:

(1) Moment Resistant Frame(MRF)

(2) Braced Moment Resisting Frame(BMRF)

(3) Friction Damped Braced Frame(FDBF)

(4) Shearwall Frame(SWF)

These frames are shown in Fig.2.1. The dimensions, member size, and other properties of the moment resisting frame are the same as the first example in the original DRAIN-2D manual[14] as shown in Fig.2.2.

The analyses were carried out by using the program DRAIN-2D developed at the University of California[14]. The earthquake record of El-Centro 1940 NS component was used, and the peak ground acceleration is 0.2g. An integration time-step of 0.01 sec. was deemed to be adequate based on extensive trial runs.

Deflection envelopes of the four frames are shown in Fig.2.3. It is seen that the deflection at the top of the FDBF is about 38% of MRF and about 69% of the BMRF, and the deflection of SWF is almost the same as the FDBF.

The permanent damage in terms of plastic hinges in columns and beams experienced by different frames is shown in Fig.2.4. It is seen that 100% of the beams and 5% of the columns yielded in the MRF, 93% of the beams and 28% of the columns yielded in the BMRF, 97% of the beam and 3% of the column yielded in the SWF, the shearwall itself yielded at all levels, while 53% of the beams and no columns yielded in the FDBF.

2.2 Behaviour of FDBF under earthquake excitations.

To demonstrate the response of multi-bay multi-storey friction damped braced frame during a earthquake excitation, a 10-storey all-steel office building located in Montreal[15] was chosen for analysis. The dimension and member size

of the frame is shown in Fig.2.5.

Four earthquake excitations as shown in Table 2.1 and Fig.2.6 to Fig.2.9 were chosen. For each excitation, two intensities were assigned, and an integration time-step of 0.01 sec. was used.

Flexural and axial deformations were considered. Interactions between axial force and moments for columns, P-Δ effect, were taken into account by including the geometric stiffness based on the axial force under static loads.

Table 2.1 Earthquake record

1940 EL-Centro Earthquake (NS 0-12 Sec.)
1952 Taft Earthquake (0-15 Sec.)
Newmark-Blume-Kapur Artificial Earthquake (0-15 Sec.)
1977 Romania Earthquake (NS 0-16 Sec.)

The dynamic responses of the frame were shown in Fig.2.10 to Fig.2.17 which show the deflection of top floor and the number of plastic hinges in columns and beams for slip loads ranging from 0 to 1200kN covering the elastic region of the braces. Fig.2.10 to Fig.2.17 clearly show the effectiveness of the friction devices in improving the seismic response of the frame, and there is a range of optimum slip-loads which either minimizes the deflection or the permanent damage.

As shown in Fig.2.10 to Fig.2.17, the deflections of the top floor exhibit a general trend: starting from zero slip load which represents the unbraced moment resisting frames, the deflection responses decrease rapidly with increasing slip load until a low flat range was reached, after that, there is very little variation in the deflection response. The number of plastic hinges decreases rapidly with

increasing slip-load, and then increases again as the slip-load further increases. This phenomenon is more evident in the case of higher excitation intensity, where as the slip-load deviates from the optimum value, the decreased energy dissipation in the friction dampers is compensated by an increase in the number of plastic hinges.

As seen in Figs. 2.11&2.15, the optimum slip-load with respect to deflection may be different from the optimum slip-load based on the number of plastic hinges, and that it varies with the type and intensity of earthquakes. It is evident that this exhaustive search approach is tedious and impractical for routine design.

In summary, this chapter confirms the general findings of previous studies and it sets the stage for the development of an efficient package which aids the engineer in his quest for an optimum design.

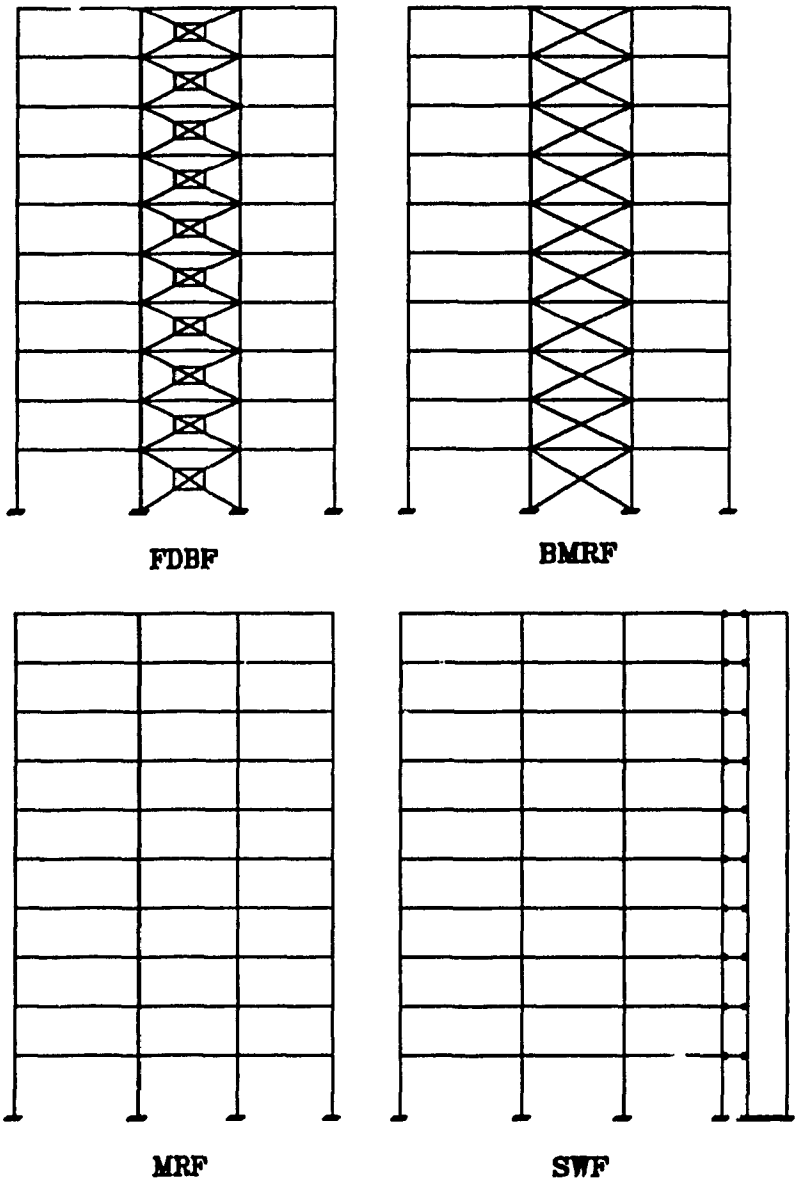

Fig.2.1 A family of 10-storey 3-bay frames

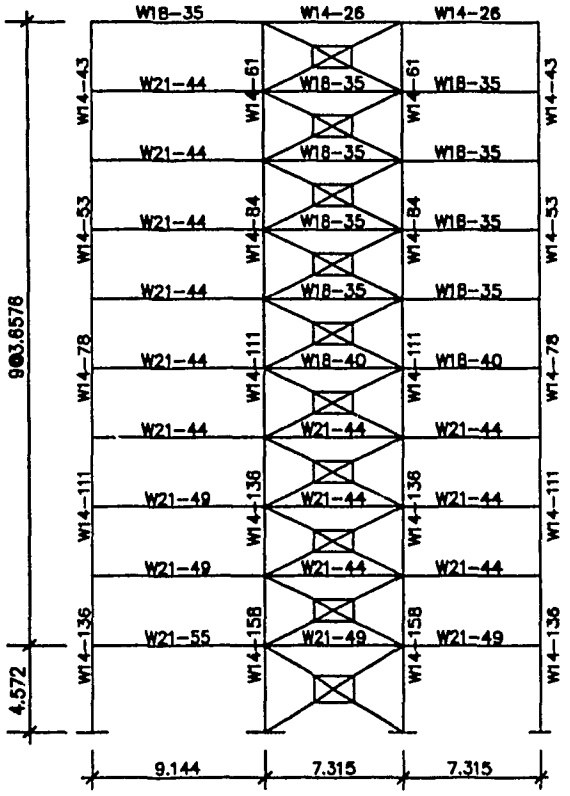

(a) Element Sizes

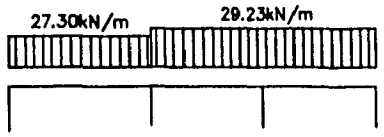

(b) Roof

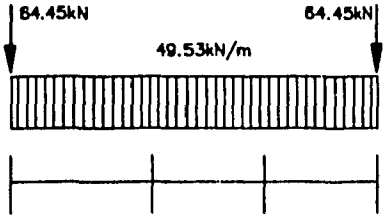

(c) All Floors

Fig.2.2 10-storey, 3-bay frame from Drain-2D manual

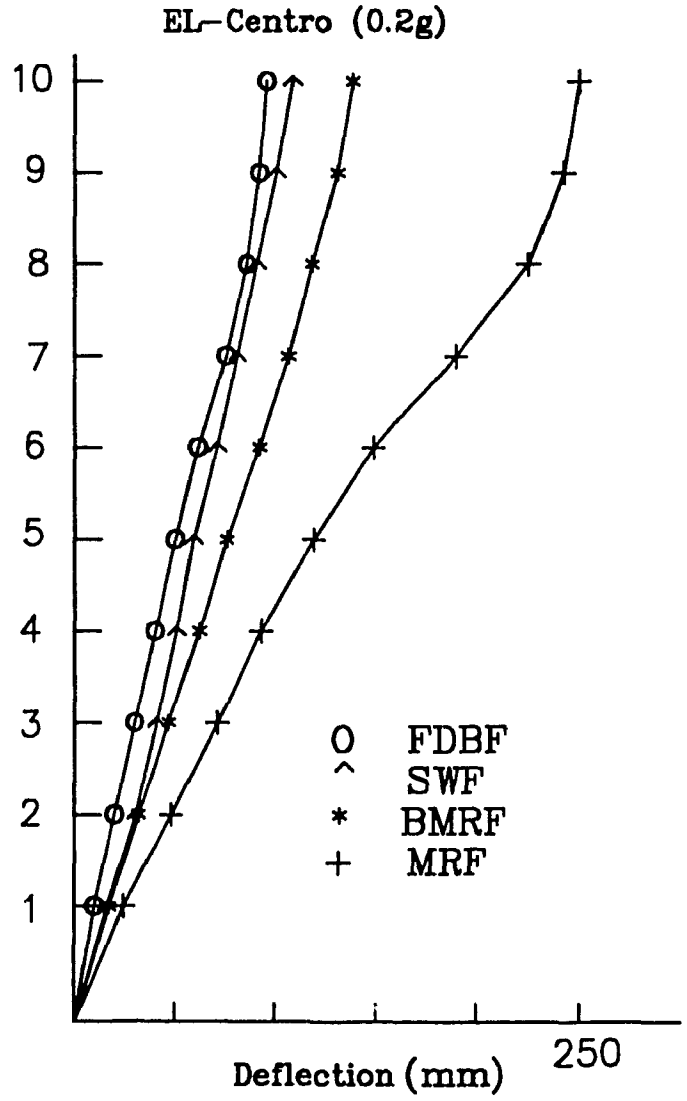

Fig.2.3 Deflection envelopes of the frame

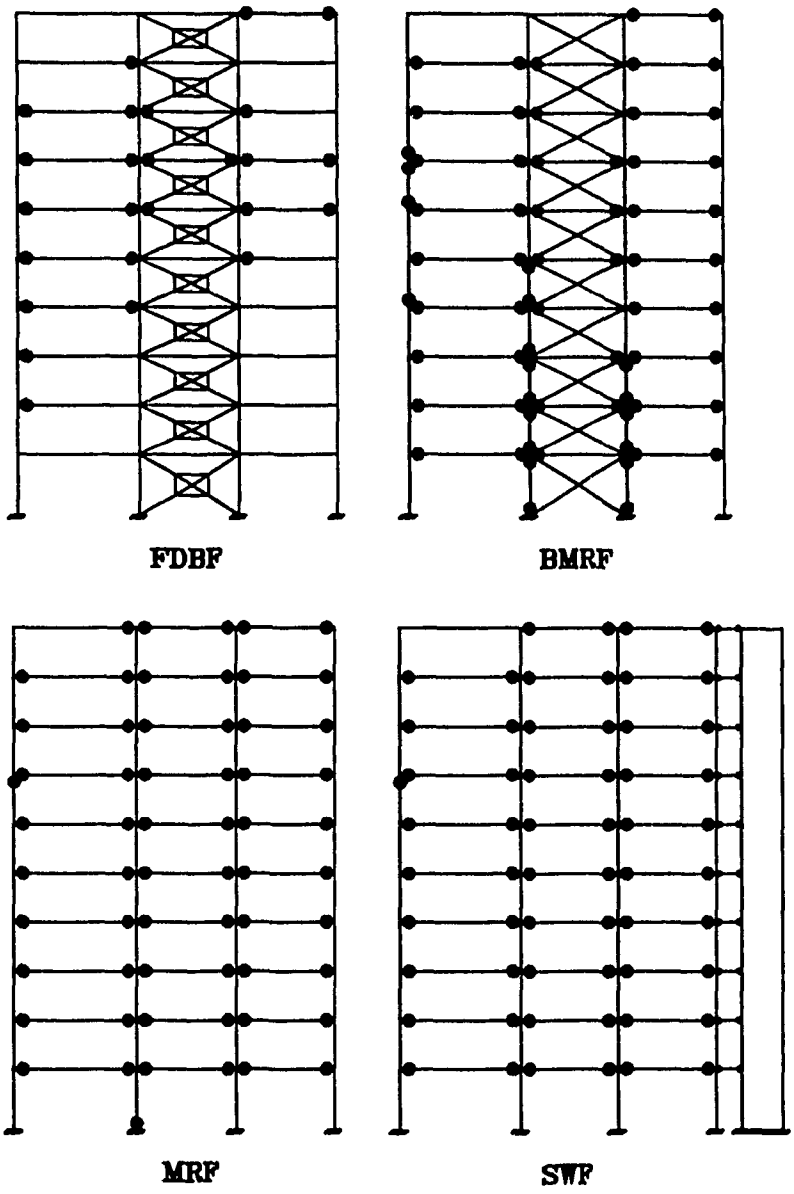

Fig.2.4 Plastic hinges in beams and columns

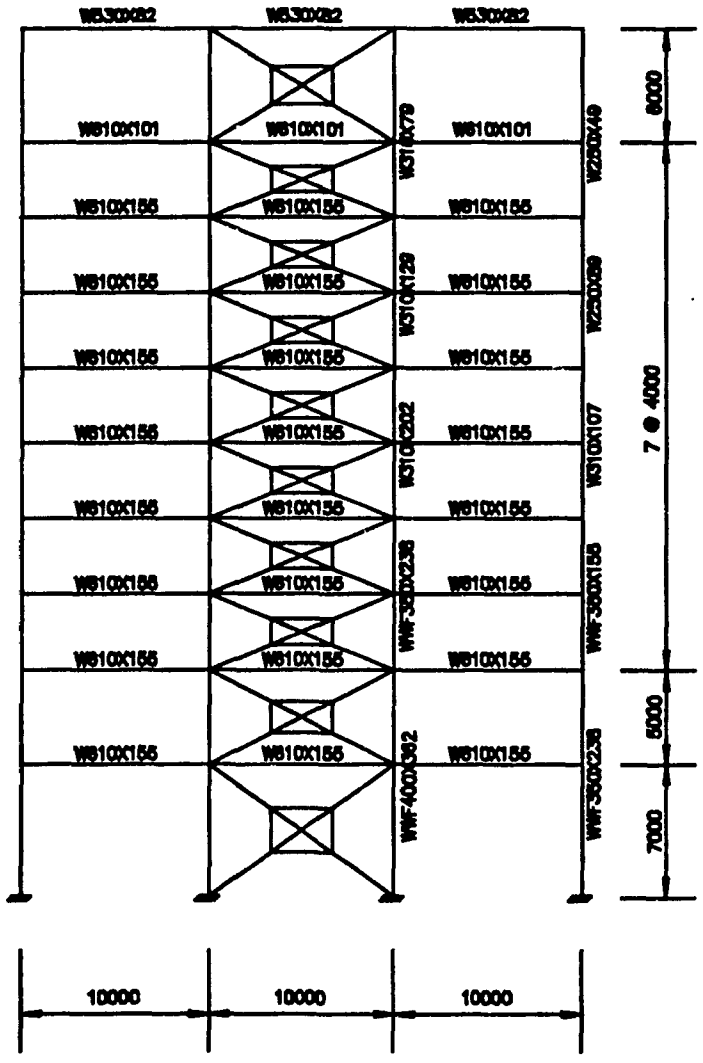

Frame dimensions are in mm

Fig.2.5 A 10-storey 3-bay steel FDBF

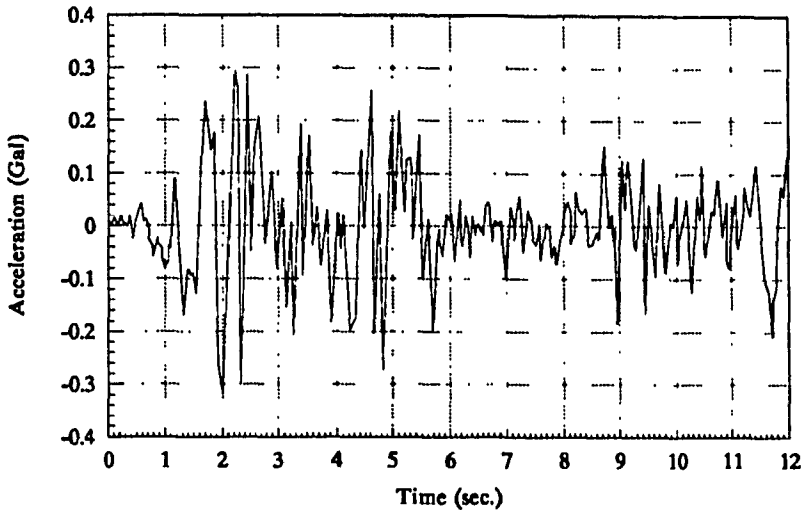

Fig.2.6 1940 El-Centro Earthquake

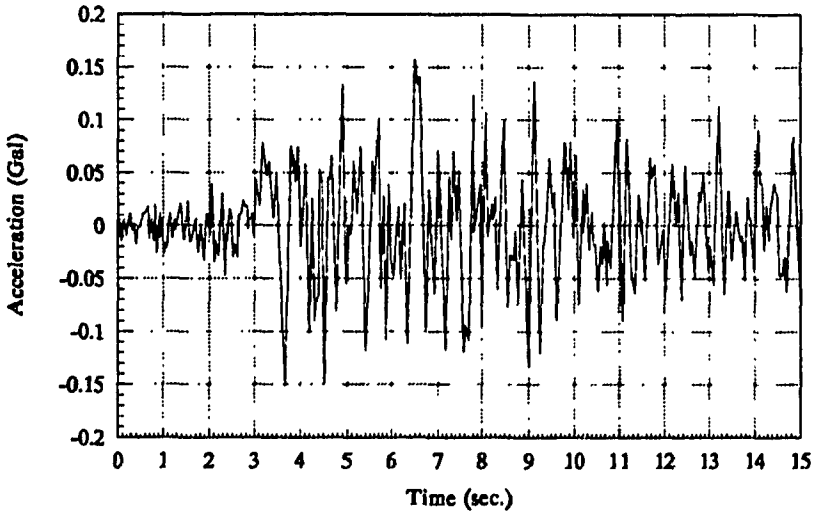

Fig.2.7 1952 Taft Earthquake

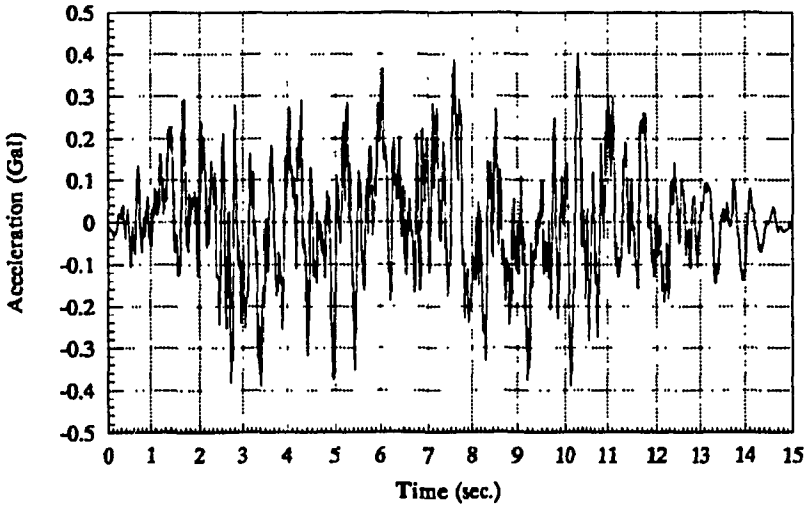

Fig.2.8 NBK Artificial Earthquake

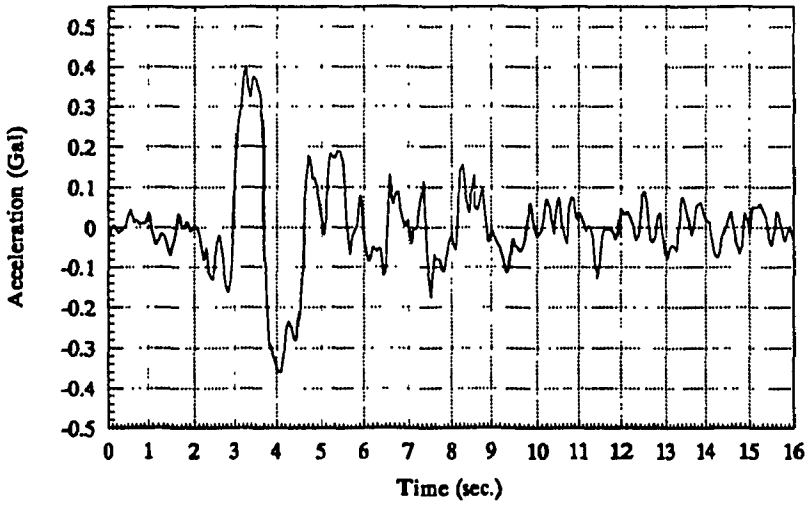

Fig.2.9 1977 Romania Earthquake

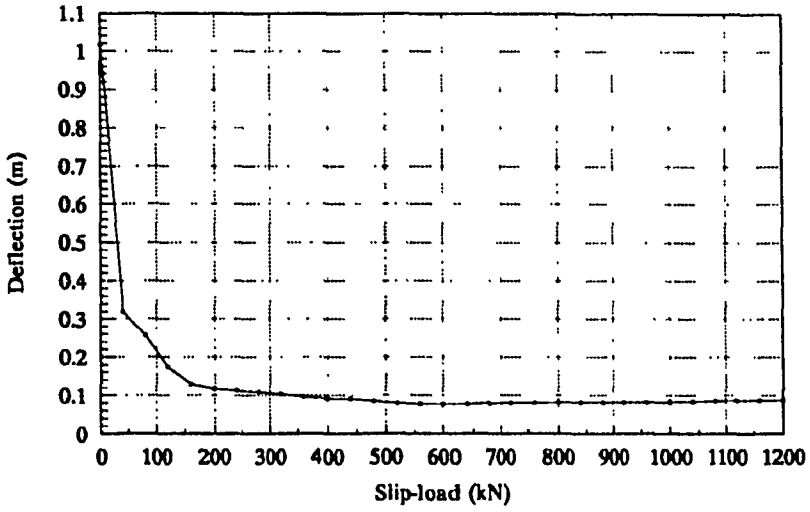

(a). Deflection at top

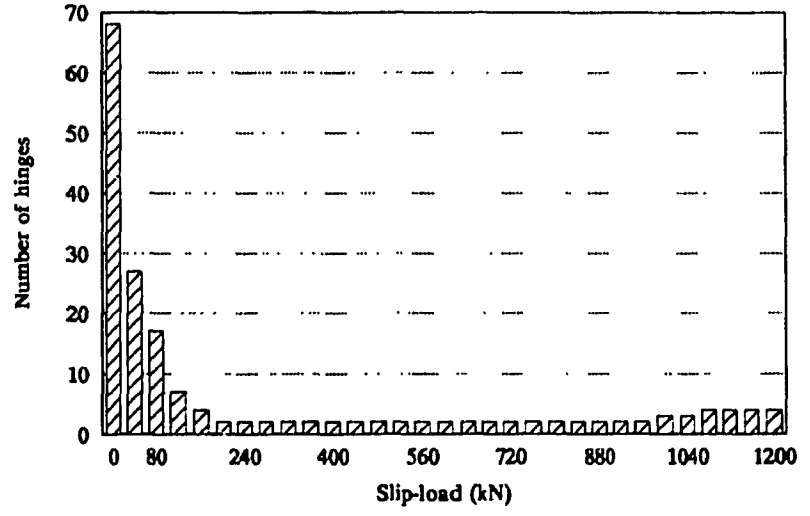

(b). Plastic hinges in beams & columns

Fig.2.10 Dynamic responses of 10-storey steel frame El-Centro 0.2g

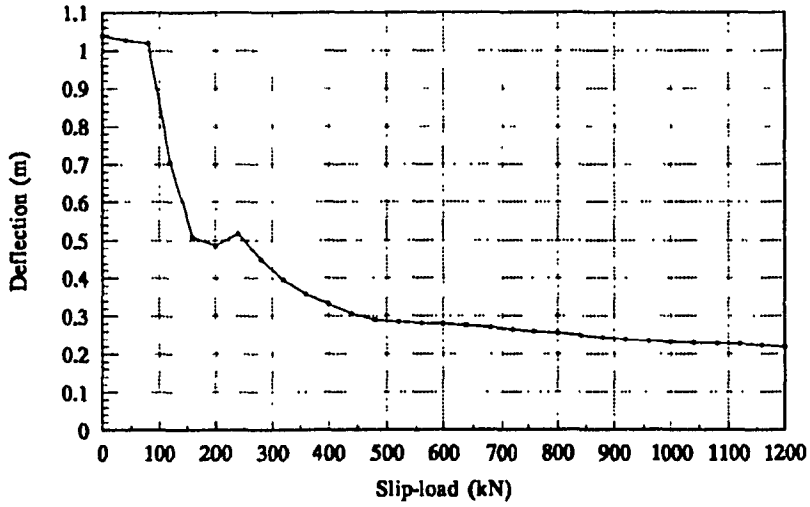

(a). Deflection at top

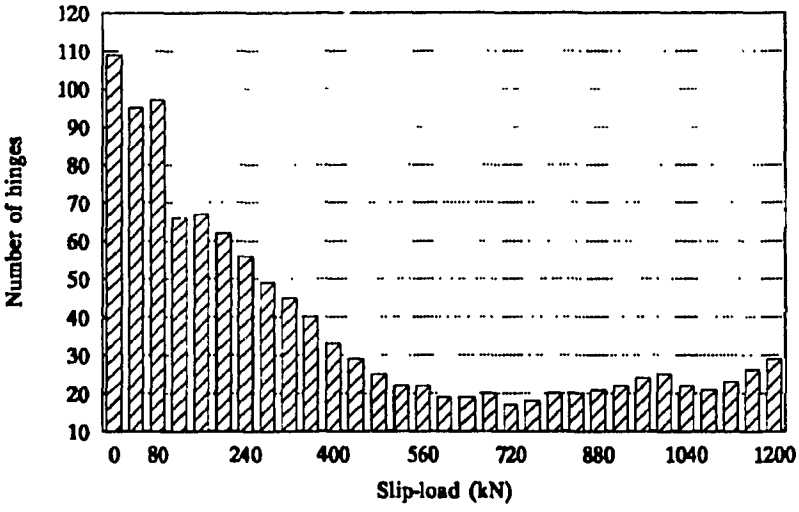

(b). Plastic hinges in beams & columns

Fig.2.11 Dynamic responses of 10-storey steel frame El-Centro 0.5g

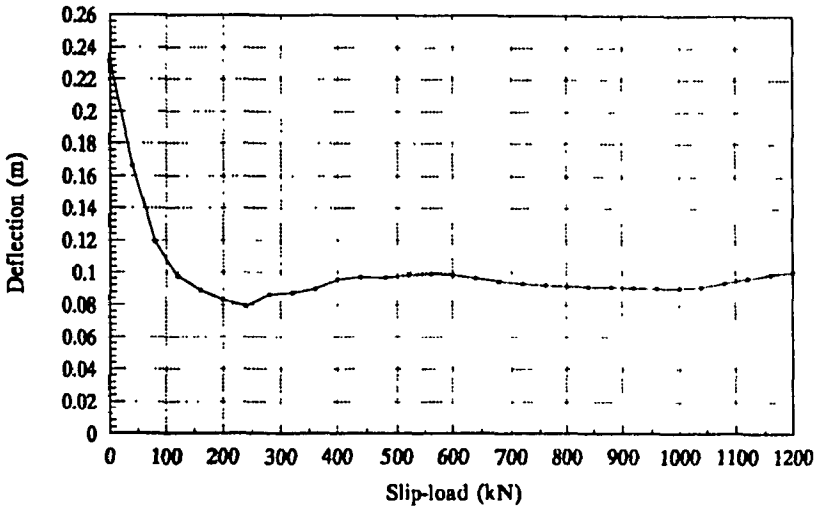

(a). Deflection at top

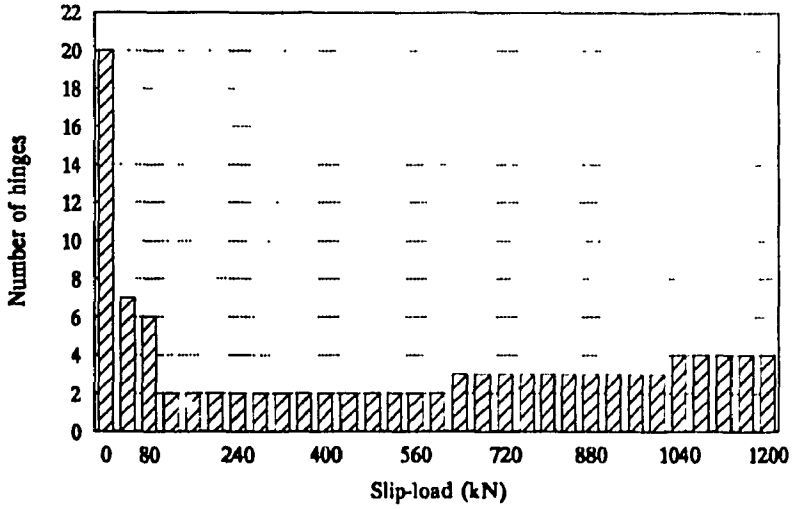

(b). Plastic hinges in beams & columns

Fig.2.12 Dynamic responses of 10-storey steel frame Taft 0.2g

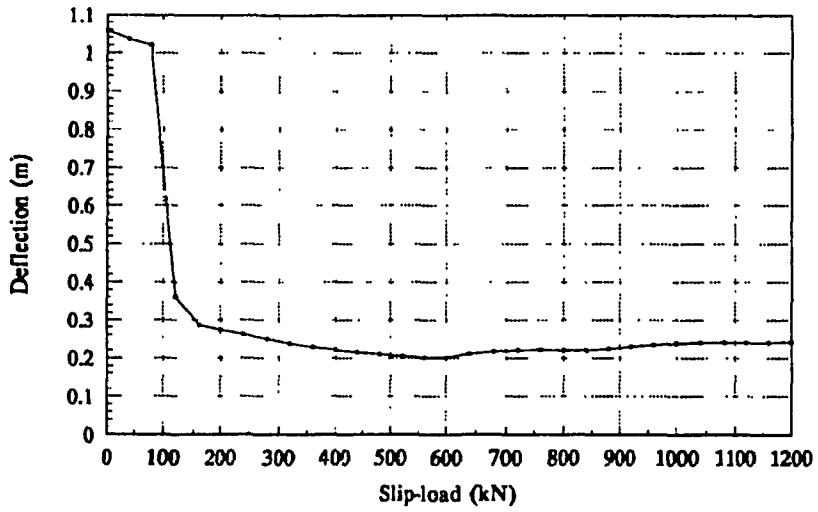

(a). Deflection at top

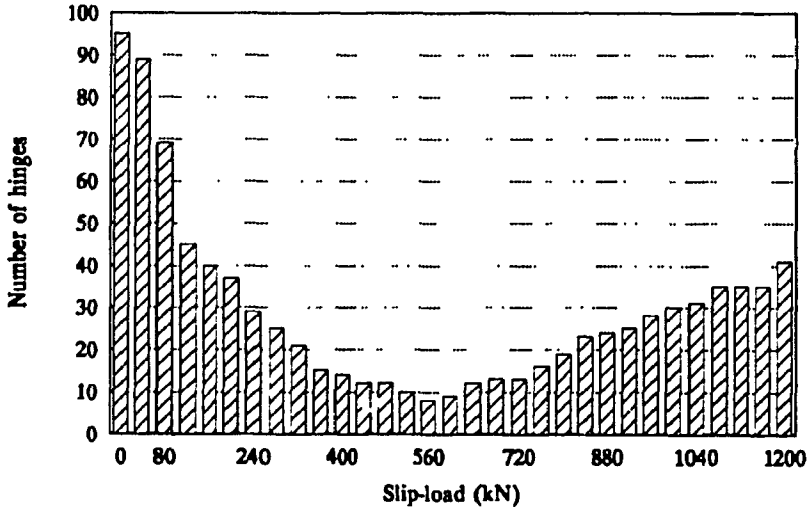

(b). Plastic hinges in beams & columns

Fig.2.13 Dynamic responses of 10-storey steel frame Taft 0.5g

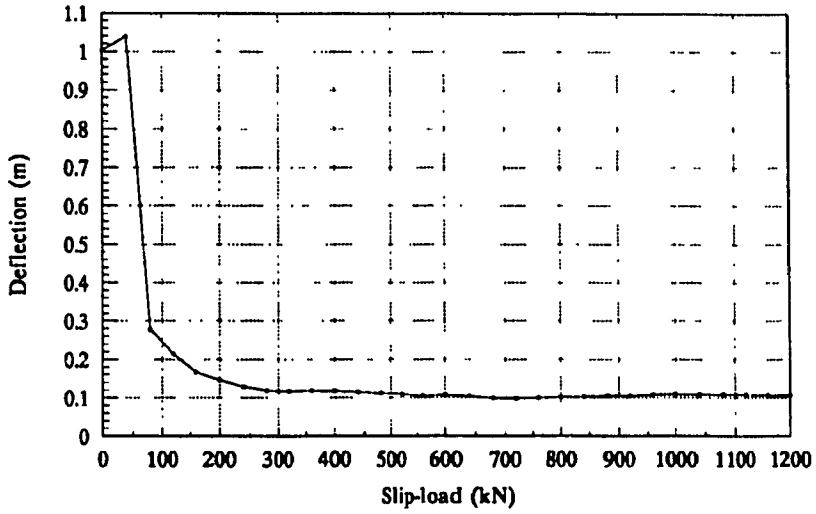

(a). Deflection at top

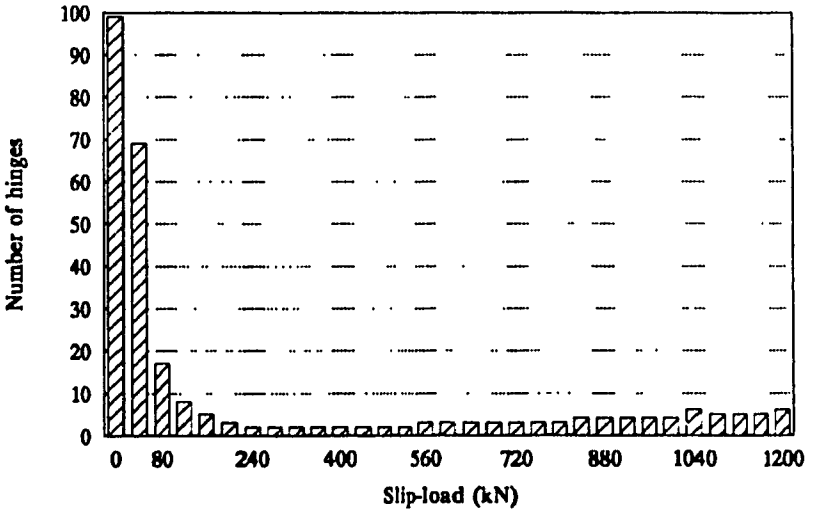

(b). Plastic hinges in beams & columns

Fig.2.14 Dynamic responses of 10-storey steel frame Newmark-Blume-Kapur 0.2g

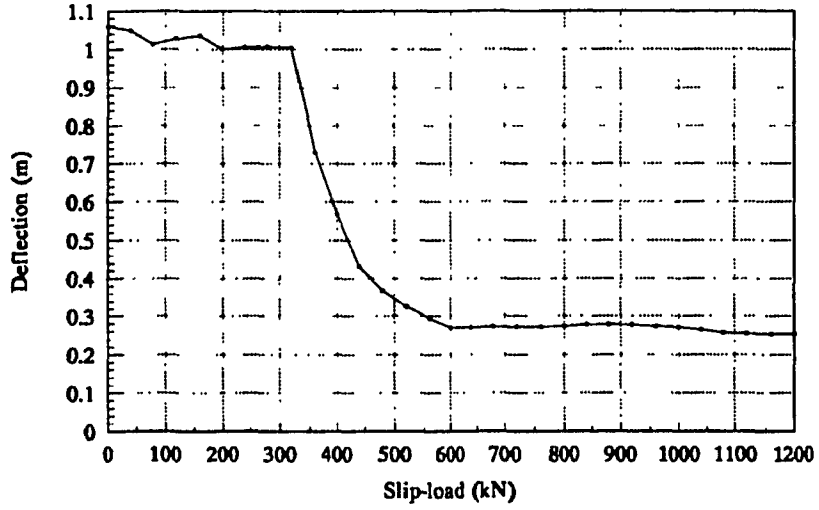

(a). Deflection at top

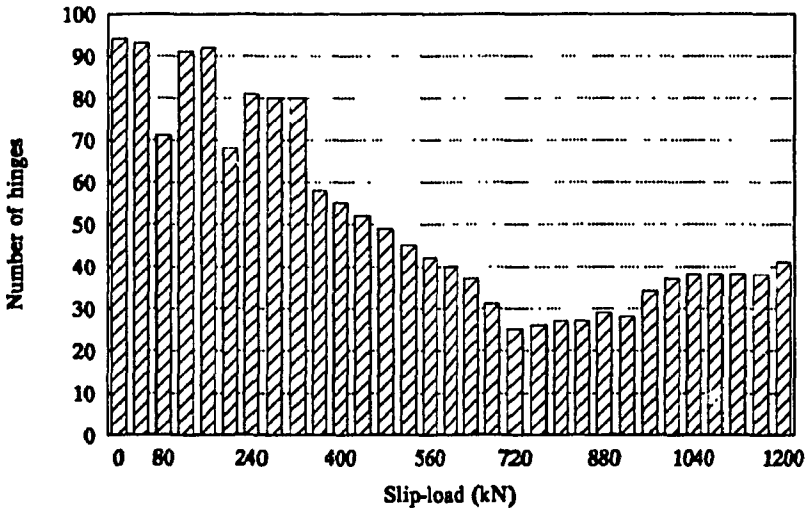

(b). Plastic hinges in beams & columns

Fig.2.15 Dynamic responses of 10-storey steel frame Newmark-Blume-Kapur 0.5g

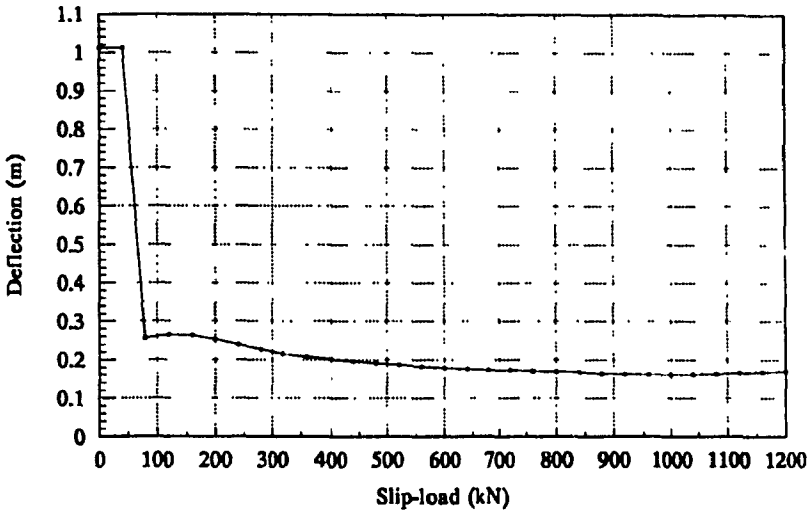

(a). Deflection at top

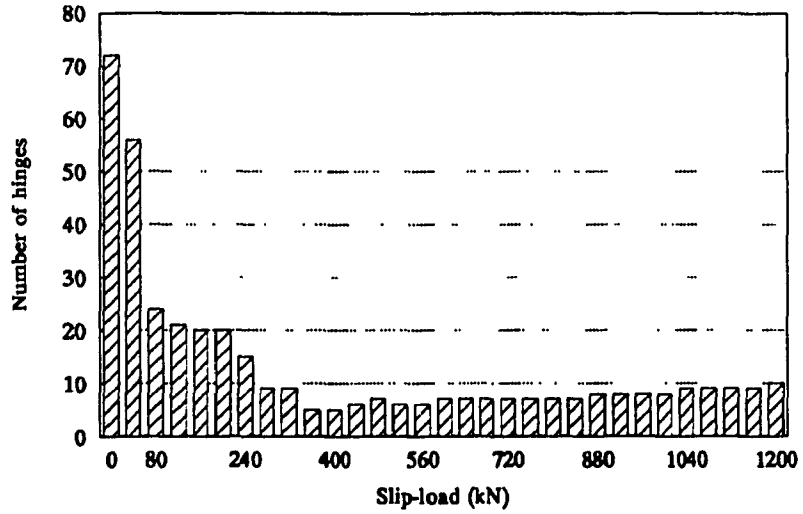

(b). Plastic hinges in beams & columns

Fig.2.16 Dynamic responses of 10-storey steel frame Romania 0.1g

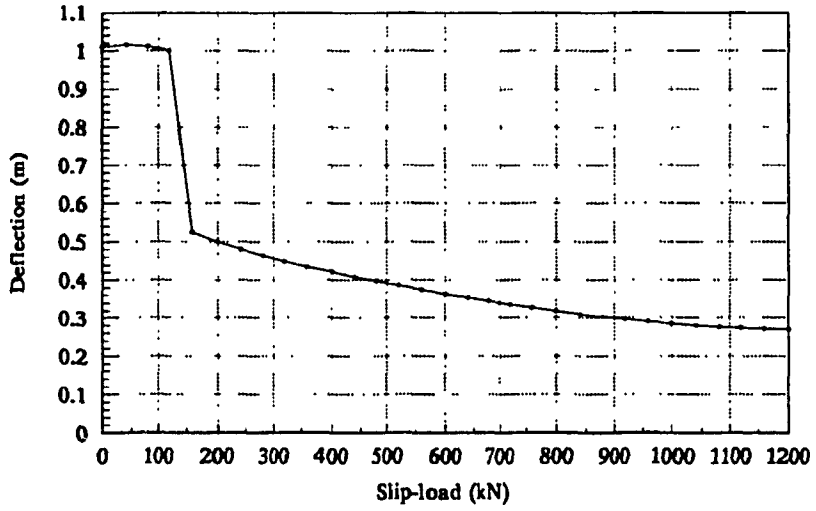

(a). Deflection at top

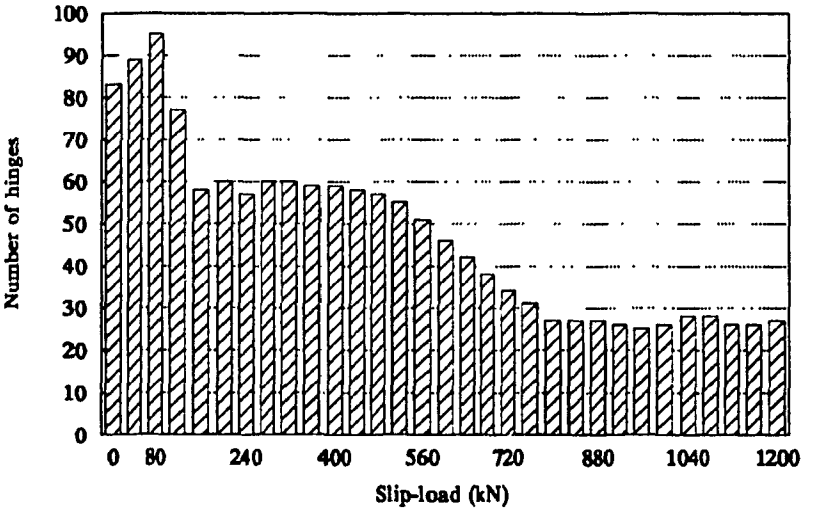

(b). Plastic hinges in beams & columns

Fig.2.17 Dynamic responses of 10-storey steel frame Romania 0.2g

CHAPTER 3 Computer program for the analysis and design of FDBF

Elastic analysis or simplified procedure are often used for earthquake resistant design of conventional structural systems. But for buildings equipped with energy dissipating devices, such as the friction damped braced frame, engineers have to deal with their inelastic behaviour. The previous chapter points out the need for a practical and efficient computer program to assist the designer in making decisions based on the likely structural performance versus design criteria. In this chapter, a computer program for the analysis and design of FDBF is presented.

3.1 Design procedure for the FDBF

The NBCC 1990 clause 83 of commentary J of the supplement stated: "Special mechanical protection systems such as base isolation or controlled friction damping devices can significantly alter the seismic response of buildings. It must be demonstrated through non-linear analysis and representative experimental data that the building so equipped will perform at least equally well in seismic events as the same building designed following the NBCC seismic requirements." Thus, for the design of buildings equipped with friction dampers, according to the NBCC

1990, the procedure should be:

1. Analyze and design the FDBF in elastic range for dead, live, wind and quasi-static seismic loads, and the FDBF should meet all the statutory requirements of the building code.

2. Perform non-linear time-step dynamic analysis to assess the seismic response of the FDBF during major earthquakes, and thereby determine the optimum slip-load.

In the integrated package, the first phase is accomplished by modifying the TABS-80 program, and the second by modifying the DRAIN-2D program.

3.2 Models for friction dampers

Two models of the friction damper device have been proposed. One is the so called simplified model first used by Pall and Marsh[2], and the other is a refined model used by Filiatrault and Cherry[8]. The refined model represents the behaviour of FDBF marginally better than the simplified model, but it needs much more computer time and data preparation. For simplicity, the simplified model has been used throughout; however, the developed program can readily accommodate the refined model.

3.2.1 Simplified model for friction damper

This model replaces the friction device by two diagonal braces endowed with elasto plastic behaviour. As shown in Fig.3.1, truss elements are used to

model these braces. A fictitious yield stress in tension is defined for the truss element to correspond with the stress in the tension brace when the device slips. A very low fictitious compression yield stress is also defined corresponding to the buckling stress of the compression brace. It must be noted that the simplified model is based on assumption that the slippage of the tension brace is large enough to straighten the buckled brace so that in the reversed load cycle, this straightened brace can immediately absorb energy in tension. It has been found that during some cycles of an actual earthquake excitation, the tension brace may not slip right away after the buckling, or the slippage is not large enough. Under such condition, the buckled braces will not absorb the energy and the simplified model will overestimate the energy absorption of the friction damper.

3.2.2 Refined model for friction damper

The refined model proposed by Filiatrault and Cherry (shown in Fig.3.2) consist of truss elements and beam-column elements. The truss elements are endowed with their own hysteretic behaviour. The four outside diagonal elements yield in tension and buckle elastically in compression and the two inside diagonal friction pads slip in tension and compression. The four links yield in tension and compression. To maintain stability, beam-column elements with zero axial stiffness are superimposed on the diagonal truss elements. Zero plastic moments are specified at one end of the beam-column elements to represent the pinned connections at the four corners of the frame.

3.3 Computer program description

To implement the design procedure mentioned previously, the two programs TABS-80[16] and DRAIN-2D were suitably modified and integrated into one package. These two programs were developed at the University of California, Berkeley, and are widely accepted and used by engineers.

3.3.1 TABS-80 elastic analysis program

TABS-80 program is for static and dynamic analysis of multistorey frame and shear wall buildings within the elastic range. The element library includes column, beam, shear panel, and brace elements. Gravity loads (dead or live) and lateral loads (wind, seismic static equivalent loads, elastic response spectrum analysis) may be applied. The mode shapes and periods(frequencies) of the structure may also be calculated.

3.3.2 DRAIN-2D inelastic analysis program

DRAIN-2D is a plane frame inelastic dynamic analysis program. It has routines for different structural elements, however, the elements which will be used in this study are:

1) Truss element, which may yield in tension and yield or buckle elastically in compression. The non-linear behaviour of truss element is shown in Fig.3.3.

2) Beam-column element, which yields through the formation of concentrated plastic hinges at its ends. Interaction between axial force and moment may be

taken into account for cross sections of steel or reinforced concrete type, and P-Δ effect may be taken into account by including the geometric stiffness based on the axial force under static loads. The hysteretic behaviour and yield interaction surface are shown in Fig.3.4 and Fig.3.5.

3) Shear panel element, which has shear stiffness only, and may yield and/or fail in a brittle fashion, its non-linear behaviour is shown in Fig.3.6.

4) Reinforced concrete beam element with degrading stiffness. Yielding may take place only in concentrated plastic hinges at the element ends. Strain hardening and degrading flexural stiffness are approximated by assuming that the element consists of a linear elastic beam element with non-linear rotational springs at each end, as shown in Fig.3.7. All plastic deformation effects, including the effects of degrading stiffness, are introduced by means of the moment-rotation relationships for the hinge spring. The moment-rotation relationship for each hinge is an extended version of Takeda's model, which has the behaviour illustrated in Fig.3.8.

3.3.3 The integrated design system

The macro flow chart of the combined computer program is shown in Fig.3.9. Since the original programs TABS-80 and DRAIN-2D were primarily for analysis, their integration into a design-oriented package requires extensive modifications. The major ones are:

- Merging of the data structures of the two programs so that they share the

same set of data input.

- Implementation of multiple load cases to produce response envelopes for the resultant force distribution.
- Verification for code requirements.
- Computation of the system's masses based on the specified gravity load.
- Implementation of an efficient search algorithm for locating the optimum slip load.
- Pre- and post-processors for plotting of the structure's geometry and dynamic responses.

This integrated program is not intended to be completely automatic in the sense that it is still the designer's responsibility to specify the initial member sizes as well the revised sizes for use in the next cycle.

In any one run, gravity load (dead or live) and lateral load (wind, seismic static equivalent loads, elastic response spectrum analysis) may be combined in different ratios. As an option, the gravity load can also be included in the non-linear time-step dynamic analysis.

For seismic analysis, the structure is assumed to be subject to rigid base excitation, which is defined by a time history of the ground acceleration at the base of the structure. Under random earthquake excitations, the optimum slip-load distribution of a friction-damped structure will be influenced by the characteristics of the earthquake ground motion anticipated at the building construction site. These characteristics include the excitation intensity, its frequency contents,

duration, number, size, and sequence of acceleration pulses. To accommodate these requirements, the original DRAIN-2D program was also modified to handle many earthquake excitations in one run. The optimum slip-loads and the responses of the structure corresponding to different excitations are output separately.

3.4 Optimization algorithm

It is known that the optimum slip-load is a function of the type and intensity of the earthquake and the stiffness of the structure.[9][12] Since earthquake excitations are random in nature, the optimum slip-load obtained by using one record may not be valid for other earthquake records. It is thus necessary for the designer to exercise his judgment in selecting the type and number of earthquake records. The present computer program helps to perform a speedy analysis while given the designer the option to define the objective functions as explained below.

3.4.1 Objective functions

In the assessment of the seismic response of buildings, the lateral deflection and the structural damages are the two main indicators[17],[18]. Thus, the optimum slip-load will be determined by minimizing the floor deflections and permanent damage (in terms of plastic hinges occurred in the structural elements).

Two objective functions are chosen to reflect these two criteria. One is the deflection of top floor, and the other is the number of plastic hinges that occur in

columns and beams during the earthquake.

3.4.2 Design parameters

According to the design procedure for the FDBF described in 3.1, except the cross-sectional area of the braces, all other properties of the frame are assumed to be known. To reduce the complexity, the design parameters chosen for the optimization of FDBF under non-linear and dynamic conditions are:

1) the slip-load of the friction devices.

2) the stiffness of the braces in terms of their cross-sectional area.

For a general structure subject to earthquake excitations, the floor shears are higher at the lower level, and thus the slip-load should also be higher there. In other word, there is an optimum slip-load distribution along the height of the structure. The effect of various slip-load distributions along the height of friction-damped structures was investigated earlier by Filiatrault and Cherry[19]. They contend that very little benefit is derived from the use of this optimum distribution. As a consequence, in this work the slip-load distribution is assumed to be uniform or in proportion to the base slip-load (normally the slip-load in the first floor); i.e. no attempt is made to alter the distribution during the optimization process. This approach not only simplifies the design procedure and the optimization process but also simplifies the fabrication and installation of the devices.

With the preceding simplification, the vector of design variables thus has only two components, and the problem can be stated as:

$$\begin{matrix} \min\ D(X,Y) \\ \min\ N(X,Y) \end{matrix} \qquad (3.1)$$

where X is the base slip-load, Y is the stiffness of the brace in terms of section area of the diagonal element, D(X,Y) and N(X,Y) are objective functions representing the deflection of top floor and the number of plastic hinges, respectively.

Eq.(3.1) is a multi-objective and multi-variable optimization problem. The coordinate rotation approach is adopted for its solution. In this approach, either the slip-load or the brace stiffness is fixed and the other is found by using one dimensional search algorithm[20]. The iterative process continues until convergence is obtained.

3.4.3 Optimization procedure

As has be seen in chapter 2, the optimum slip-load with respect to the deflection may be different from the optimum slip-load based on the number of plastic hinges. Thus, it is desirable to allow the designer the flexibility of specifying the relative importance of the two criteria.

For this purpose, two parameters N_0 and D_0 are introduced, where N_0 and D_0 are the tolerance values for convergence of the optimum N and D, respectively. The meaning of N_0 and D_0 is illustrated by the two extreme cases as follows:

1. N_0=0, D_0=large number: the optimum point is based exclusively on the number of plastic hinges. The large tolerance specified for displacement allows

unrestrictive displacements.

2. D_0=0, N_0=large number: the optimum point is based solely on limiting the displacement D since the damage in terms of plastic hinges in columns and beams is not restricted.

Between these two extremes, the designer may choose some intermediate values to reflect his perception on the relative importance of the criteria. Fig.3.10(a) illustrates the case where the two criteria lead to the same optimum slip load X_2. In Fig 3.10(b), the optimum points for N and D are different and contradictory. In this case where

$$N(X_2)-N(X_1)=n<N_0$$

$$D(X_1)-D(X_2)=d>D_0$$

if we consider only permanent damage then the optimum point should be X_1. But as $n<N_0$, there is room for accommodating the deflection as well. For instance, if $d>D_0$, although $N(X_2)>N(X_1)$, X_2 will be chosen as the optimum point.

Suppose that if the deflection of the building is of higher priority while the permanent damage has to be limited, then we may specify a small value for D_0 (say 0.005m) and a reasonable limit for N_0 (say 30). During the optimum procedure, as long as

$$|N(X_1)-N(X_2)|<N_0$$

the minimum deflection will always be chosen as optimum point. If $|N(X_1)-N(X_2)|>N_0$, then both objective functions will be considered together. The procedure for the two-objective optimization is illustrated in Fig.3.11.

3.5 Elastic analysis and design of FDBF

In proportioning the structure to meet the various design requirements, the distribution of internal forces and bending moments may be determined under the specified loads by using the elastic analysis.

3.5.1 Lateral loads due to wind

There are three different approaches to the problem of determining design wind loads on buildings in the Subsection 4.1.8., "Effects of Wind" of the 1990 edition of the National Building Code of Canada. The first approach, the "simple procedure" is appropriate for use with the majority of wind loading applications. The equivalent static loads given by the NBCC is:

$$p=qC_eC_eC_p \qquad (3.2)$$

where p is the specified external pressure or suction due to wind on the surface of the building. q is the reference velocity pressure. C_e is the exposure factor increase along the height of the building. C_g is the gust effect factor, C_g=2.0 for the building as a whole and main structural members. C_p is the external pressure coefficient averaged over the area of the surface considered. In the case of tall rectangular buildings, C_p=0.8 for the pressure directed towards the surface, C_p=-0.5 for the suction directed away from surface.

3.5.2 Lateral loads due to earthquake

According to the National Building Code of Canada the earthquake design criteria is to design structures to resist moderate earthquakes without significant damage and resist major earthquakes without structural collapse, multi-storey buildings located in moderately seismic zones such as Montreal therefore must be designed to have sufficient structural capacity and integrity to resist the minimum lateral seismic force.

The specified loading due to earthquake motion is determined as follows:

(1) The minimum lateral seismic force, V, shall be calculated in accordance with the following formula:

$$V=(V_e/R)U \tag{3.3}$$

where U=0.6; R is the force modification factor that reflects the capability of a structure to dissipate energy through inelastic behaviour. Since friction damped braced frames may be classified as ductile braced frames, the R factor to be used is 3.0, while appears to be extra conservative in view of their superior performance to equivalent ductile moment resisting frames whose R value is 4.0. For buildings more than 60 m in height with a structural system having R=2.0 or R=1.5, the value of V shall be increased by 50 per cent in velocity-related seismic zones of 4 and higher.

(2) The equivalent lateral seismic force representing elastic response, V_e, shall

be calculated in accordance with the following formula:

$$V_e = v \cdot S \cdot I \cdot F \cdot W \qquad (3.4)$$

where v is the specified zonal horizontal ground velocity expressed as a ratio to 1 m/s, S is the seismic response factor. It is a function of the fundamental period, T, of the structure, and the relative values of the velocity-related and acceleration-related seismic zones, Z_v and Z_a. S is illustrated in Fig.3.12. I is the importance factor, I=1.0 for buildings except as schools and post-disaster buildings. F is foundation factor. W is the dead load, which includes the weight of the permanent equipment (mechanical floor), 25% snow load and 60% storage load(retail floor).

(3) The total lateral seismic force, V, shall be distributed as follows:

A portion, F_t, shall be applied as a concentrated load at the roof and

$$F_t = 0.07TV \quad (\text{where } F_t \le 0.25V) \qquad (3.5)$$
$$= 0 \qquad (\text{when } T < 0.7s)$$

the remainder, $V-F_t$, shall be distributed along the height of the building, including the top level in accordance with the formula

$$F_x = (V - F_t) W_x h_x / \left(\sum_{i=1}^{n} W_i h_i\right) \qquad (3.6)$$

where F_x is the lateral force applied to level **x**, h_x, h_i are the height above the base to level "**x**" or "i", W_x, W_i are that portion of W which is located at or is assigned to level "**x**" or "i".

Lateral deflections obtained from the elastic analysis using the loads given in (3.5) and (3.6) shall be multiplied by R, and the interstorey deflection based on the lateral deflections shall be limited to $0.01h_s$ for post-disaster buildings and $0.02h_s$ for all other buildings, where h_s is the interstorey height (h_i-h_{i-1}).

All the provisions mentioned above have been introduced into the computer program.

3.5.3 Member size checking

According to NBCC, the structural members should be designed to have sufficient strength and stability, such that:

Factored Resistance ≥ Effect of Factored loads (3.7)

where Effect of factored loads is determined as follows:

$$\alpha_D D + \gamma\psi(\alpha_L L + \alpha_Q Q + \alpha_T T) \quad (3.8)$$

where D is Dead loads, L is Live loads, Q is wind or earthquake loads, and T causes from temperature change, shrinkage etc..

In eq.(3.8), α are load factors, ψ is the load combination factor, and γ is the importance factor.

Load factors, α, shall be taken as follows:

$\alpha_D = 1.25$;

$\alpha_L = 1.50$;

$\alpha_Q = 1.50$ for wind or 1.00 for earthquake;

$\alpha_T = 1.25$.

The load combination factor, ψ, shall be taken as follows:

(a) When only one of L, Q and T act, $\psi = 1.00$;

(b) When two of L, Q and T act, $\psi = 0.70$;

(c) When all of L, Q and T act, $\psi = 0.60$.

The most unfavourable effect shall be determined by considering L, Q and T acting alone with $\psi = 1.00$ or in combination with $\psi = 0.70$ or 0.60.

The importance Factor, γ, usually is taken as 1.00.

The factored member resistance is different for different type of structural member. For instance, according to design provisions[21], for the axial compression and bending member (Class 1 sections of I-shape), the following equations should be satisfied:

$$\frac{M_f}{M_r} \leq 1.0$$

$$\frac{C_f}{C_r} + \frac{0.85\omega M_f}{M_r(1-\frac{C_f}{C_e})} \leq 1.0 \qquad (3.9)$$

where

C_f = factored axial force.

M_f = factored bending moment.

C_r = factored axial compressive resistance.

M_r = factored bending moment resistance.

C_e = Euler buckling strength.

ω = Coefficient used to determine equivalent uniform bending effect.

The member resistance formulas for axial tension member, axial compression member, bending members, axial compression and bending members etc., have been introduced to the computer program. If eq.(3.7) is satisfied, then the program will go to the next step; i.e. to perform non-linear time-step dynamic analysis. If the verification fails, then the designer will have the option to revise the member sizes and another analysis and verification cycle is carried out. As currently implemented, the program can only perform member size verification based on CSA Standard CAN/CSA-S16.1-M89[21] i.e. for steel structural members.

3.6 Interface with AutoCAD[22]

Pre- and post-processing are performed primarily by means of an interface to AutoCAD. AutoCAD is a general purpose Computer-Aided Design/Drafting software. It provides powerful tools for graphics applications. The interface program creates script files. The script file is a ASCII file which contains a predetermined

sequence of command for AutoCAD taking advantage of the facilities provided by AutoCAD to draw and print out the graphics.

The pre-processing phase produces the drawing of the frame and its nodes and elements numbering. Post-processing concerns with the plotting of the time history displacement of a specified node, the deformed structure and the location of the plastic hinges within the frame. Most of the results shown in this thesis are the product of this post-processor.

3.7 Examples analysis

In this section, a 20-storey all-steel office building and a 10-storey reinforced concrete office building will be used as the application examples to demonstrate the use of the computer program as a tool for assisting engineers in seismic design of FDBF consistent with the design criteria. Emphasis is placed on the proposed automatic optimization scheme and its effectiveness as compared to the exhaustive search procedure.

3.7.1 A twenty-story steel office building

The case-study building is a hypothetical 20-storey all-steel office building as described by K.S. Sivakumaran[15]. Fig.3.13 shows the floors and roof plan and Fig.3.14 shows the elevation and member sizes of the W-E direction perimeter frames(column lines A and B). The concentric bracing system used by Sivakumaran (N-S direction column lines 2 and 3) was modified by changing the

brace member sizes and adding friction damper devices to all floors. The girder sizes for the internal frames(N-S direction) are assumed to be same as the perimeter frames(W-E direction). The dead and live load act on the internal frames are shown in Fig.3.15. For the wind loads, q is taken as 0.37kPa (Montreal area) based on a probability of being exceeded in any one year of 1 in 30. For the seismic forces, v, Z_a, Z_v, I, F are taken as follows:

v=0.1
Z_a=4 (Montreal area)
Z_v=2
I=1.0
F=1.0 (for rock and dense soil conditions)

And thus:

v:	Zonal Velocity Ratio	=	0.10
Za:	Acceleration-Related Seismic Zone	=	4
Zv:	Velocity-Related Seismic Zone	=	2
I:	Seismic Importance Factor	=	1.00
F:	Foundation Factor	=	1.00
R:	Force Modification Factor	=	3.00

The first five natural periods and mode shapes of the FDBF, the lateral deflections and story drifts under the design loads (wind and seismic) are listed respectively in Table 3.1 and 3.2.

The elastic analysis results show that the deflections and interstory drift due to wind and specified seismic loads all meet the statutory requirements of the

NBCC. The elastic analysis also produces the design member forces (which are not shown here) for member size verification. In addition, the maximum brace force was established at approximately 100kN which becomes the lower limit for the slip loads of the friction devices.

Table 3.1 First five natural periods and mode shapes of the 20-story frame

MODE NUMBER	TIME PERIOD
1	2.24876
2	.59904
3	.31319
4	.21625
5	.16311

	MODE SHAPES:				
LEVEL	MODE 1	MODE 2	MODE 3	MODE 4	MODE 5
20	-.1374	.1198	.0968	.0919	-.1021
19	-.1271	.0870	.0563	.0393	-.0258
18	-.1193	.0564	.0085	-.0266	.0615
17	-.1114	.0249	-.0383	-.0823	.1152
16	-.1033	-.0066	-.0777	-.1121	.1104
15	-.0950	-.0363	-.1037	-.1078	.0496
14	-.0865	-.0628	-.1124	-.0704	-.0374
13	-.0784	-.0840	-.1033	-.0142	-.1038
12	-.0702	-.1004	-.0786	.0469	-.1230
11	-.0622	-.1111	-.0428	.0944	-.0860
10	-.0542	-.1165	-.0009	.1170	-.0110
9	-.0465	-.1163	.0412	.1084	.0684
8	-.0389	-.1105	.0779	.0707	.1161
7	-.0317	-.0999	.1037	.0151	.1108
6	-.0248	-.0848	.1159	-.0445	.0558
5	-.0183	-.0669	.1134	-.0913	-.0212
4	-.0138	-.0557	.1047	-.1040	-.0565
3	-.0099	-.0438	.0894	-.1029	-.0784
2	-.0064	-.0313	.0690	-.0893	-.0843
1	-.0030	-.0170	.0409	-.0599	-.0681

Table 3.2 Lateral deflections and story drifts

LATERAL DISPLACEMENTS (WIND LOAD):						
LEVEL	Deflec-tions		h/500	Story drift		Hs/500
20	.09067	<	0.172	.00654	<	.012
19	.08413	<	0.160	.00451	<	.008
18	.07962	<	0.152	.00463	<	.008
17	.07499	<	0.144	.00479	<	.008
16	.07020	<	0.136	.00494	<	.008
15	.06526	<	0.128	.00506	<	.008
14	.06020	<	0.120	.00500	<	.008
13	.05520	<	0.112	.00510	<	.008
12	.05010	<	0.104	.00509	<	.008
11	.04501	<	0.096	.00515	<	.008
10	.03986	<	0.088	.00514	<	.008
9	.03472	<	0.080	.00514	<	.008
8	.02958	<	0.072	.00502	<	.008
7	.02456	<	0.064	.00499	<	.008
6	.01957	<	0.056	.00478	<	.008
5	.01479	<	0.048	.00335	<	.008
4	.01144	<	0.040	.00303	<	.008
3	.00841	<	0.032	.00275	<	.008
2	.00566	<	0.024	.00284	<	.010
1	.00282	<	0.014	.00282	<	.014

LATERAL DISPLACEMENTS (QUASI-STATIC EARTHQUAKE LOAD):					
NO. OF STOREY	LATERAL DEFLECTION	DEFLECTION MULT. BY R	INTERNAL DEFLECTION		(0.02Hs)
20	.05611	.16833	.01394	<	.120
19	.05146	.15439	.01004	<	.080
18	.04812	.14435	.01011	<	.080
17	.04475	.13424	.01025	<	.080
16	.04133	.12400	.01030	<	.080
15	.03790	.11370	.01032	<	.080
14	.03446	.10338	.00991	<	.080
13	.03116	.09347	.00987	<	.080
12	.02786	.08359	.00959	<	.080
11	.02467	.07400	.00947	<	.080
10	.02151	.06453	.00922	<	.080
9	.01844	.05531	.00896	<	.080
8	.01545	.04635	.00851	<	.080
7	.01261	.03784	.00822	<	.080
6	.00987	.02961	.00764	<	.080
5	.00732	.02197	.00536	<	.080
4	.00554	.01661	.00472	<	.080
3	.00396	.01189	.00413	<	.080
2	.00258	.00775	.00407	<	.100
1	.00123	.00368	.00368	<	.140

Non-linear dynamic analysis

After the elastic analysis, the non-linear time-step dynamic analysis should be carried out to make sure that the frame equipped with friction dampers will perform better or at least equally well in seismic events as the same frame designed following the NBCC seismic requirement, and at the same time, the optimum slip-load for the friction dampers may be established.

The yield strength of the structural steel used for the beam and column elements is 300MPa. The Young's modulus of steel is 2×10^5MPa.

The cross sectional areas of the braces have been previously selected, and thus only the slip-load is the optimizing parameter for this problem.

EL-Centro 1940 NS component(0-12 Sec.), Taft 1952(0-15 Sec.) earthquake record, Newmark-Blume-Kapur Artificial Earthquake(0-15 Sec.) were used as the base excitations. All the earthquake records are scaled to 0.18g and 0.36g.

The values for N_0 and D_0 are chosen as:

$$N_0=10,\ D_0=0.01\ (m)$$

The optimum slip-load for different ground motions and peak accelerations are listed in table 3.3. All computations were performed on an IBM-compatible PC (486DX-33).

To evaluate the correctness and effectiveness of the optimization scheme, the exhaustive search approach was performed for the same frame. Time costs of the two approaches are also listed in table 3.3. The dynamic responses of the frame from the exhaustive search approach and the optimization search points are

shown in Fig 3.16 to Fig.3.21. In these figures, the slip loads varying from 100kN to 1800kN, where 100kN is the maximum axial force in braces due to static loads(combination of dead, live, and wind/or quasi-static seismic loads) so that the friction devices will not slip under the action of wind forces or minor earthquakes, and 1800kN is the strength limit of the braces.

Table.3.3 Comparison of Results (20-story frame)

Earthquake Excitation	Peak value Acce.	Optimum slip-load(kN)	Max dis. at top (m)	Hinges in Col. & Beam	CPU Time (h:m:s) Optimi-zation	Exhaustive search
El-Centro	0.18g	363	0.136	0	14:33	1:29:51
El-Centro	0.36g	749	0.268	11	14:58	1:31:52
Taft	0.18g	263	0.116	0	18:45	1:52:10
Taft	0.36g	687	0.234	3	18:50	1:55:26
NBK	0.18g	1112	0.213	4	17:59	1:51:15
NBK	0.36g	1637	0.432	59	18:41	1:46:46

Observation of the results in table 3.3 and Fig.3.16 to Fig.3.21 shows that the optimization procedure leads to similar conclusion as the exhaustive search however with much less time. The CPU time in the exhaustive search approach does not include the time spent by the analyst for data preparation and plotting of results.

Fig.3.22 shows the time histories of deflections at the top of the frame of the FDBF and the BMRF for the Newmark-Blume-Kapur Artificial Earthquake excitation (0.36g). The base optimum slip-load for the FDBF was chosen as 1600kN. The damage in terms of plastic hinges in columns and beams experienced by the FDBF and the BMRF are shown in Fig.3.23 and Fig.3.24. It is shown that the FDBF performs better than the BMRF in seismic events.

Influence of N_0 and D_0

To assess the influence of values of N_0 and D_0 on the optimum slip-loads, three different sets of N_0 and D_0 were chosen for controlling the optimization:

Case 1: N_0=0 , D_0=0.1m (minimize the number plastic hinges only)

Case 2: N_0=30 , D_0=0.0m (minimize the deflection only)

Case 3: N_0=10 , D_0=0.01m (both criteria are considered)

The earthquake excitation is NBK, and the intensity is 0.36g. The results are listed in Table 3.4.

Table.3.4 Results for different cases of N_0 & D_0

Peak value of Acce.	No & Do Cases	Optimum slip-load(kN)	Max dis. at top (m)	Hinges in Col. & Beam
0.36g	Case 1	1000	0.567	40
	Case 2	1700	0.426	65
	Case 3	1637	0.432	59

As shown in Fig.3.21, the optimum slip-load in terms of minimum deflection (case 2) should be around 1700kN, while the optimum slip-load in terms of minimum damage (case 1) should be around 1000kN. By choosing an intermediate values of N_0 and D_0, the deflection and damage of the frame could be taken into account together. As shown in Table 3.4, the optimum slip-load is 1637kN, which corresponds to the maximum deflection of 0.432m and 59 plastic hinges.

3.7.2 A ten-story reinforced concrete office building

This frame was chosen from the New Library Building Complex of

Concordia University, Montreal, Canada. Details of the building are described in reference[3]. The plan view of the complex structure and the location of the chosen 10-storey frame are shown in Fig.3.25. Fig.3.26 shows the elevation of the frame to be considered.

As the building was designed as an (unbraced) moment resistant frame, only the time-step dynamic analysis was carried out to obtain the optimum slip-load and the corresponding dynamic responses. The Newmark-Blume-Kapur Artificial Earthquake(0-15 Sec.) is used with the maximum acceleration scaled to 0.18g and 0.36g, where 0.18g is the peak horizontal ground acceleration with a probability of exceedance of 10% in 50 years in Montreal (NBCC table J-2). The Takeda model for the degrading stiffness of flexural concrete members was used. The integration time step was 0.005 seconds. As foundations of the building rest on rock, the soil-structure interaction was neglected. The optimization results (N_0=10, D_0=0.01m) are listed in table 3.5.

Table.3.5 Optimum slip-load under excitations

Earthquake Excitation	Peak value Acce.	Optimum slip-load(kN)	Max dis. at top (m)	Hinges in Col. & Beam
NBK	0.18g	642	0.056	0
NBK	0.36g	519	0.111	48

The dynamic responses of the same frame for slip-load ranging from 0 to 1100kN are shown in Fig.3.27 to Fig.3.28 for the purpose of evaluating the correctness of the obtained optimum slip-loads.

The time histories of deflections at the top of the FDBF and the MRF for the 0.18g and 0.36g NBK excitation are shown in Fig.3.29 and Fig.3.30. The optimum slip-load for the FDBF was chosen as 650kN. The damage in terms of plastic hinges in columns and beams experienced by the FDBF and the MRF are shown in Fig.3.31 and Fig.3.32. It is shown that the FDBF performs better than the MRF in seismic events.

3.8 Summary

The current design procedure of FDBF is first to design the FDBF in elastic range, and next, to perform the non-linear dynamic analysis. The computer program developed in this study can handle the elastic design and the non-linear dynamic analysis in one run, and only one set of data needs to be prepared. In addition, the program can handle more complex distributed loading, such as the triangular distribution in the 20-storey example building. It can also accumulate the dead loads acted on frame, and convert them to masses and then lump the masses to the corresponding column-beam joints for the dynamic analysis. These two features make the data preparation much easier.

The proposed optimization scheme eliminates the much more tedious task of data preparation and plotting of results by using an automatic search procedure. The designer has the option of placing relative importance on the two criteria for the optimum, which may or may not be in conflict with each other.

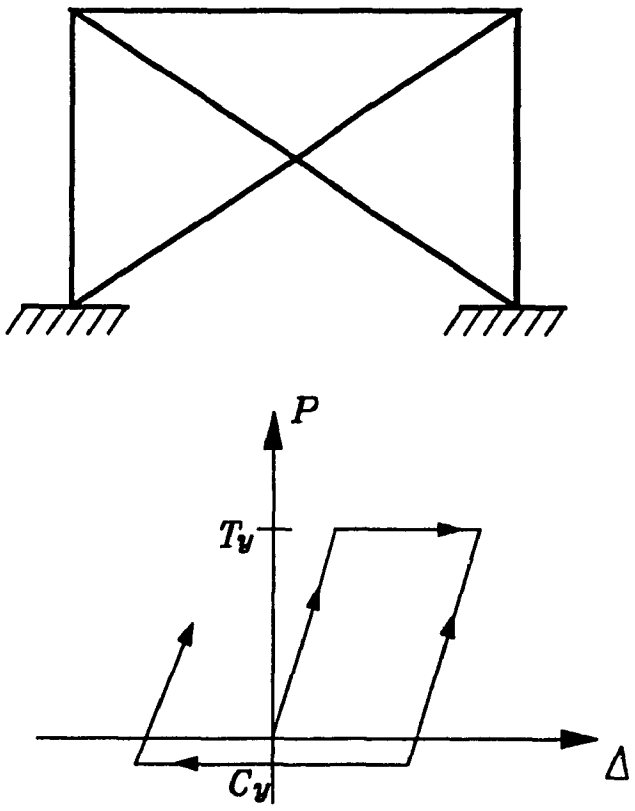

T_y, C_y = Fictitious yield loads of braces

Fig.3.1 Simplified model for friction damper[2]

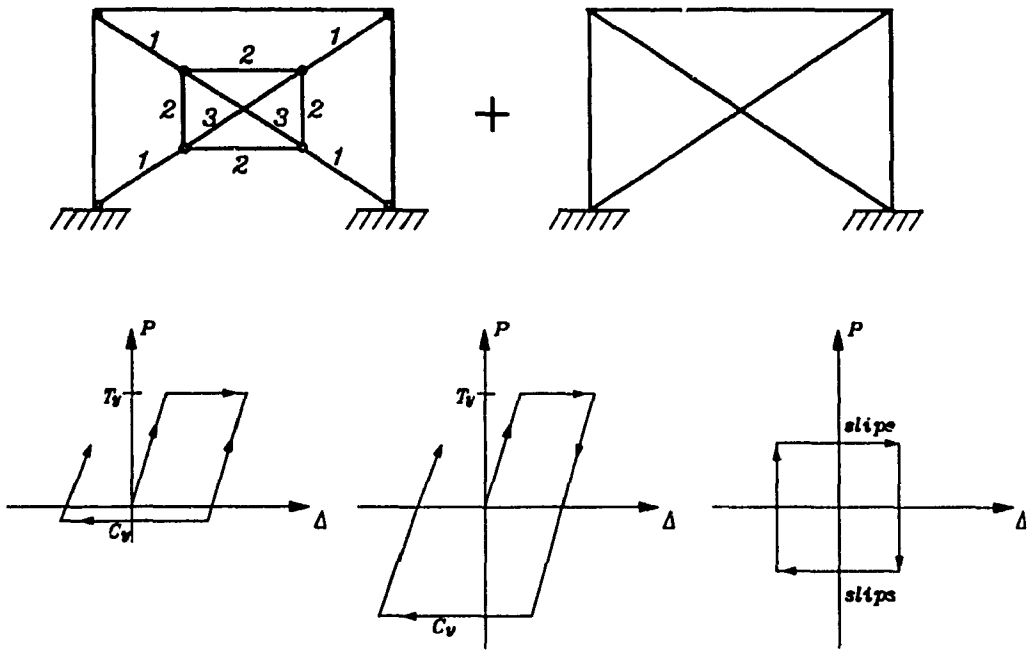

Fig.3.2 Refined model for friction damper[8]

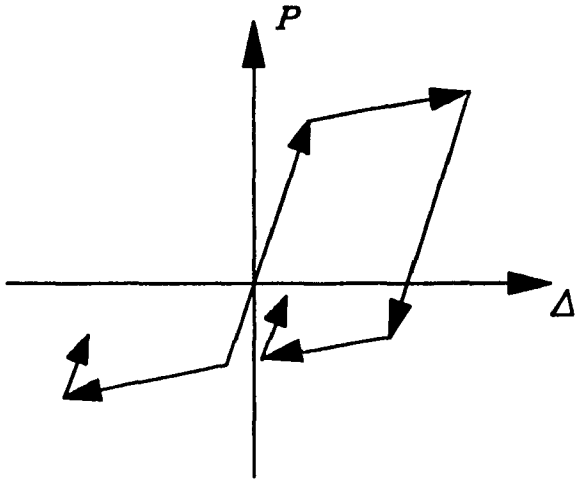

(a) Yield in tension and compression

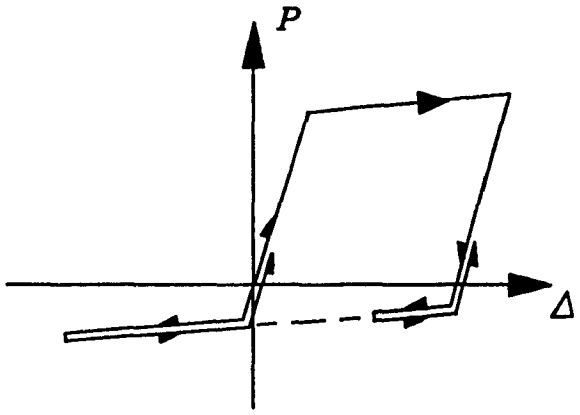

(b) Yield in tension, buckling in compression

Fig.3.3 Truss element behaviour[14]

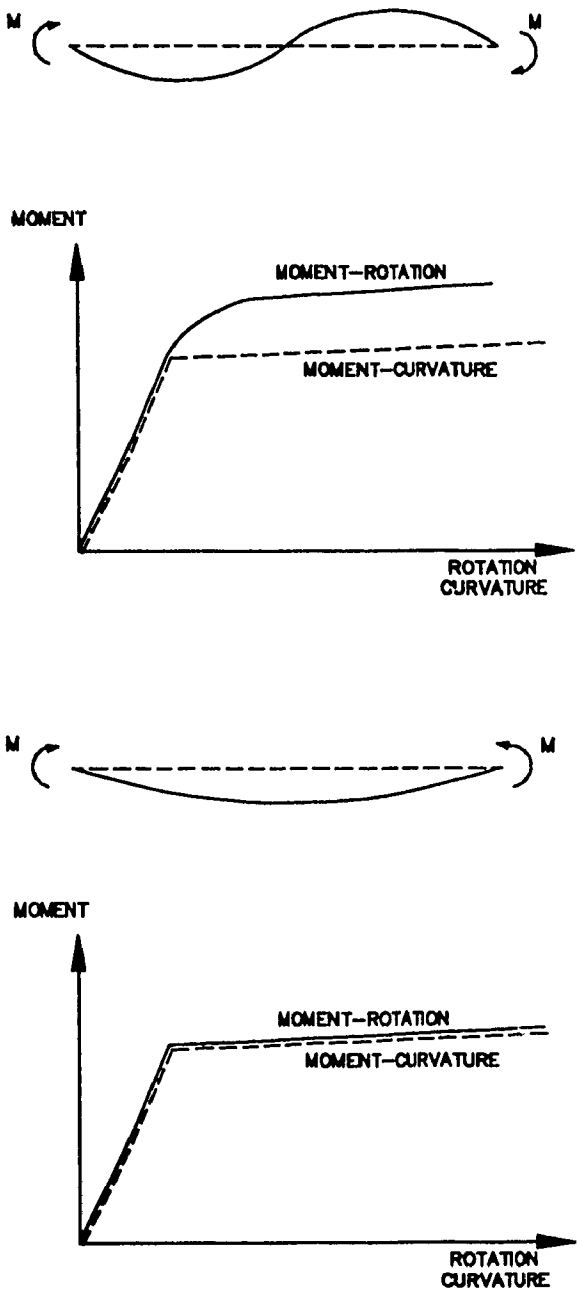

Fig.3.4 Moment-Curvature and Moment-Rotation relationship for the Beam-Column element[14]

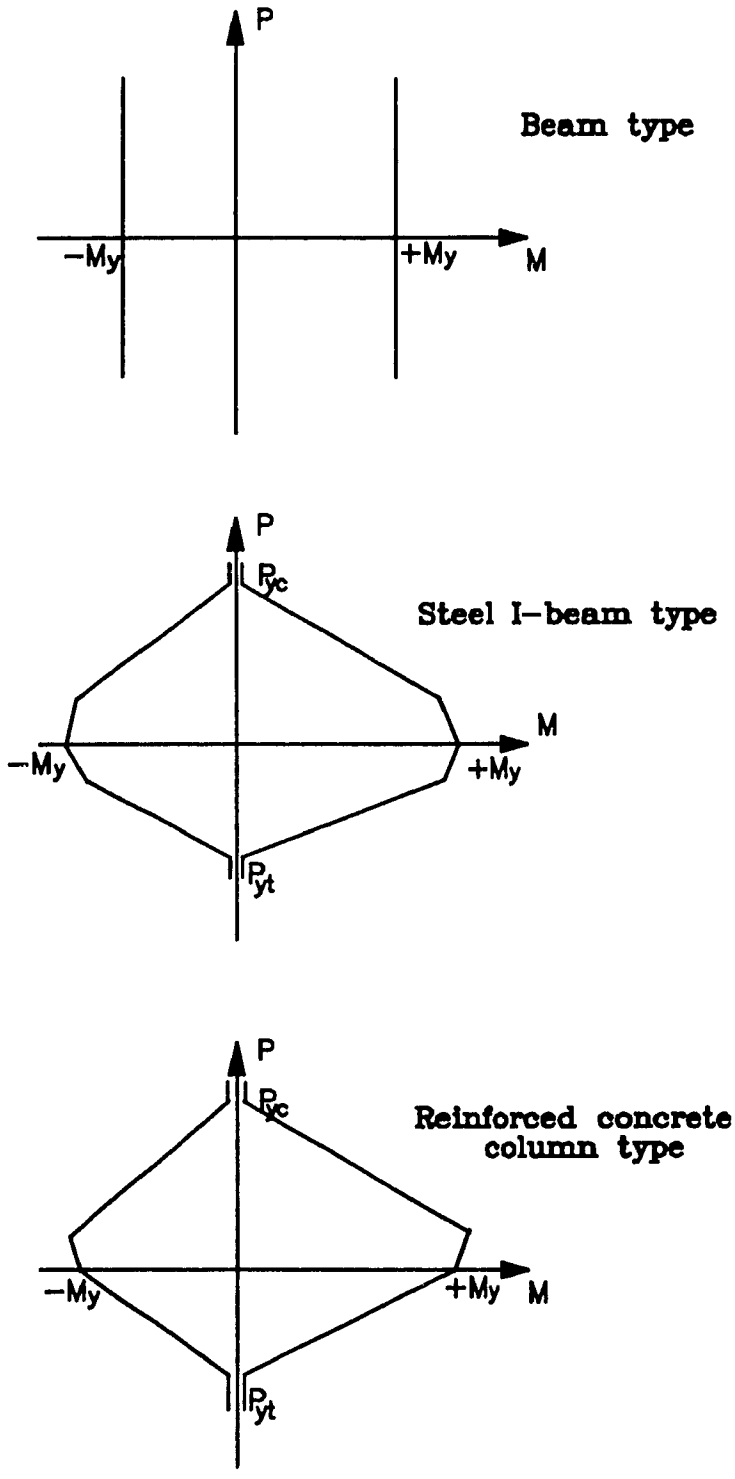

Fig.3.5 Yield interaction surfaces[14]

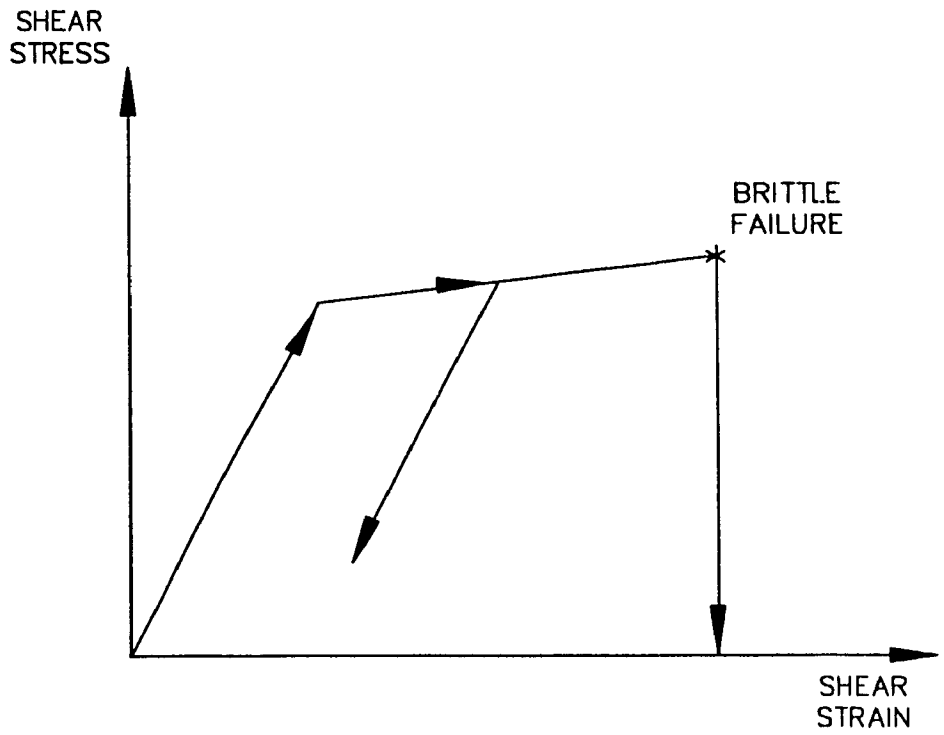

Fig.3.6 Stress-strain relationship for infill panel[14]

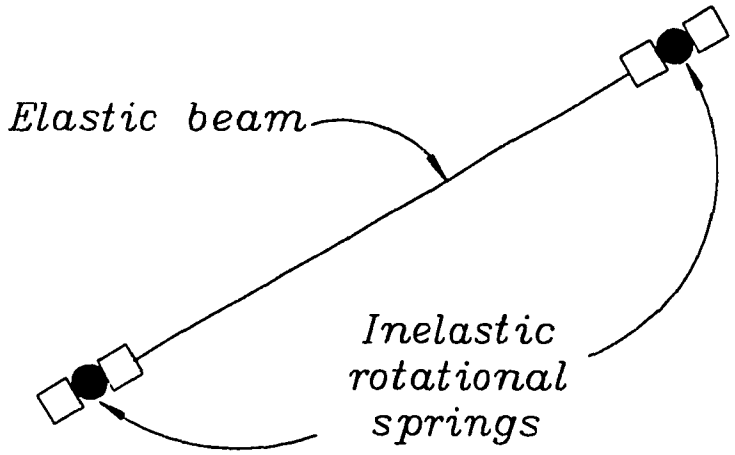

Fig.3.7 Element idealization[14]

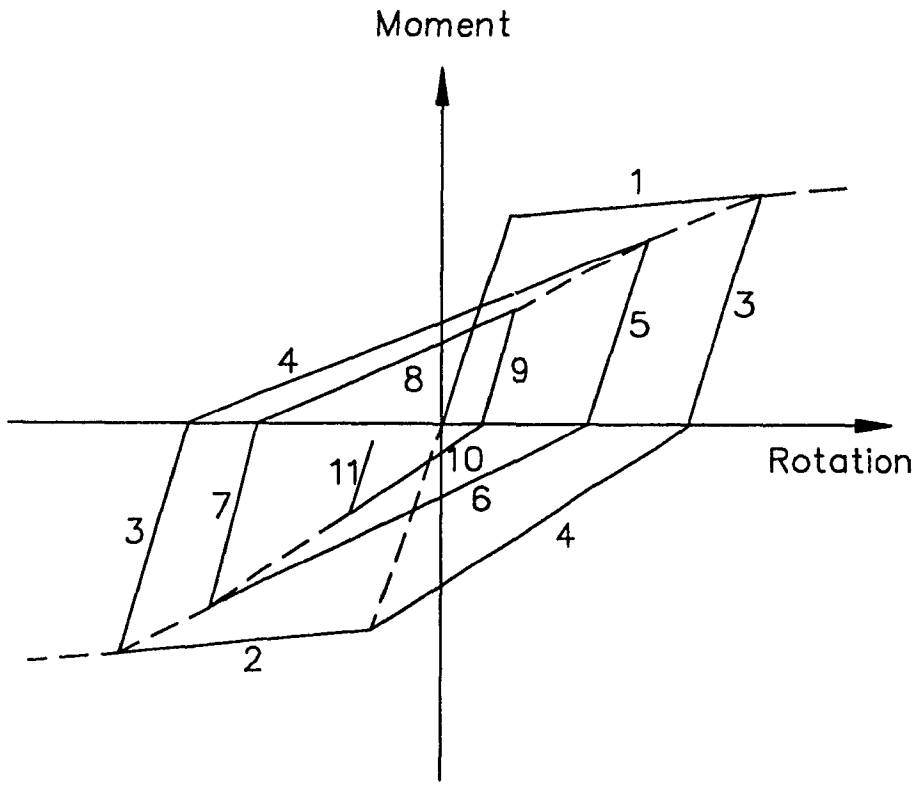

Fig.3.8 Hinges moment-rotation relationship for TAKEDA model[14]

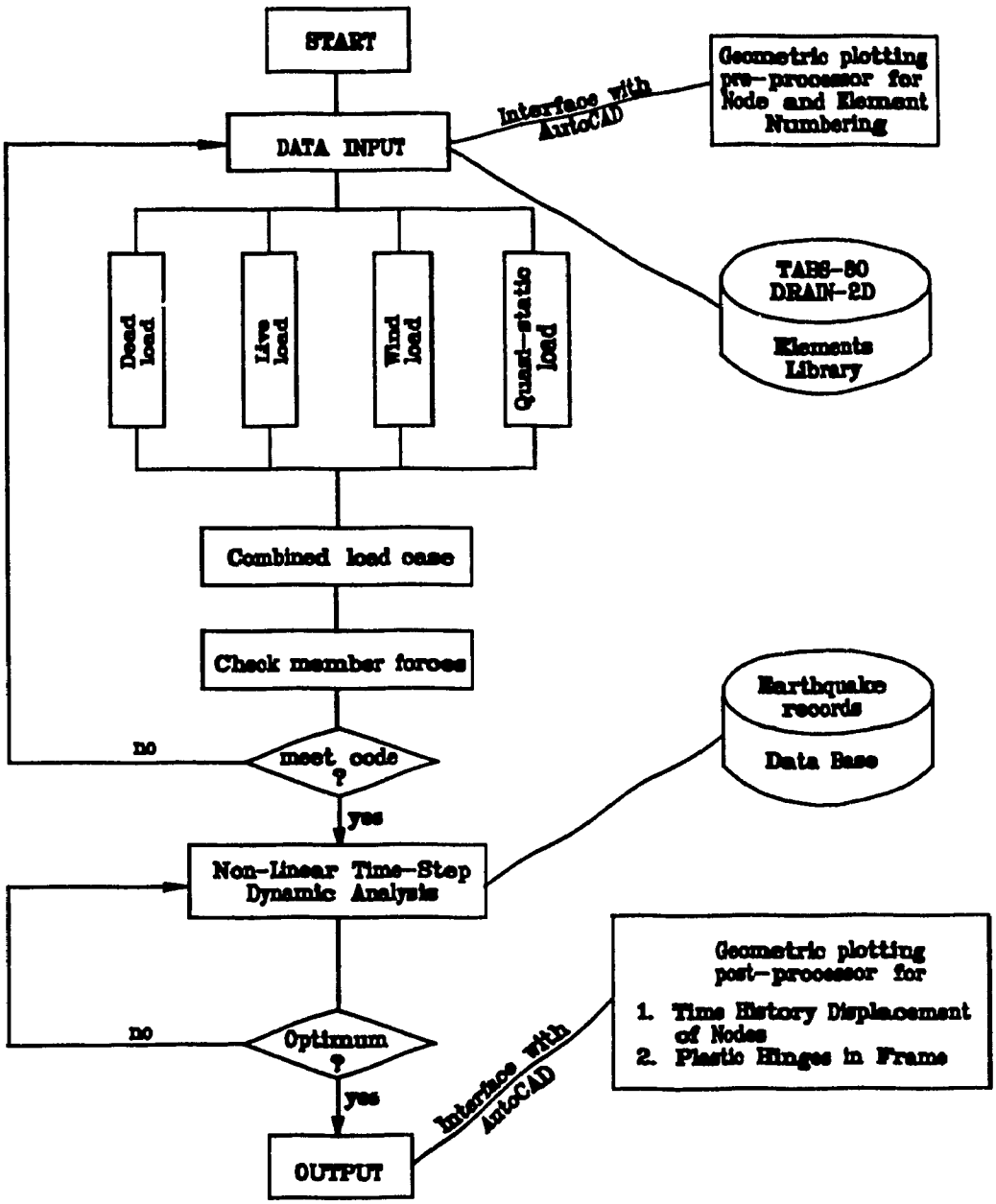

Fig.3.9 Macro flow chart of the integrated program

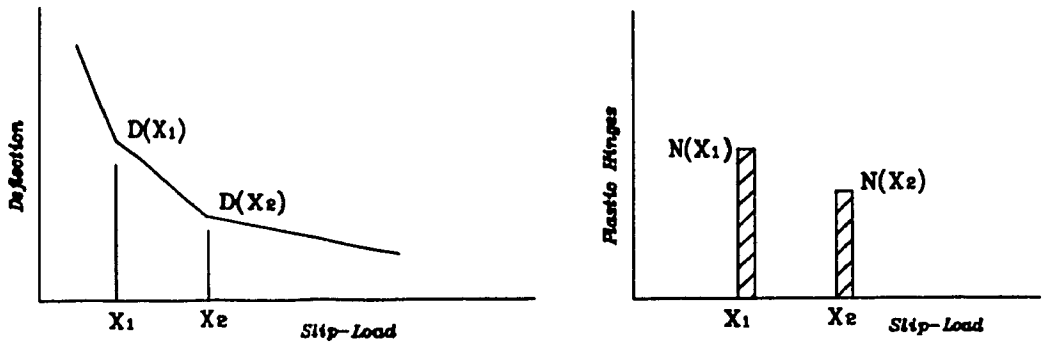

a) optimum slip load=X_2

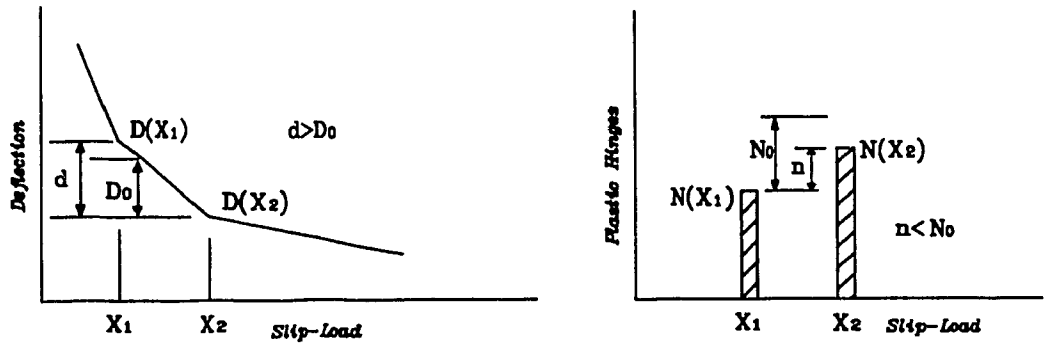

b) optimum slip load=X_2

Fig.3.10 Decision procedure

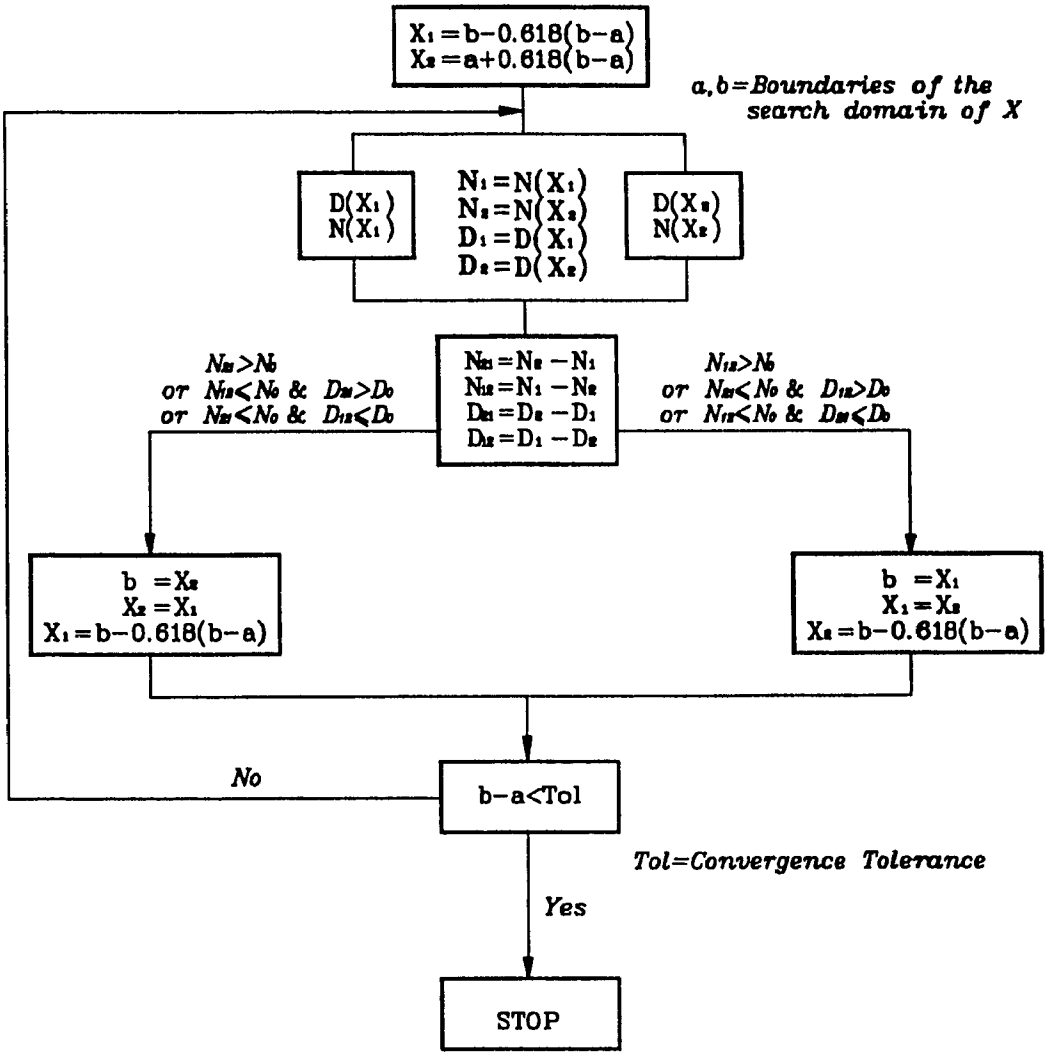

Fig.3.11 Optimization procedure

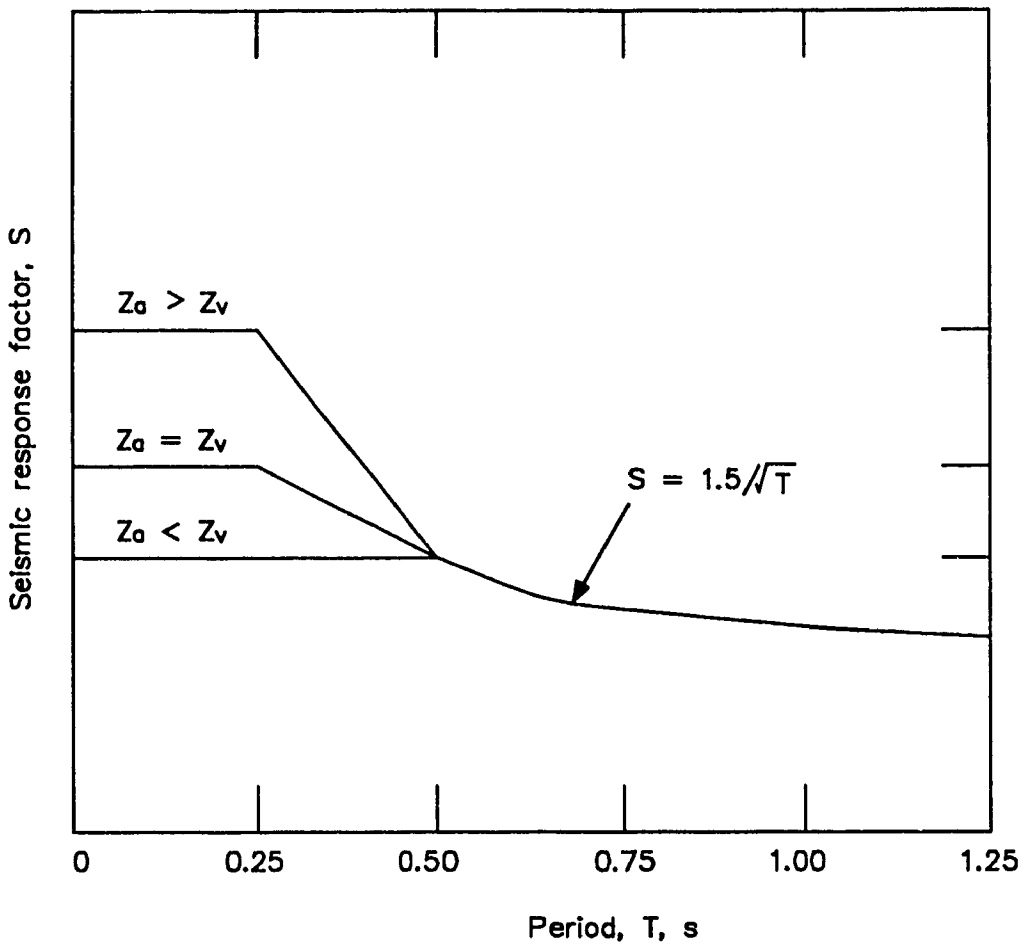

Fig.3.12 Seismic response factor S for 1990 NBC

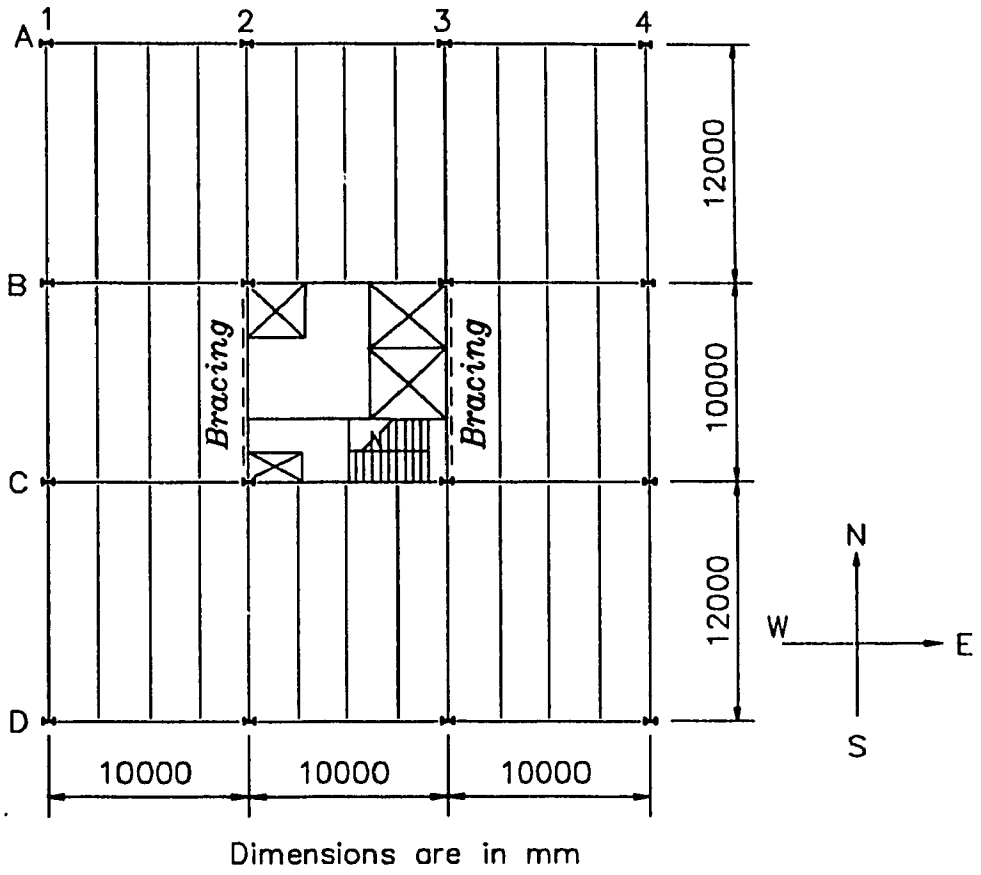

Fig.3.13 Floor plan of the 20-storey steel building

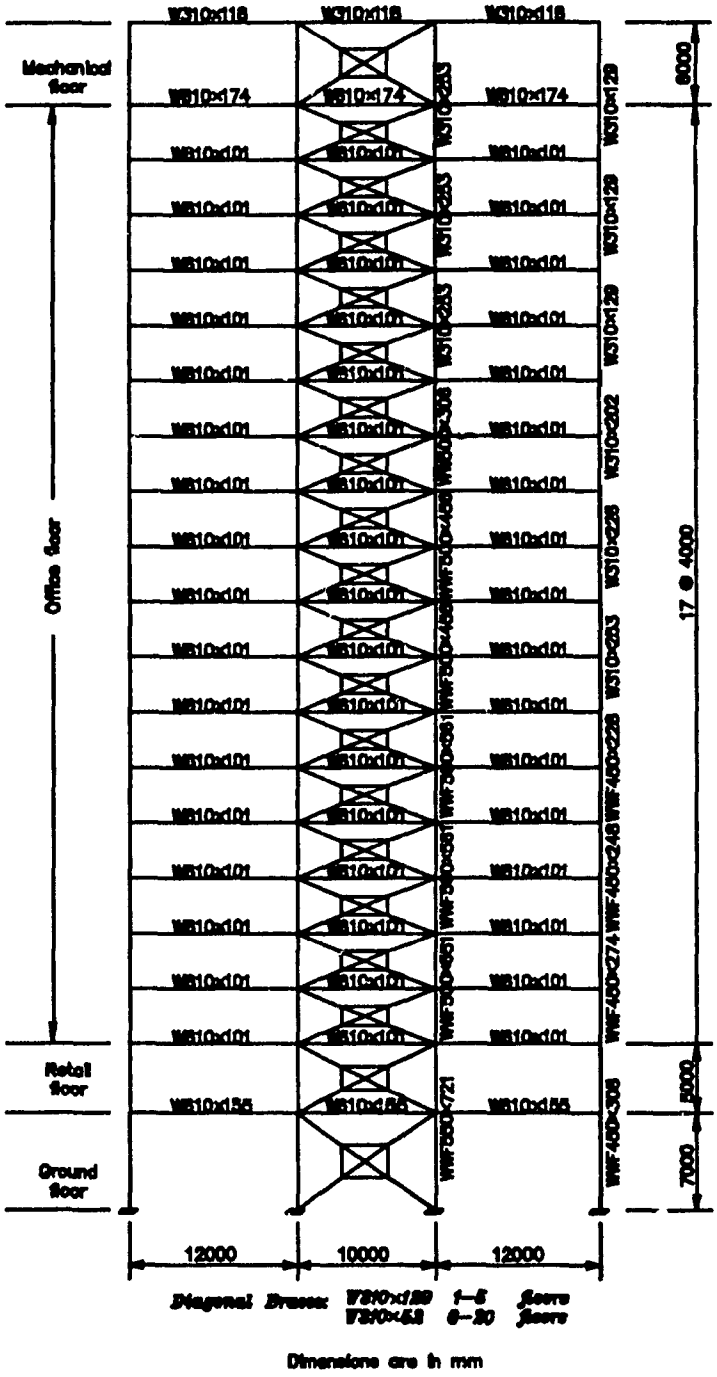

Fig.3.14 Elevation and member sizes of FDBF (N-S direction, column lines 2 and 3)

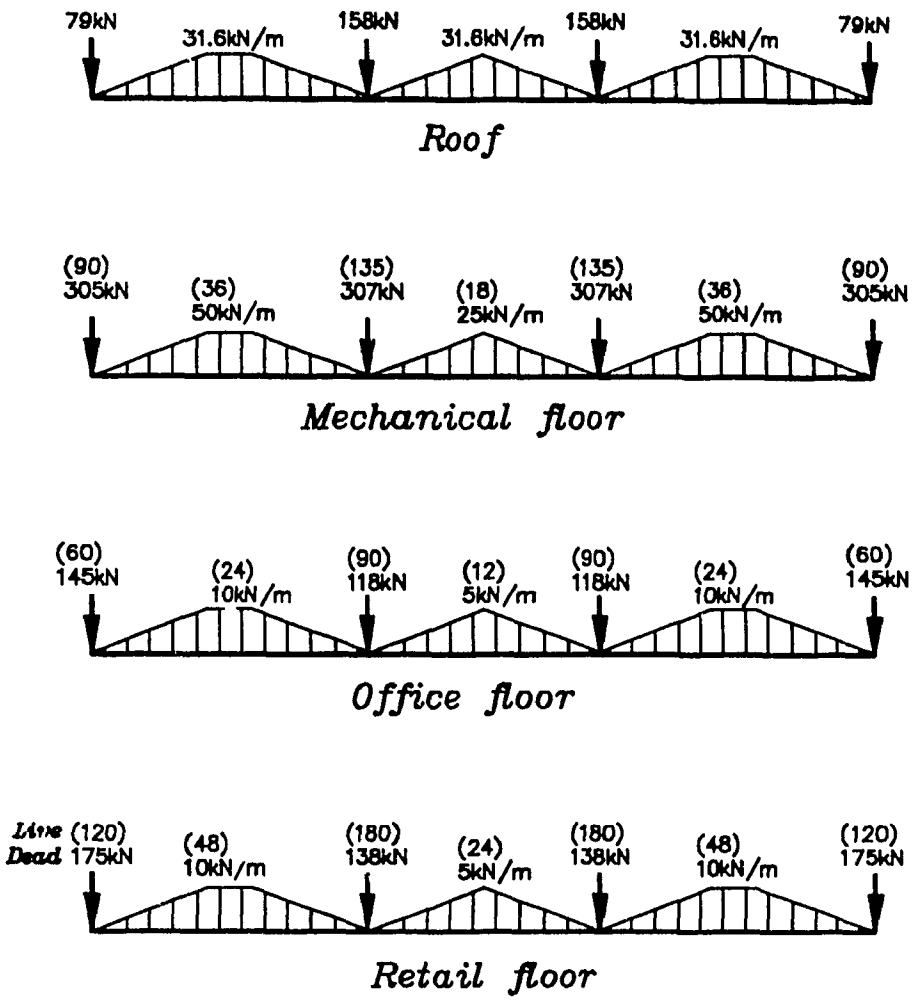

Fig.3.15 Dead and live loads

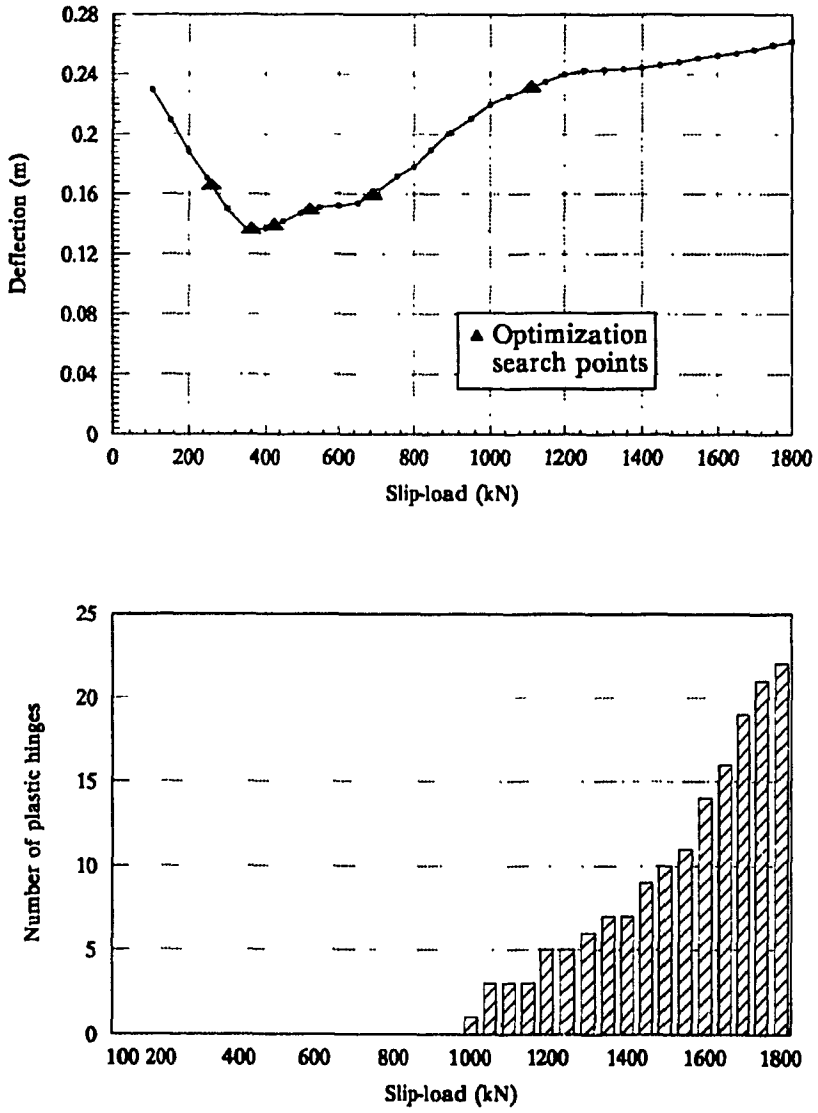

Fig.3.16 Dynamic responses of 20-storey steel frame El-Centro 0.18g

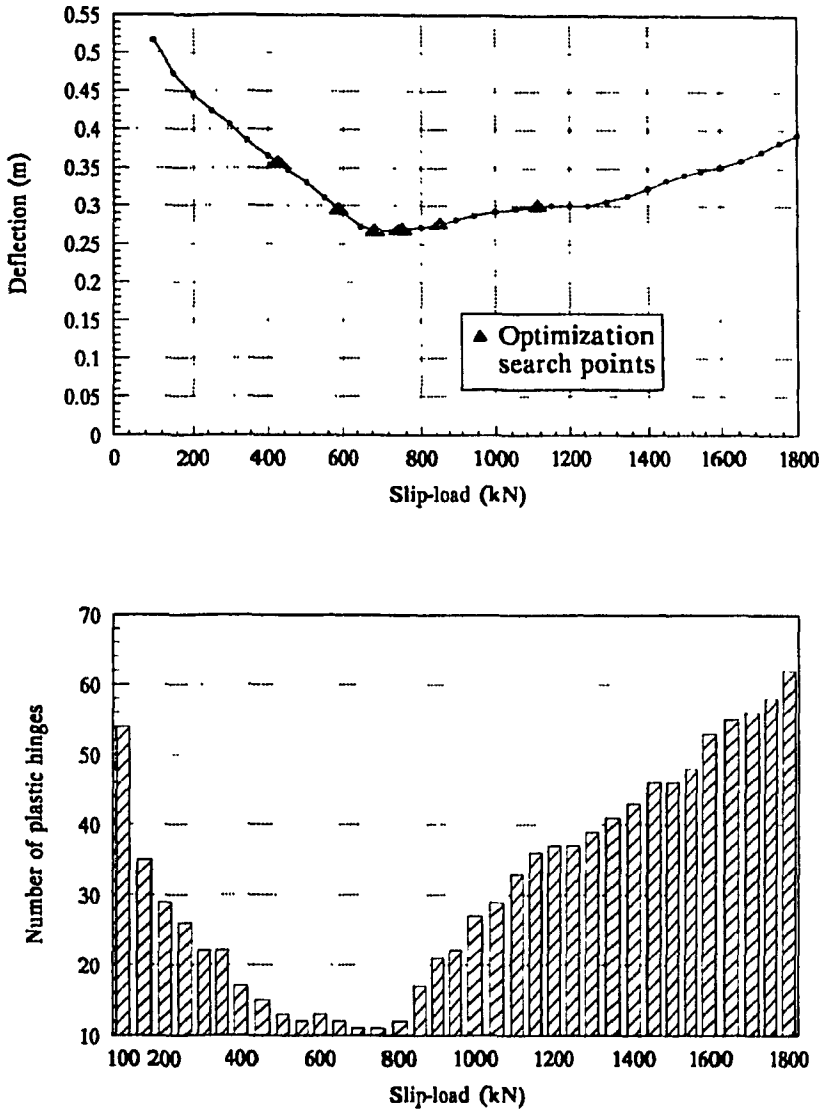

Fig.3.17 Dynamic responses of 20-storey steel frame El-Centro 0.36g

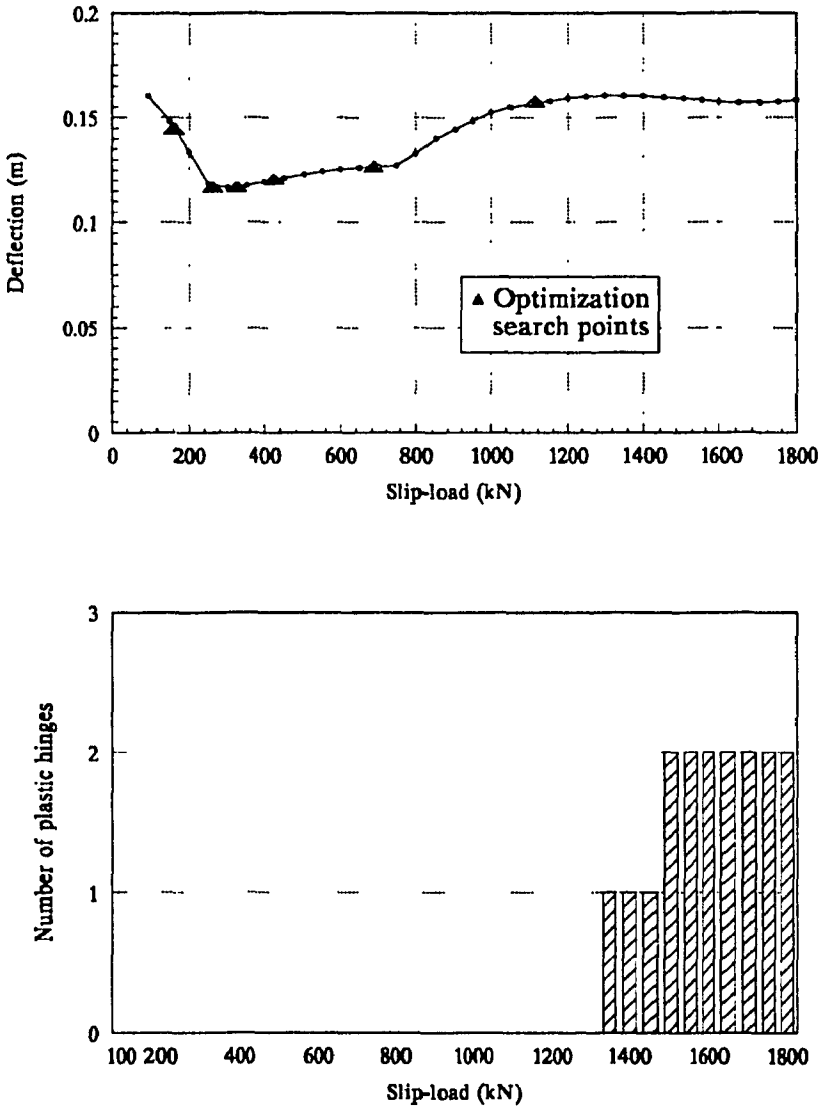

Fig.3.18 Dynamic responses of 20-storey steel frame Taft 0.18g

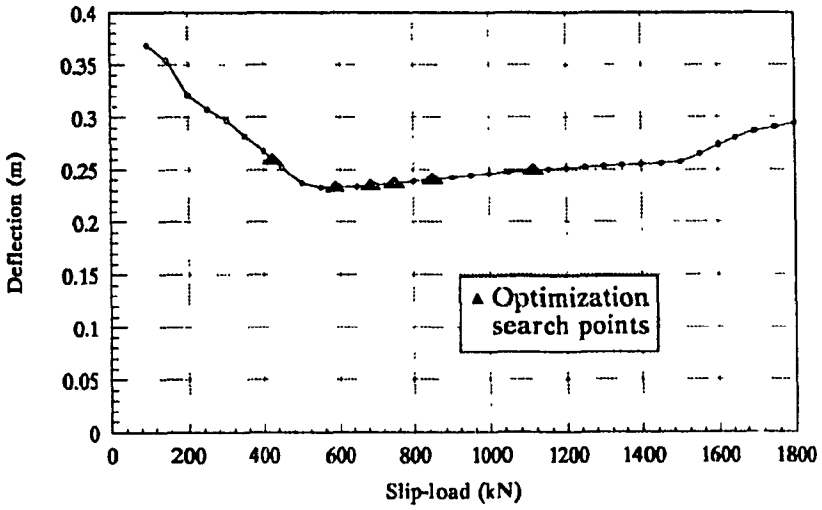

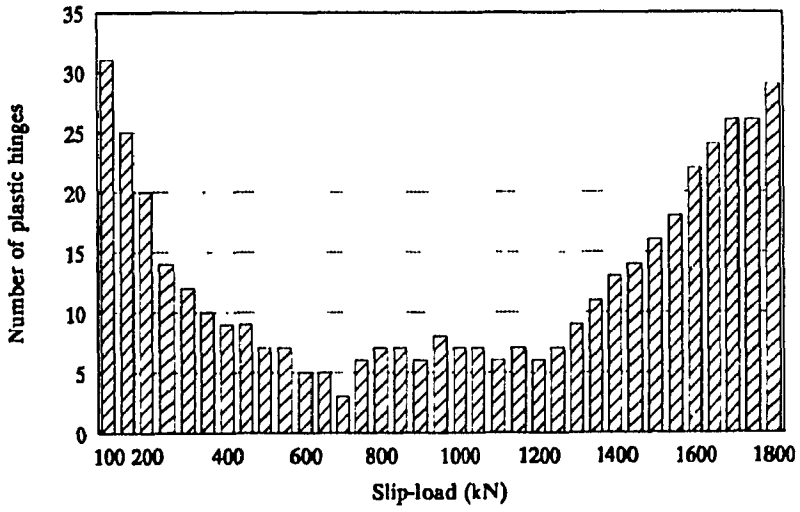

Fig.3.19 Dynamic responses of 20-storey steel frame Taft 0.36g

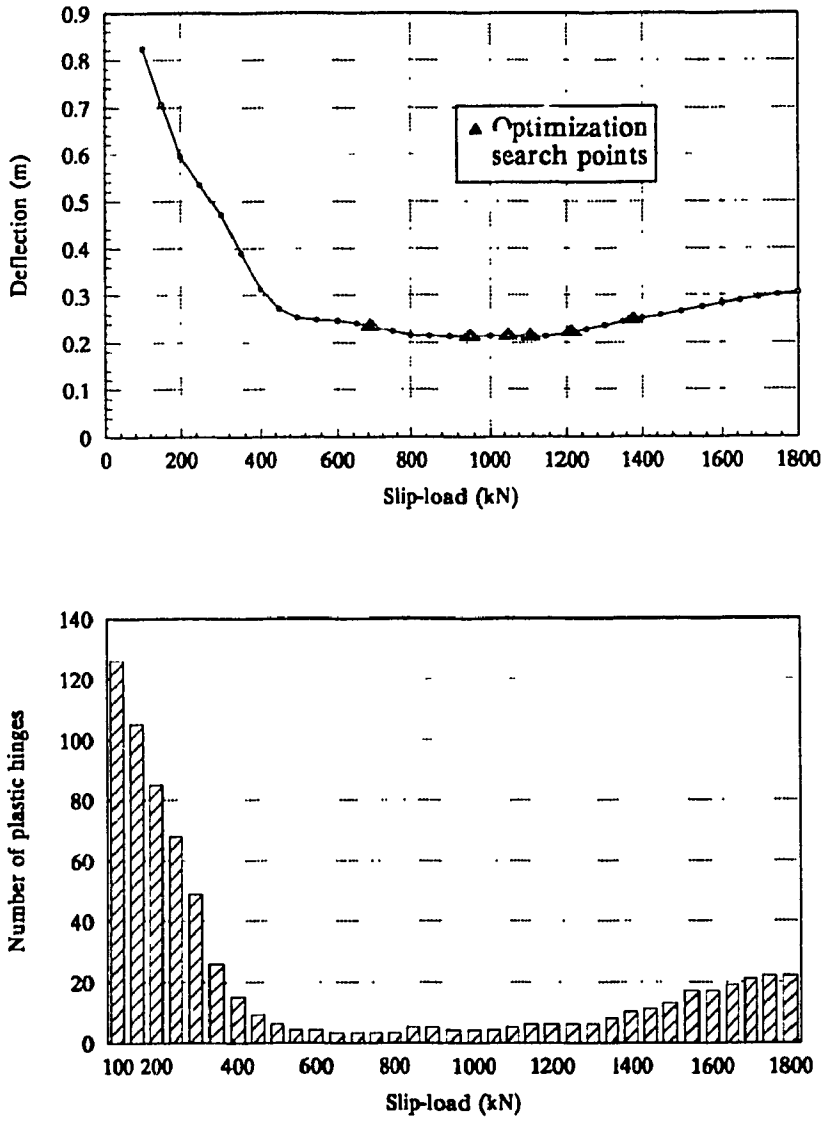

Fig.3.20 Dynamic responses of 20-storey steel frame NBK 0.18g

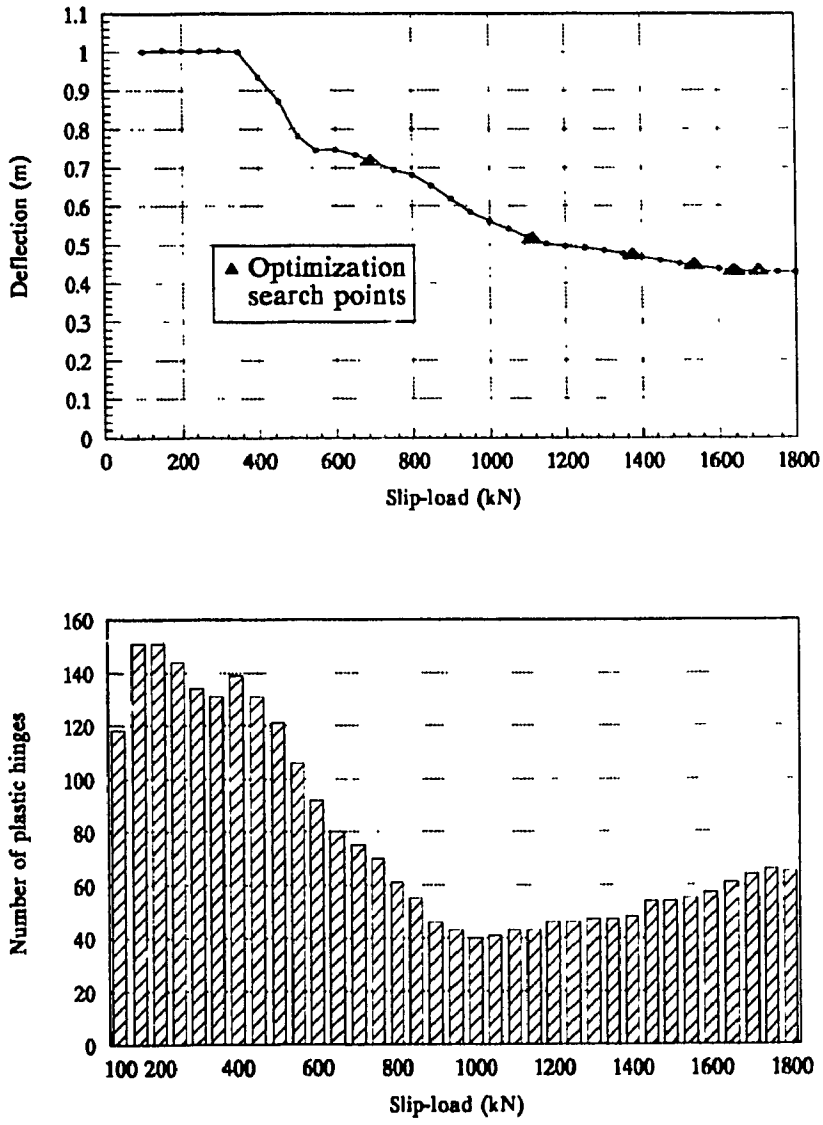

Fig.3.21 Dynamic responses of 20-storey steel frame NBK 0.36g

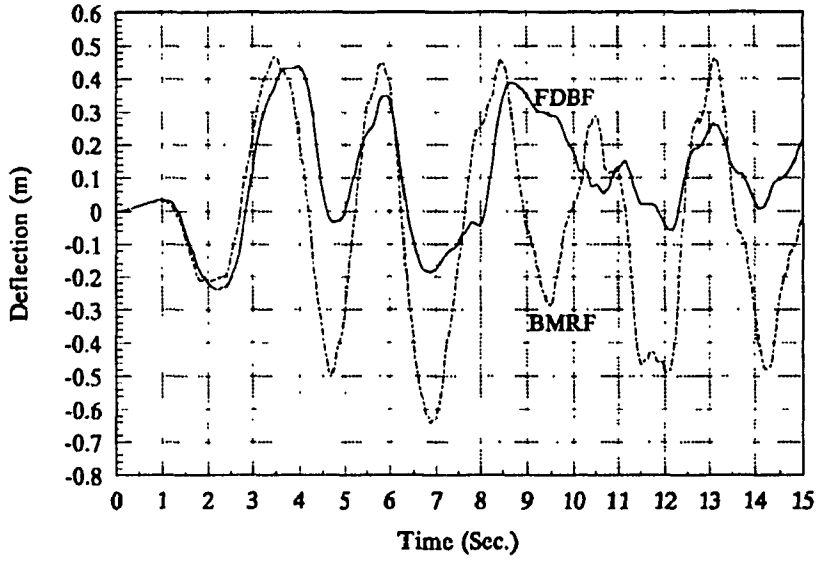

Fig.3.22 Time histories of deflection at the top of the frame NBK Earthquake (0.36g)

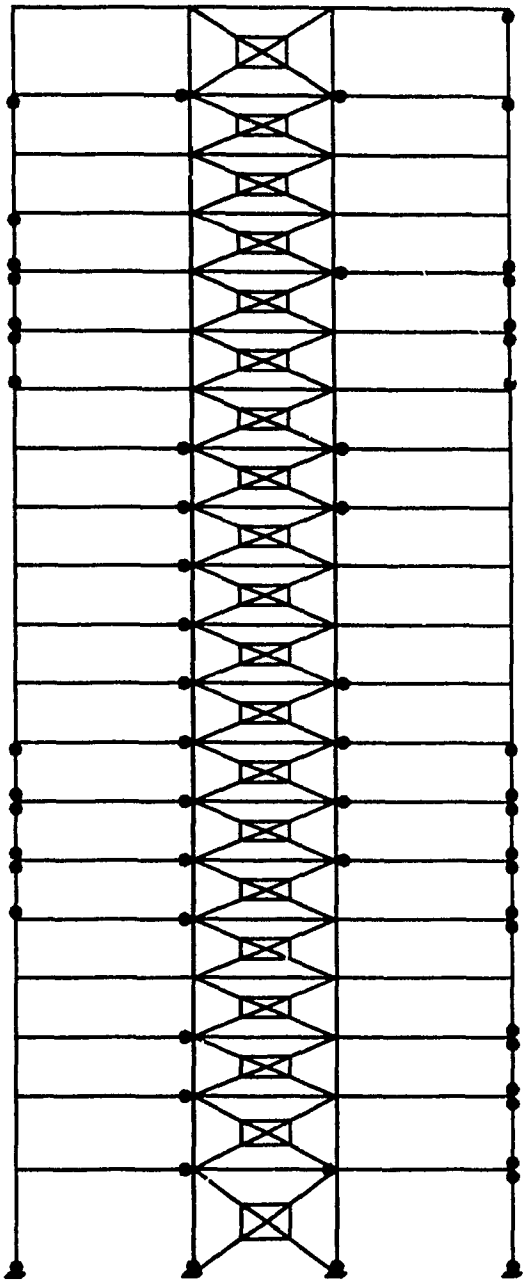

Fig.3.23 Plastic hinges in beams and columns experienced by FDBF (NBK 0.36g)

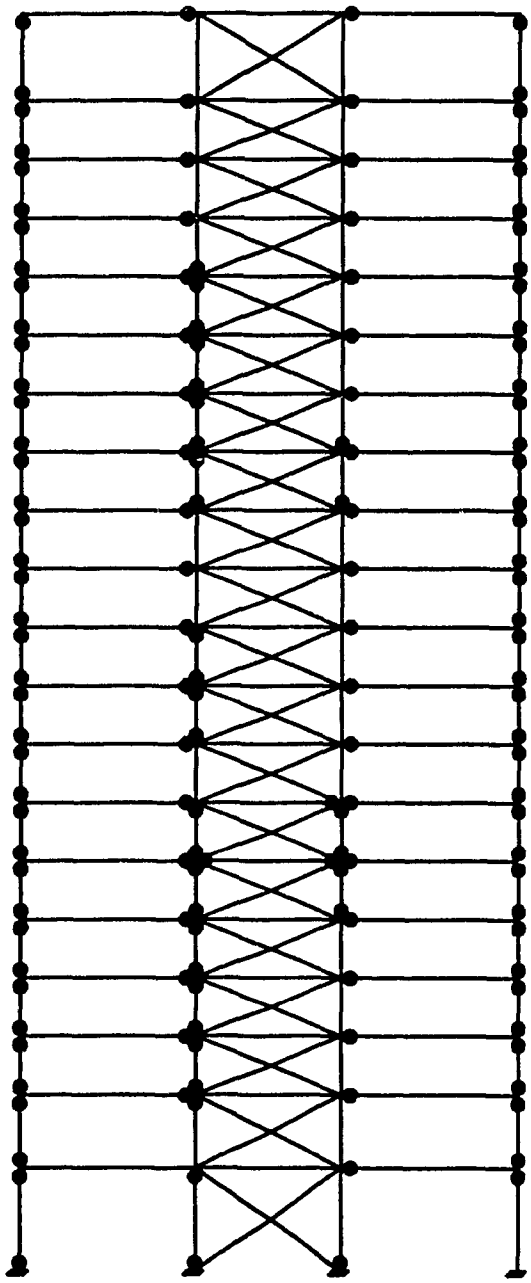

Fig.3.24 Plastic hinges in beams and columns experienced by BMRF (NBK 0.36g)

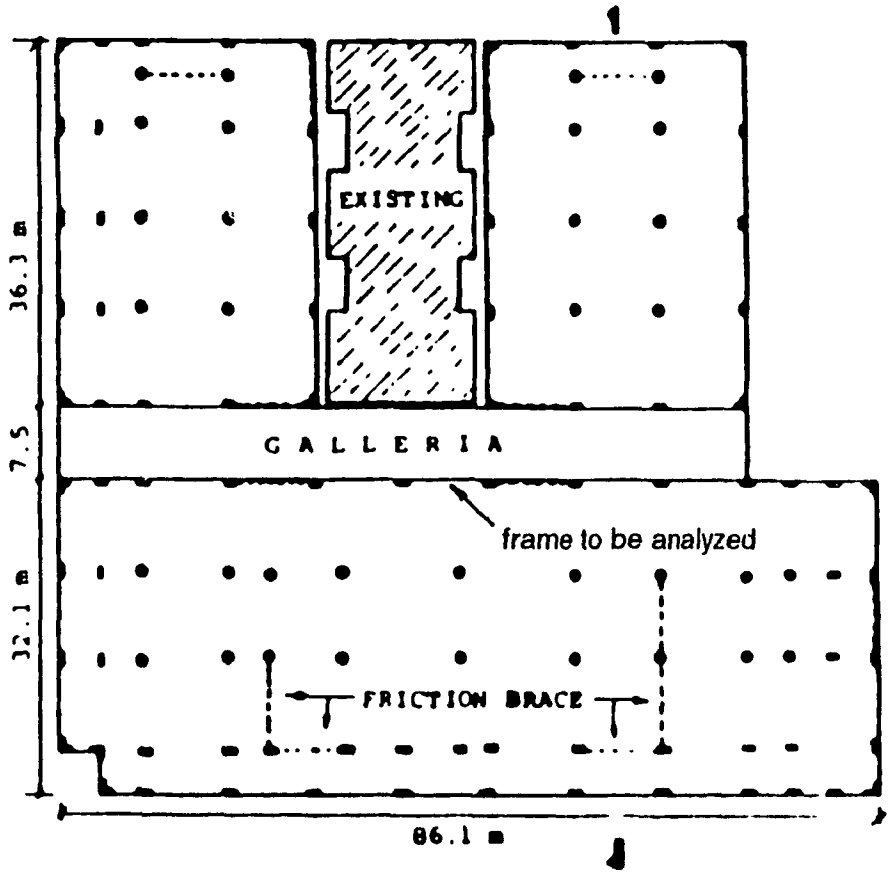

Fig.3.25 Ground floor plan of the library building[3]

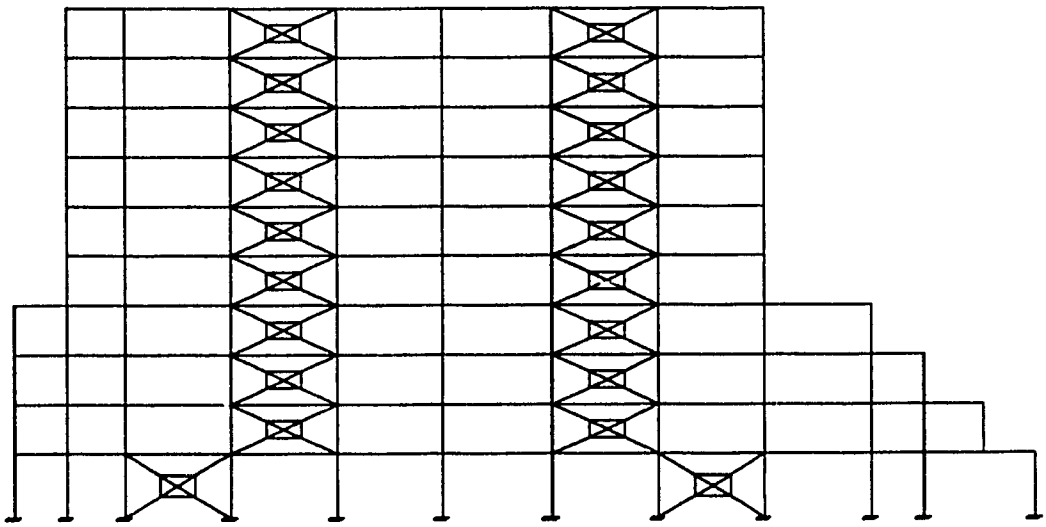

Fig.3.26 Elevation of the concrete frame equipped with friction dampers[3]

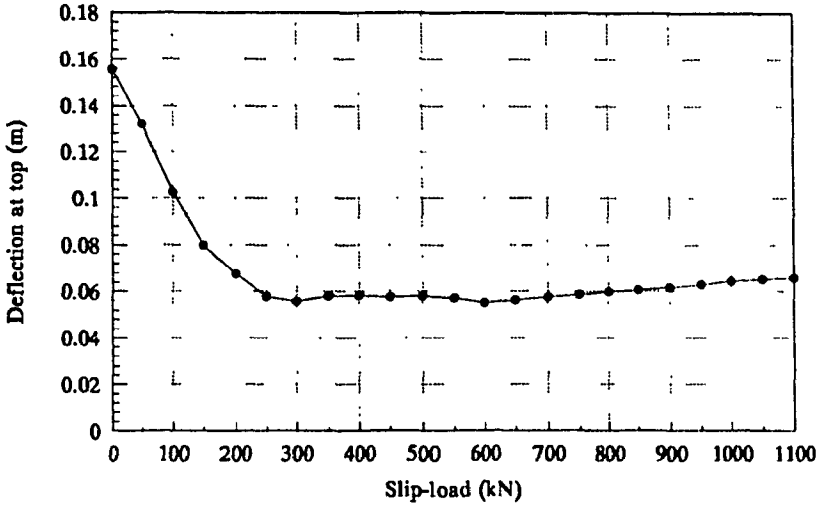

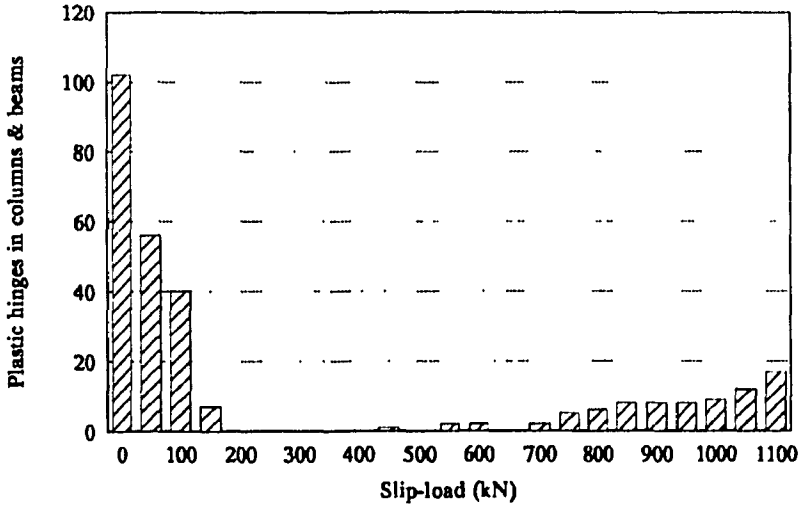

Fig.3.27 Dynamic responses of 10 storey concrete FDBF NBK 0.18g

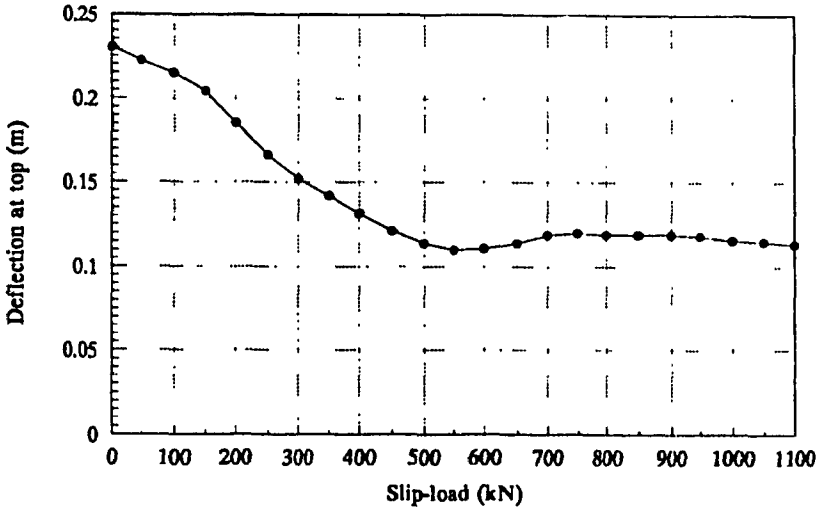

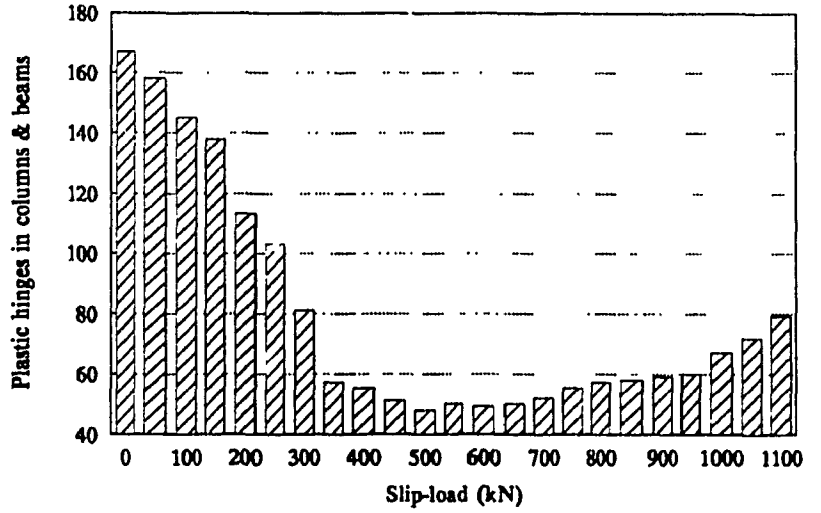

Fig.3.28 Dynamic responses of 10 storey concrete FDBF NBK 0.36g

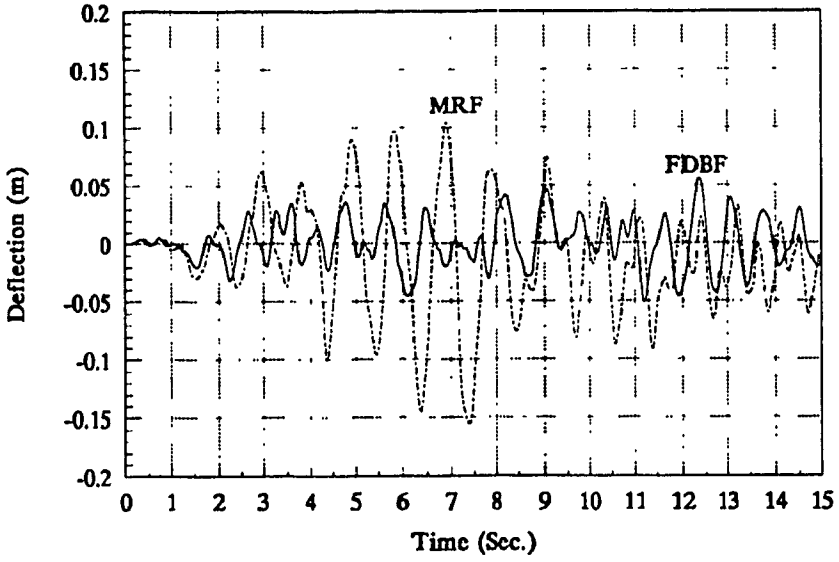

Fig.3.29 Time histories of deflection of the roof NBK Earthquake (0.18g)

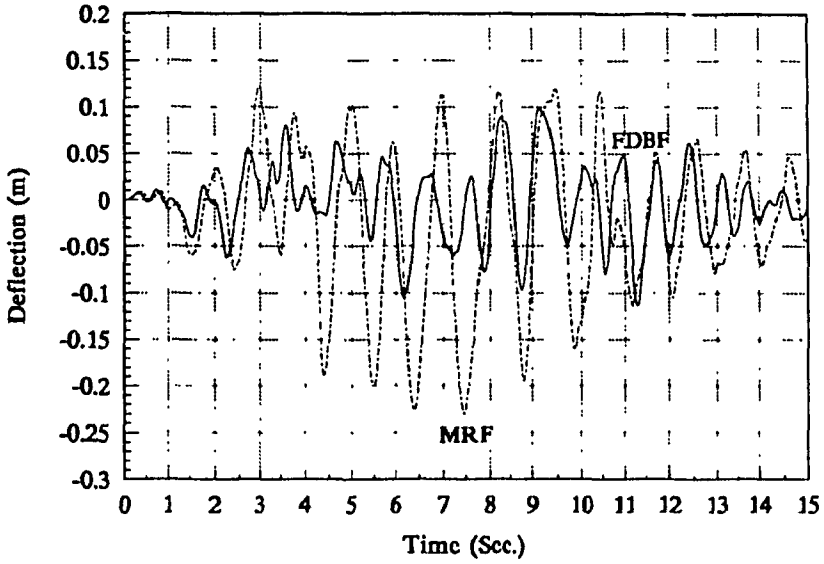

Fig.3.30 Time histories of deflection of the roof NBK Earthquake (0.36g)

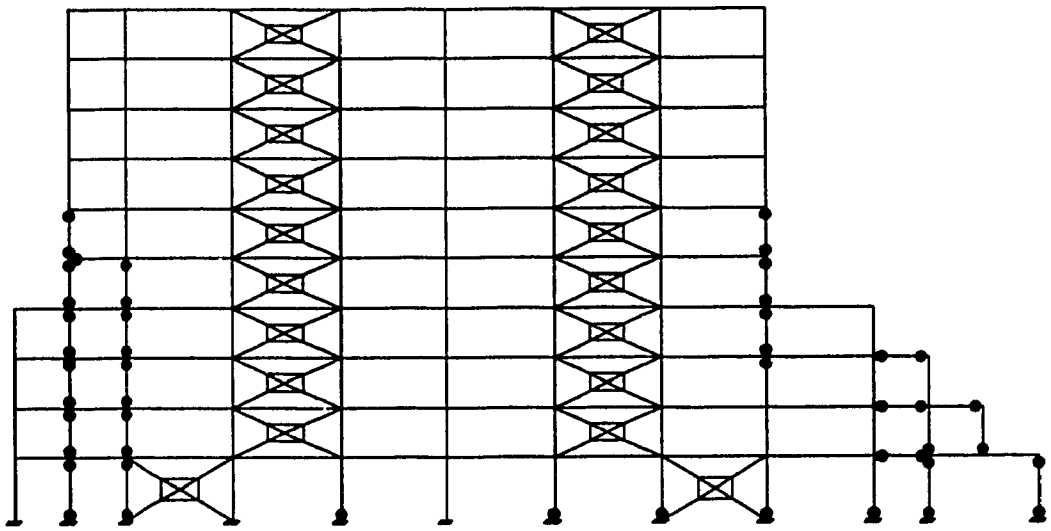

Fig.3.31 Plastic hinges in beams and columns experienced by FDBF (NBK 0.36g)

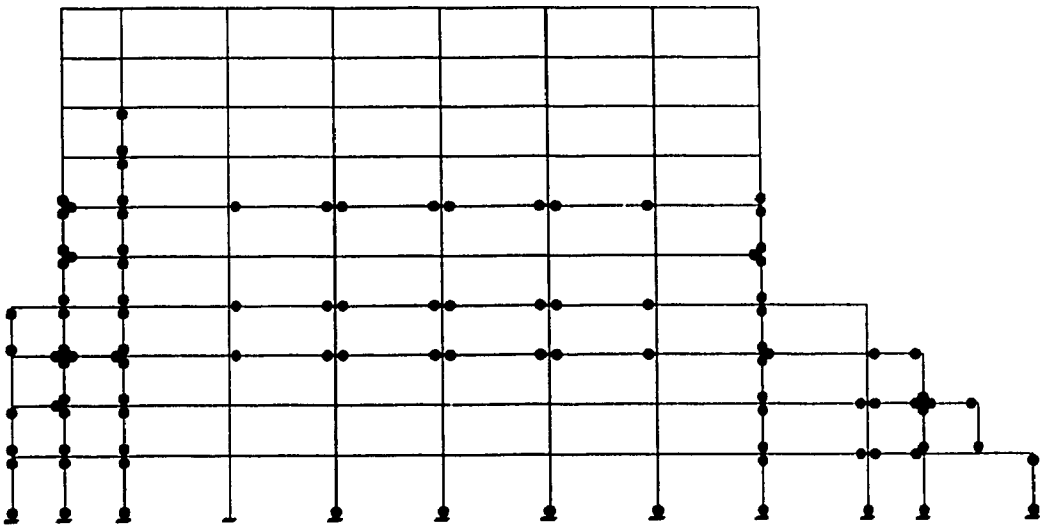

Fig.3.32 Plastic hinges in beams and columns experienced by MRF (NBK 0.36g)

Chapter 4 Soil-Structure interaction of friction damped braced frame-soil system

In all previous studies of the dynamic response of FDBF, it has been assumed that the earthquake excitations were introduced at the structural support points and that the foundation was rigid, and thus ignoring the soil condition and the effects of soil-structure interaction (SSI).

The importance of considering the site's soil condition is reflected in many modern building codes,[1],[23] which modify the lateral seismic design loads based on the knowledge of the soil condition. Since the traditional quasi-static method is inadequate for FDBF, non-linear analysis must be conducted and at the same time, the site soil condition may also be taken into account.

In this chapter, an approach for the dynamic analysis of FDBF-soil system is proposed, and the dynamic responses of the coupled FDBF-soil system are evaluated with some conclusions drawn for the design of FDBF.

4.1 General

Methods for analysis of soil-structure interaction have been published by a number of researchers. These methods can be divided into two categories: the

impedance function approach[24],[25],[26] and the complete method[27],[28],[29],[30]. The impedance approach was implemented in two steps: the half-space soil domain is analyzed first to establish the free-field motion impedance and the scattering properties at the soil-structure interface; and in the second step, these properties are used as boundary conditions in the dynamic analysis together with the loading calculated from the free-field motions.

The complete method means that the motions of the soil mass and structure are determined simultaneously. Complete methods are often implemented by using the finite element method. In recent years, hybrid methods such as BEM-FEM[31], FDM-FEM[32] have been proposed to deal with the soil-structure interaction problem.

The major advantage of complete methods over the impedance function methods is that the dynamic analysis is performed at the actual stress level for all soil elements and thus the soil's non-linear behaviour can be easily incorporated. The disadvantage of the complete methods is that more computer time is needed to perform the analysis.

As computers become more powerful and efficient while their use less costly, the complete method once considered too expensive and time consuming are becoming viable. It will be used to deal with the soil-structure interaction of FDBF system in this chapter. For this purpose, a new finite element and the free-field soil-structure interface earthquake input model are incorporated into the previously described computer program to model the soil medium for soil-structure

interaction analysis.

4.2 Isoparametric quadrilateral element for the soil medium

Since the DRAIN-2D program does not have an appropriate element to model the soil media, the isoparametric quadrilateral plane strain element shown in Fig.4.1 was added to the computer program. Its formulation follows the standard procedure and is briefly described below.

For an isoparametric finite element, the same interpolation functions are used for both the element geometry and displacements:

$$x-\sum_{i-1}^{4} h_i x_i$$
$$y-\sum_{i-1}^{4} h_i y_i$$

$$u-\sum_{i-1}^{4} h_i u_i$$
$$v-\sum_{i-1}^{4} h_i v_i$$

in which x_i, y_i are the coordinates of element's nodes. The interpolation functions h_i are defined in the natural coordinates of the element as:

$$h_1=(1+r)(1+s)/4$$

$$h_2=(1-r)(1+s)/4$$

$$h_3=(1-r)(1-s)/4 \qquad (4.3)$$

$$h_4=(1+r)(1-s)/4$$

where $-1 \le r,s \le 1$. The strain-displacement relations are:

$$\epsilon_{xx}=\frac{\partial u}{\partial x},\ \epsilon_{yy}=\frac{\partial v}{\partial y},\ \gamma_{xy}=\frac{\partial v}{\partial x}+\frac{\partial u}{\partial y} \qquad (4.4)$$

By using the chain rule, the derivatives with respect to the natural coordinates can be written as:

$$\begin{bmatrix} \frac{\partial}{\partial r} \\ \frac{\partial}{\partial s} \end{bmatrix} = \begin{bmatrix} \frac{\partial x}{\partial r} & \frac{\partial y}{\partial r} \\ \frac{\partial x}{\partial s} & \frac{\partial y}{\partial s} \end{bmatrix} \begin{bmatrix} \frac{\partial}{\partial x} \\ \frac{\partial}{\partial y} \end{bmatrix}$$

or

$$\frac{\partial}{\partial \boldsymbol{r}}=\boldsymbol{J}\frac{\partial}{\partial \boldsymbol{x}} \qquad (4.5)$$

where **J** is the Jacobian matrix of the coordinate transformation specified by Eq.4.1. Thus,

$$\frac{\partial}{\partial \boldsymbol{x}}=\boldsymbol{J}^{-1}\frac{\partial}{\partial \boldsymbol{r}} \qquad (4.6)$$

Using (4.1) to (4.6) we can express the strain at any point in the element in terms of the nodal displacements as:

$$\epsilon = Bu$$

where $\epsilon^T=\{\ \varepsilon_{xx},\ \varepsilon_{yy},\ \gamma_{xy}\ \}$, $\mathbf{u}^T=\{u_1,v_1,u_2,v_2,u_3,v_3,u_4,v_4\}$ and **B** is the strain-displacement transformation matrix. For any point (r_i,s_i) in the element:

$$B_{ij}=\frac{1}{4}J_{ij}^{-1}\begin{bmatrix} 1+s_j & 0 & -(1+s_j) & 0 & -(1-s_j) & 0 & 1-s_j & 0 \\ 0 & 1+r_i & 0 & 1-r_i & 0 & -(1-r_i) & 0 & -(1+r_i) \\ 1+r_i & 1+s_j & 1-r_i & -(1+s_j) & -(1-r_i) & -(1-s_j) & -(1+r_i) & 1-s_j \end{bmatrix}$$

The element stiffness matrix is then:

$$K=\int_V B^T CB dv=\int_{-1}^{1}\int_{-1}^{1} B^T CB(detJ)\,dr\,ds \qquad (4.7)$$

where t is the thickness of the element, det**J** is the determinant of the Jacobian matrix, **C** is the stress-strain matrix for plane strain condition:

$$C=\frac{E(1-\nu)}{(1+\nu)(1-2\nu)}\begin{bmatrix} 1 & \frac{\nu}{1-\nu} & 0 \\ \frac{\nu}{1-\nu} & 1 & 0 \\ 0 & 0 & \frac{1-2\nu}{2(1-\nu)} \end{bmatrix}$$

It is assumed for simplicity that the entire soil mass behaves linear-elastically throughout the loading history.

To evaluate the integral in (4.7), the two-point Gauss quadrature is used, and the stiffness matrix of the element is therefore

$$K=\sum_{i=1}^{2}\sum_{j=1}^{2}\alpha_i\alpha_j B_{ij}^{T}CB_{ij}\det J_{ij} \tag{4.8}$$

in which α_i,α_j are the weighting factors at the Gauss sampling points.

4.3 Models for earthquake input mechanism

To analyze the coupled soil-structure system, there are three alternative models for the earthquake input mechanism. These are the rigid-base input model, the massless-soil input model and the free-field soil-structure interface input model.

4.3.1 Rigid-base input model with soil mass(Model I)

In this model, the specified free-field earthquake excitation is directly applied

at the rigid-rock-base. The masses of soil are concentrated at the nodes. As illustrated in Fig.4.2, the upward propagation of earthquake motions is from the basement rock through the soil to the soil-structure interface. The equation of dynamic equilibrium of this model is:

$$[M]\{\ddot{U}\}+[C]\{\dot{U}\}+[K]\{U\}=-[M]\ddot{v}_g(t) \tag{4.9}$$

in which [M],[C] and [K] are, respectively, the mass, damping and stiffness matrices for the complete soil-structure system; {U}, {$\dot{U}$}, {$\ddot{U}$} are, respectively, the nodal displacement, velocity and acceleration vectors relative to the rigid-base, and $\ddot{v}_g(t)$ is the specified base earthquake acceleration time histories.

If the earthquake motions in the basement rock underlying the soil layer are known, the rigid-base input model is the most efficient and simplest approach. However, in most cases, only the free-field motions are known, and normally the free-field motions are directly applied at the base rock.

Using the free-field records as the rigid-base motion is relatively simple, because no modification need be made to the specified time history of the accelerograms, and the matrices [M],[C] and [K] of the complete soil-structure system can be used directly. However, this simplification is not expected to give very accurate results since the earthquake waves will propagate through the soil to reach the ground surface, and the recorded excitations at the surface are usually different from the base rock motions. An examples of this is the

acceleration records from the SCT (Secretaria de Communicacions y Transportes) site in downtown Mexico City where the maximum acceleration amplitudes are from three to five times larger than the maximum accelerations recorded at nearby rock sites during the September 19, 1985 earthquake.[33],[34]

4.3.2 Rigid-base input model without soil mass(Model II)

In this model, the governing equation is similar to Eq.(4.9), but the difference is that the soil is assumed to be massless. However, the use of finite element model for the soil as opposed to the use of impedance and scattering coefficients retains the possibility of considering the non-linear soil behaviour and avoids the need to establish the impedance and scattering properties in terms of springs and dashpots.

For the massless soil rigid-base input model, the earthquake excitations are transmitted instantaneously through the soil media to the supports of the building. As it can be seen later from the results, by using massless soil, the wave propagation in the soil media is not considered, and thus the potential problem of inadequate artificial amplification of the free-field motions is eliminated. Consequently, it appears more reasonable to apply the free-field surface motions as earthquake input at the rigid-base of the complete system.

4.3.3 Free-field interface input model(Model III)

As most of the earthquake excitations were recorded at the ground surface,

the free-field soil-structure interface input model as shown in Fig.4.3 could be considered as an appropriate earthquake input mechanism.

The free-field soil-structure interface input model is implemented by expressing the effective earthquake loading in the dynamic equilibrium equation of the soil-structure system directly in terms of the free-field motions recorded at the ground surface.

As shown in Fig.4.3, the degrees of freedom of the soil mass and the superstructure are respectively designated by the vectors $\{U_f\}$ and $\{U_s\}$, and those at the interface between the soil and the superstructure by $\{U_i\}$. The equation of dynamic equilibrium of free-field soil-structure interface input model is then[35]

$$[M]\{\ddot{U}\}+[C]\{\dot{U}\}+[K]\{U\} = -\left\{[M][r]+\begin{bmatrix} m_{fs} \\ m_{ff} \\ 0 \end{bmatrix}\right\}\ddot{U}_f \qquad (4.10)$$

where, [M], [C], [K] are the usual system matrices of the complete system. Matrix $[m_{fs}]$ represents the soil-structure mass coupling terms and $[m_{ii}]$ is the mass which corresponds to the frame-soil interface degrees of freedom. Matrix [r] is the influence coefficient matrix expressing the nodal displacements of the complete system due to unit displacements applied at the base of the superstructure. {U} is the vector of displacements relative to the free-field motion. $\{U_f\}$ is free-field motion at the interface between soil and superstructure. In practice, all the supports of building are assumed to be subjected to the same earthquake excitations as

shown in Fig.4.4. The influence-coefficient matrix [r] may be established by solving the static equilibrium equation of the soil-structure system subjected to unit prescribed displacements at the interface nodes.

As the mass of the foundation soil is taken into account in the time-step dynamic analysis and the earthquake record excludes artificial amplification, the use of free-field interface input model to represent the soil-structure interaction could give more reasonable and realistic results.

4.4 Analysis of FDBF-soil system

In this section, the dynamic responses of friction damped braced frame-soil system under different earthquake input mechanisms will be evaluated, and conclusions will be drawn for the design of FDBF when the soil condition and the soil-structure interaction need be considered.

4.4.1 Problem description

Fig.4.5 shows the FDBF-soil system which will be analyzed by using three different earthquake input mechanisms. The dimensions, member size, and other properties of the moment resisting frame are as shown in Fig.2.2. The yield strength of the structural steel used for the beam and column elements is 300MPa. The Young's modulus of steel is 2×10^5MPa. The soil layer is represented by an assemblage of four-node linear isoparametric elements with a total of 600 degrees of freedom. Three different soil conditions representing the hard, medium and soft

soil conditions are chosen and listed in table 4.1. As this study is focused on the influence of soil conditions and soil-structure interaction on the superstructure, the dynamic response quantities of interest are the deflection of the top floor and the plastic hinges in beams and columns.

Table 4.1 Soil Parameters[36]

Case	Soil modulus	Condition	Poisson ratio	Mass density
1	0.047GPa	soft	0.49	1700kg/m^3
2	1.56GPa	medium	0.35	2050kg/m^3
3	31.87GPa	hard	0.30	2650kg/m^3

4.4.2 Comparative performance of friction damped braced frames versus moment resisting frames

Previous studies[2],[7] showing the superior performance of FDBF when compared with moment resistant frame(MRF) were carried out using rigid supports earthquake input model. The MRF-soil system is created by removing the friction devices and braces off the super-structure of Fig.4.5. EL-Centro earthquake(NS 0-12 Sec.) was used with the peak ground acceleration at 0.2g. Both FDBF-soil system and MRF-soil system are analyzed by using three different earthquake input models.

The numerical results are listed in table 4.2. It is seen that for all the different earthquake input models and soil cases, the FDBF's performance is

superior to the MRF. Taking the medium soil case (case 2) as an example, the deflection envelopes of the FDBF and the MRF corresponding to the different earthquake input models are shown in Fig.4.6. The deflection of the FDBF is about 28% of MRF for earthquake input model I, and 38%, 34% for model II and model III, respectively.

The permanent damage in terms of plastic hinges in columns and beams experienced by FDBF and MRF is shown in Fig.4.7. The percentage of members that have yielded are shown in table 4.2 in parentheses.

4.4.3 Soil-structure interaction on FDBF

To evaluate the influence of the soil condition and the soil-structure interaction on the friction damped braced frame during earthquake excitations, the FDBF-soil system as shown in Fig.4.5 was analyzed for three soil conditions, and each with three earthquake input models. For the purpose of comparison, analyses were also performed assuming rigid supports. The earthquakes used are 1940 EL-Centro(NS 0-12 Sec.) and Newmark-Blume-Kapur Artificial Earthquake(0-15 Sec.), which were both scaled to 0.2g and 0.4g, respectively. The numerical results of the FDBF-soil system for the different earthquake input models and different soil cases are presented in table 4.3. It is seen that by considering the soil media and SSI, the responses have significantly increased as soil become soft for all three input models, and it is also noted that when the soil becomes hard, the dynamic responses of all three models come closer to the rigid support model.

Model I is seen to induce significant artificial amplification in the flexible soil cases, where the deflection may grow excessively large.

The responses from model II are likely more reasonable than those in model I, but the idealized massless soil does not adequately model the soil-structure interaction under dynamic excitation. From the results of table 4.3, it seems that the characteristics of the FDBF-soil coupled system was not captured by using this model, and the numerical results indicate that the massless model underestimates the dynamic responses in comparison to models I and III as the soil becomes soft.

The free-field interface input model (model III), appears to give more reasonable and realistic results, where the influence of the soil and the soil-structure interaction are reflected. The effects of soil-structure interaction increases the dynamic responses as the soil becomes soft. Comparing this model with the rigid base model, the latter underestimates the dynamic responses of the FDBF especially in relatively soft soil condition.

4.4.4 Influences of soil condition and soil-structure interaction on optimum slip-load

Fig.4.8-Fig.4.11 show the results of the massless model of FDBF-soil system for the three soil conditions and rigid supports. Fig.4.12-Fig.4.15 show the results of the free-field interface input model of FDBF-soil system for the three soil conditions and rigid supports. They are plotted for slip-loads varying from 0 to 1100kN, covering the entire spectrum of behaviour starting with the MRF and

ending with the fully braced frame.

From Fig.4.8 to Fig.4.11, it can be seen that, for the massless model, although the dynamic responses increase as the soil becomes soft, the optimum slip-load corresponding to the minimum deflection and minimum damage does not change significantly as compared to the rigid support model. In other words, if the soil media is treated as a spring, where the waves propagate and the SSI is excluded, then the optimum slip-load appears little affected by the flexibility of the soil.

With respect to the free-field interface input model,(Fig.4.12 to Fig.4.15) the optimum slip-load has greater variation in softer soil. For example, from Fig.4.13, by minimizing both displacement and damages, the optimum slip-load for the soil case 1 should be around 450kN, while the optimum slip-load for soil case 2 and 3 should be around 1000kN. For hard and medium soil, the optimum slip-load is similar to the rigid support model.

4.5 Summary

This chapter focused on the dynamic responses of friction damped braced frame by considering the soil condition and soil-structure interaction. Three different earthquake input mechanisms were applied to the FDBF-soil system. These are the rigid-base input model, the massless soil input model and the free-field soil-structure interface input model. The results derived from the application of the three earthquake input mechanisms to the friction-damped-braced-frame-soil

system have shown that the flexibility of soil and the SSI could have a significant influence on the dynamic response of FDBF during earthquake events.

Table 4.2 Results for FDBF-soil and MRF-soil system (El-Centro 0.2g)

Model Type	Soil Type	FDBF-soil system			MRF-soil system		
		Max. displ. at top(m)	Yielded column	Yielded beam	Max. dis. at top(m)	Yielded column	Yielded beam
I	1	0.607	28 (70%)	28 (93%)	9.086	39 (97%)	30 (100%)
	2	0.099	2 (5%)	19 (63%)	0.357	27 (67%)	30 (100%)
	3	0.089	1 (2%)	14 (46%)	0.254	3 (7%)	30 (100%)
II	1	0.113	1 (2%)	14 (46%)	0.276	2 (5%)	30 (100%)
	2	0.096	0	16 (53%)	0.253	2 (5%)	30 (100%)
	3	0.088	1 (2%)	15 (50%)	0.253	2 (5%)	30 (100%)
III	1	0.189	1 (2%)	28 (93%)	0.363	5 (12%)	30 (100%)
	2	0.092	1 (2%)	18 (60%)	0.263	7 (17%)	30 (100%)
	3	0.088	1 (2%)	14 (46%)	0.253	2 (5%)	30 (100%)
Rigid base		0.088	1 (2%)	15 (50%)	0.251	2 (5%)	30 (100%)

Table 4.3 Dynamic responses of FDBF-soil system

Mode Type	Soil Type	El-Centro 0.2g		NBK 0.2g		El-Centro 0.4g		NBK 0.4g	
		Max. displ. at top (m)	Number of plastic hinges	Max. displ. at top (m)	Number of plastic hinges	Max. displ. at top (m)	Number of plastic hinges	Displ. at top (m)	Number of plastic hinges
Model I	Soft	0.607	104	10.066	140	10.267	131	10.556	138
	Medium	0.099	39	0.353	87	0.209	62	10.223	140
	Hard	0.089	28	0.114	34	0.182	50	0.214	61
Model II	Soft	0.113	27	0.136	40	0.202	49	0.242	62
	Medium	0.096	25	0.113	35	0.185	51	0.215	62
	Hard	0.088	29	0.114	35	0.183	51	0.216	59
Model III	Soft	0.189	55	0.273	57	0.488	77	0.537	81
	Medium	0.092	33	0.113	49	0.203	55	0.268	83
	Hard	0.088	28	0.114	34	0.183	51	0.214	59
Rigid support		0.088	29	0.114	35	0.187	50	0.214	59

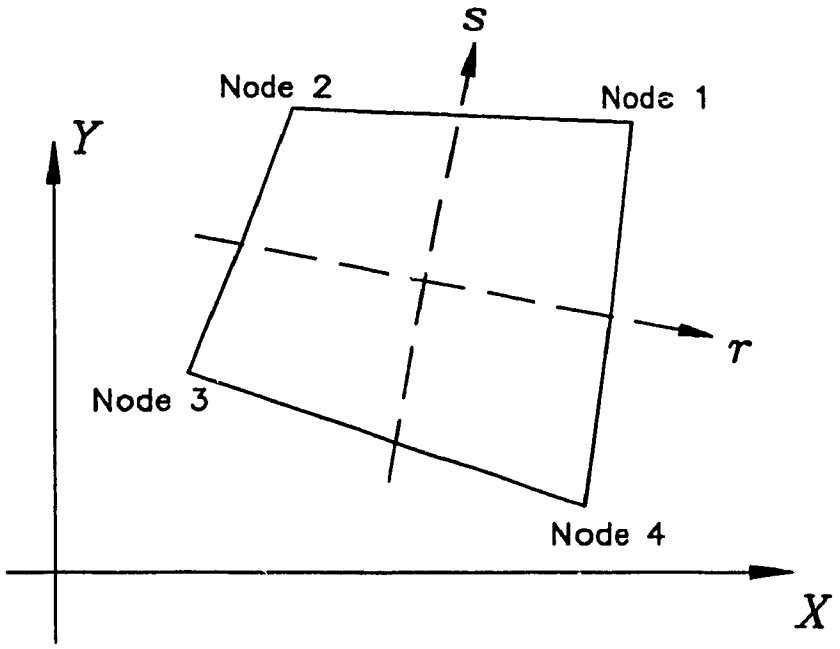

Fig.4.1 Isoparametric quadrilateral element

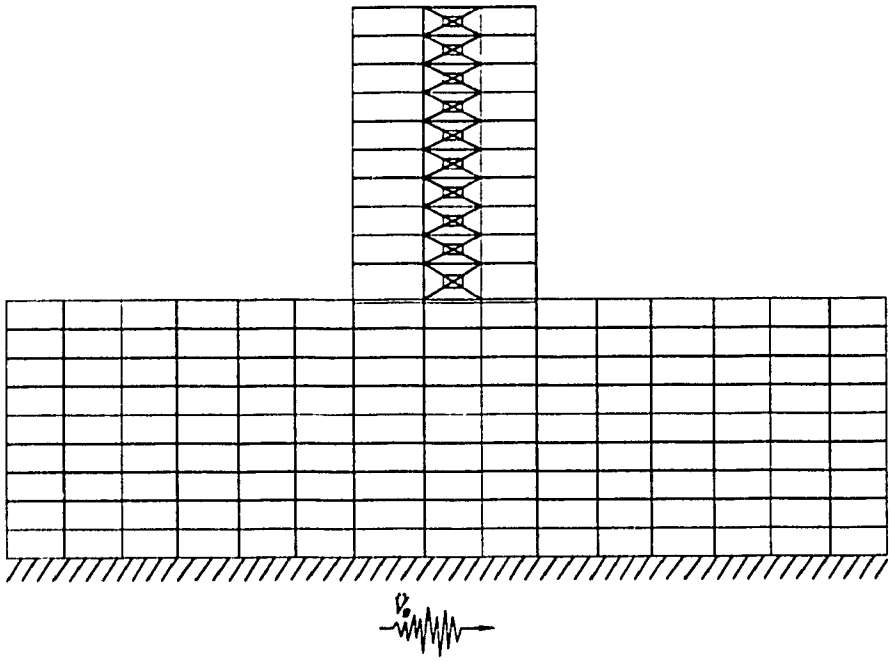

Fig.4.2 Rigid base earthquake input model

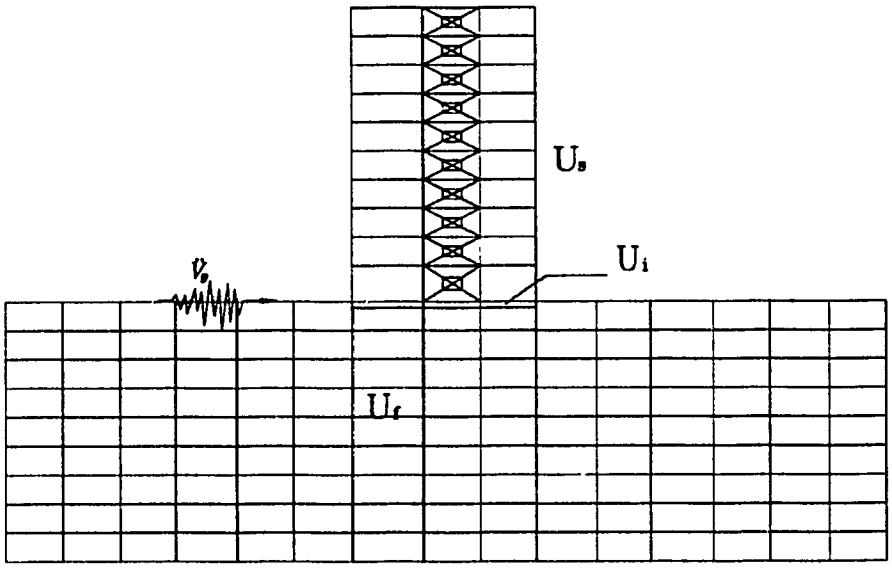

Fig.4.3 Free-field interface earthquake input model

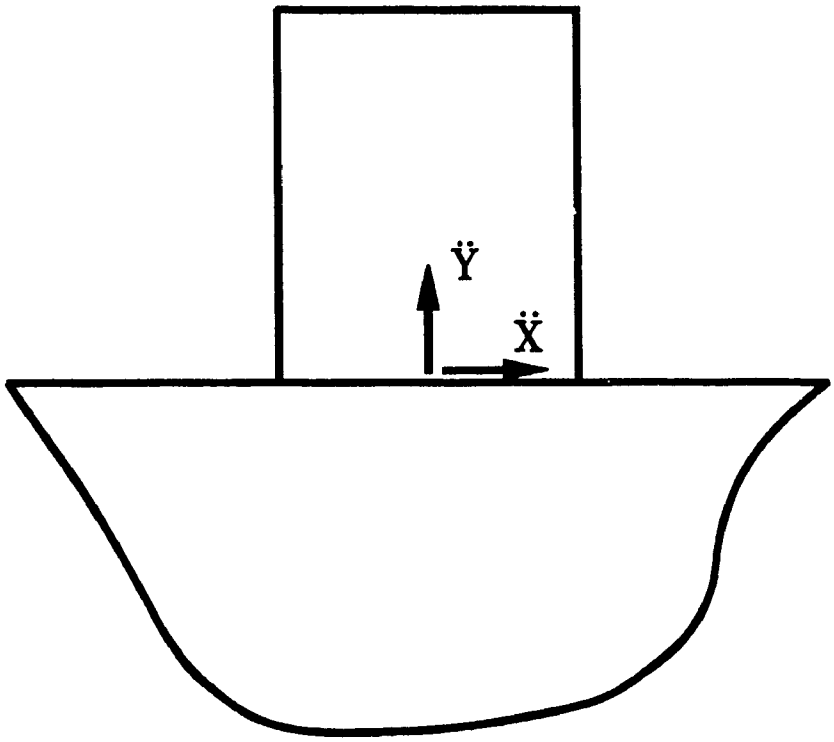

Fig.4.4 Earthquake excitation at the interface

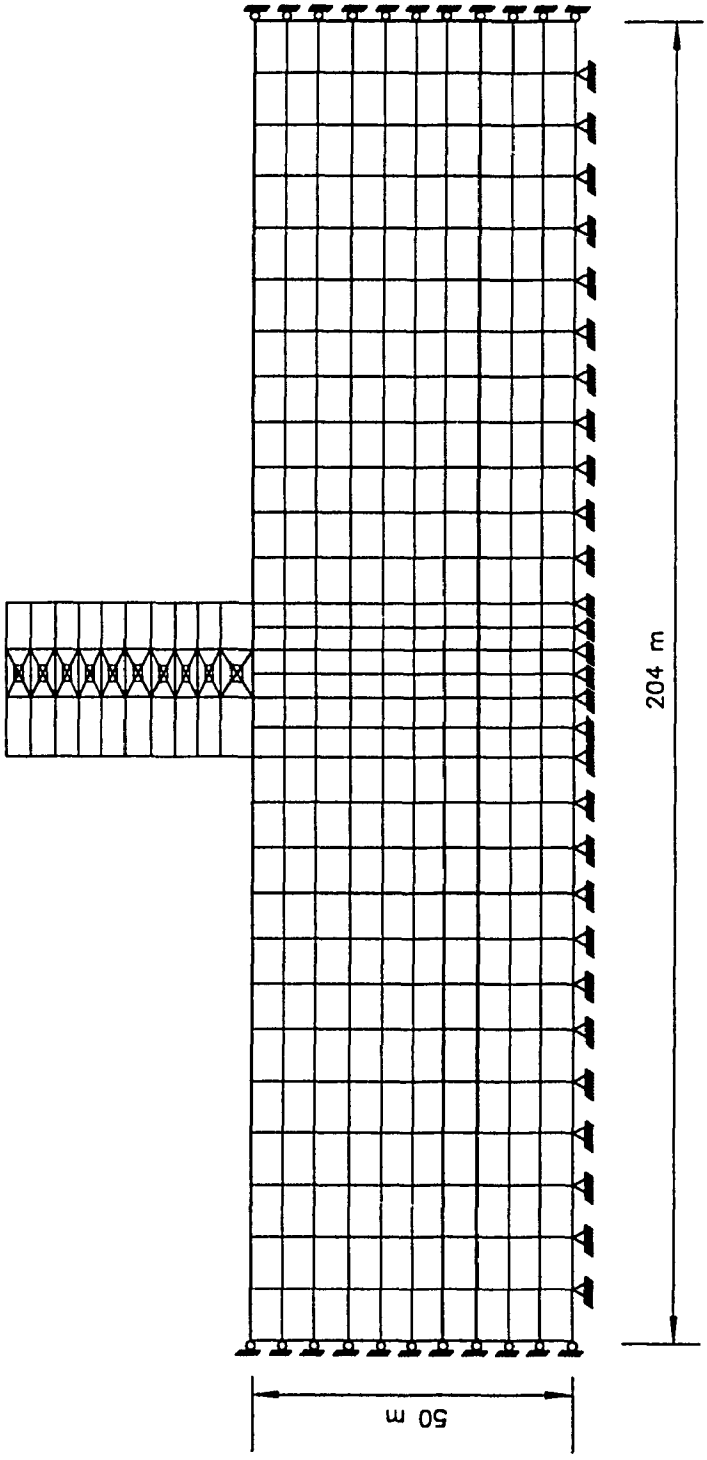

Fig.4.5 FDBF-soil coupled system for finite element analysis

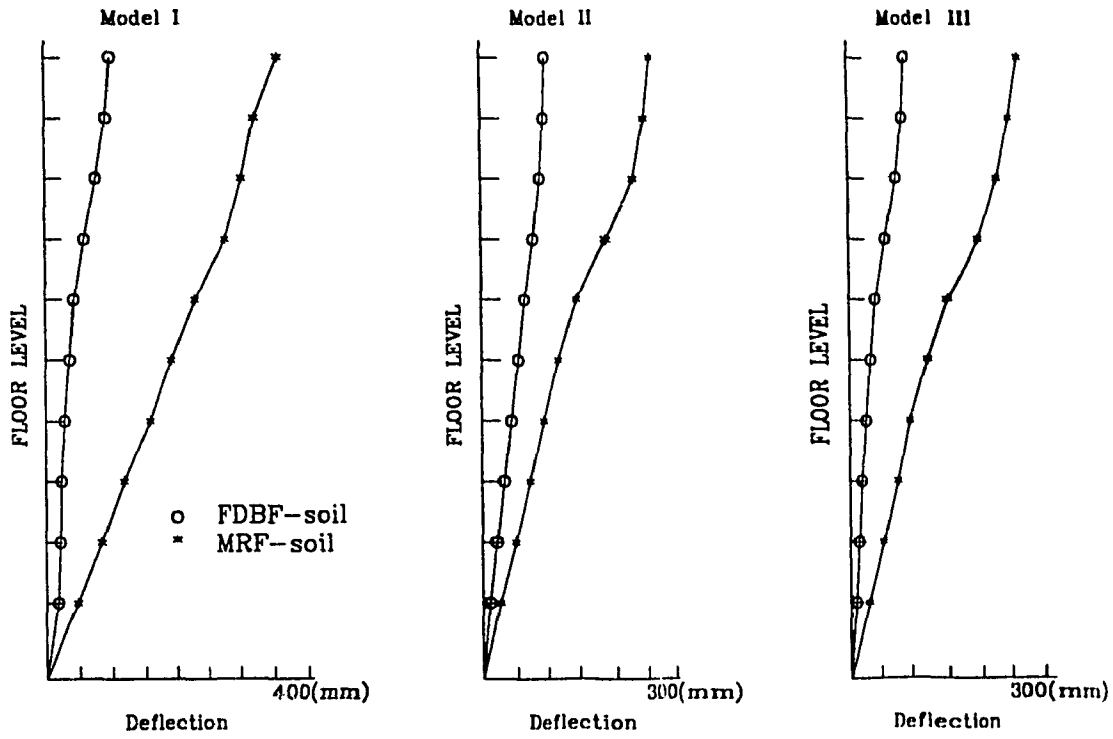

Fig.4.6 Deflection envelopes of superstructure

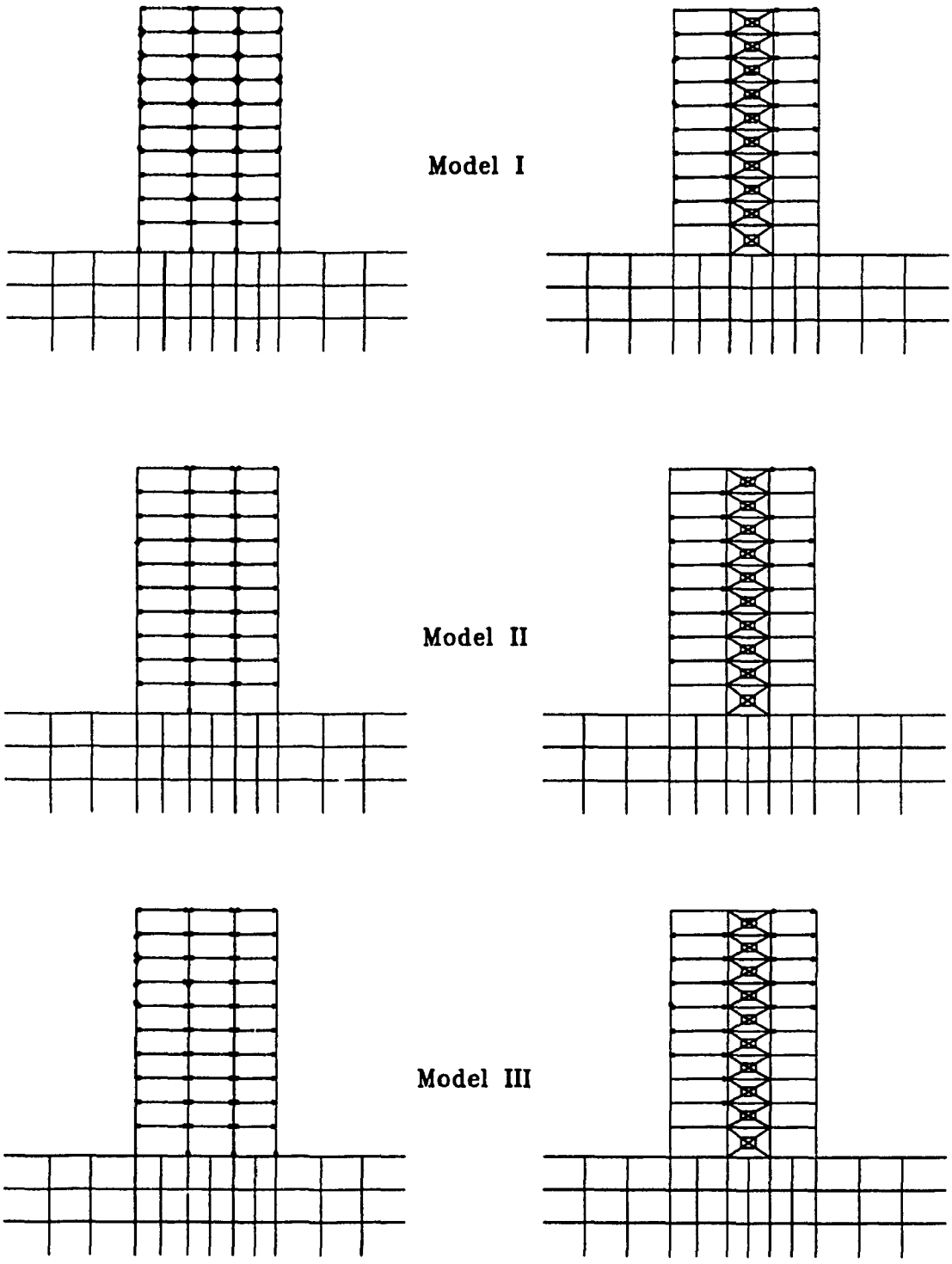

Fig.4.7 Plastic hinges in beams and columns experienced by superstructure

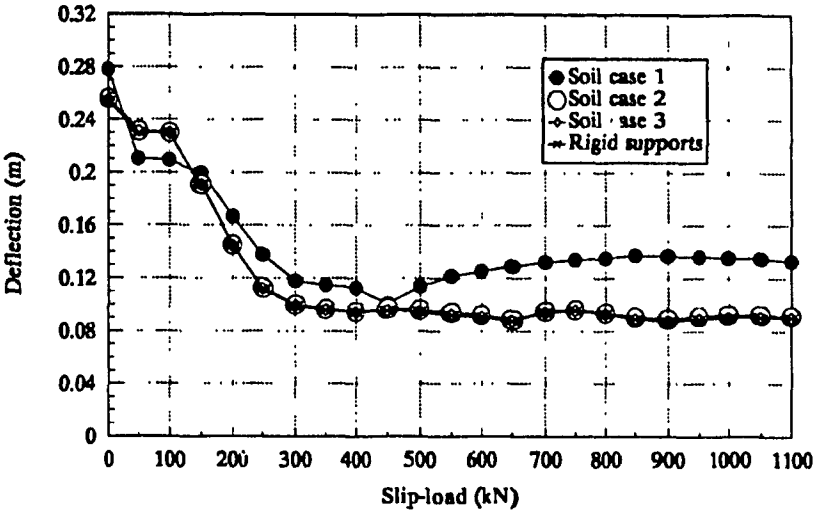

(a) Deflection at the top of the frame

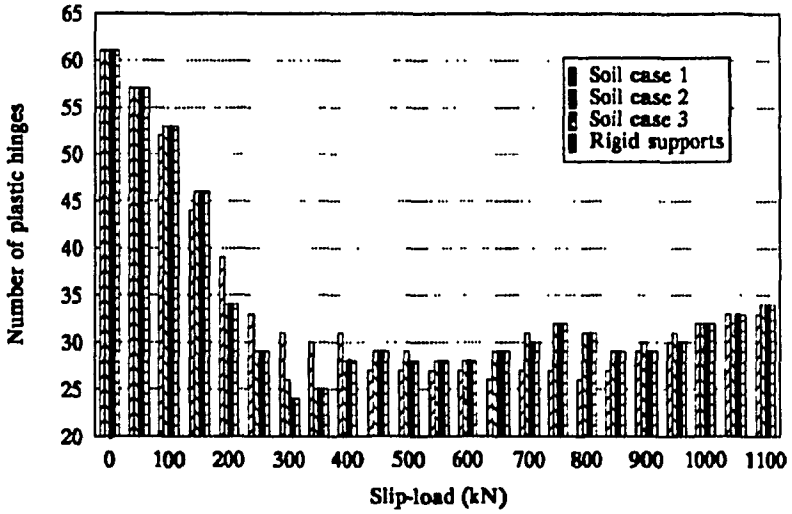

(b) Plastic hinges in beams & columns

Fig.4.8 Dynamic responses of FDBF-soil system for massless input model (El-Centro 0.2g)

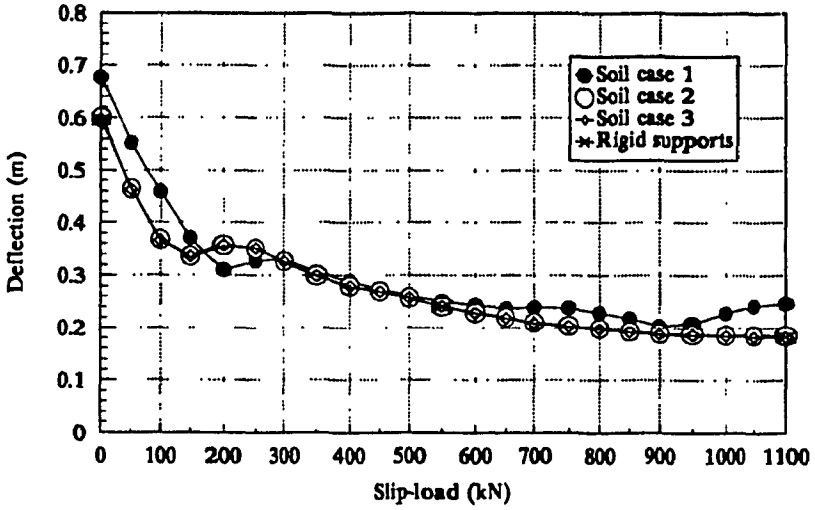

(a) Deflection at the top of the frame

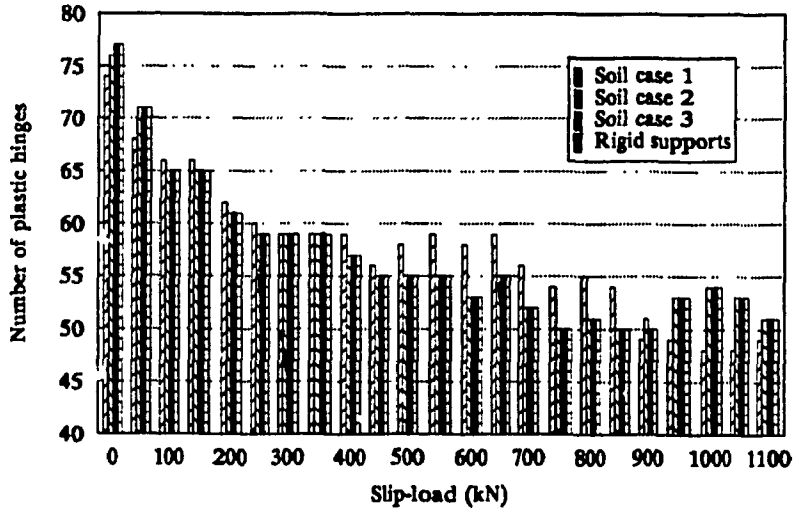

(b) Plastic hinges in beams & columns

Fig.4.9 Dynamic responses of FDBF-soil system for massless input model (El-Centro 0.4g)

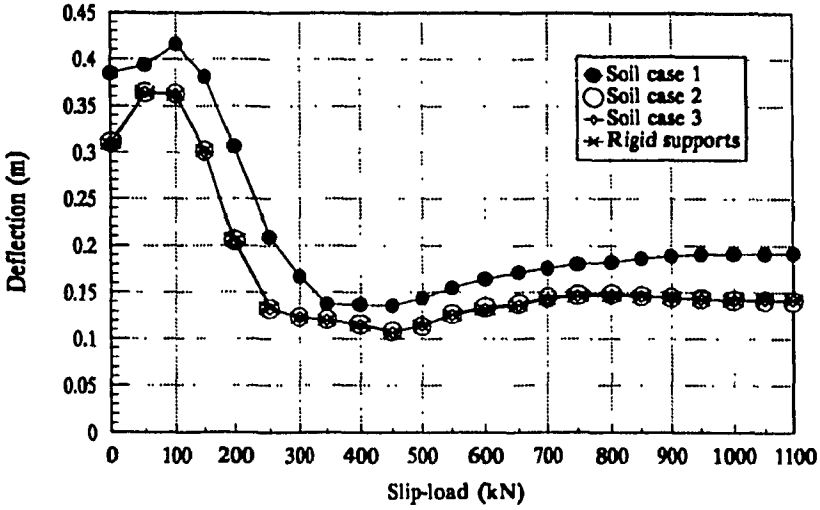

(a) Deflection at the top of the frame

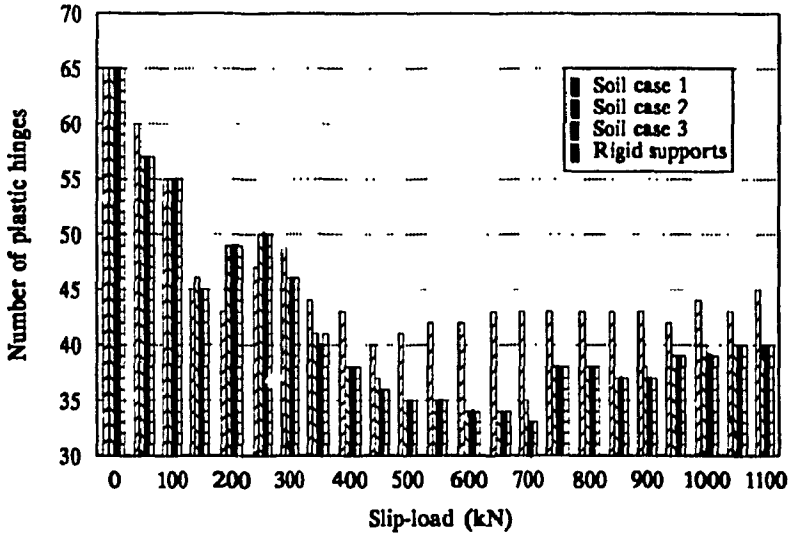

(b) Plastic hinges in beams & columns

Fig.4.10 Dynamic responses of FDBF-soil system for massless input model (NBK 0.2g)

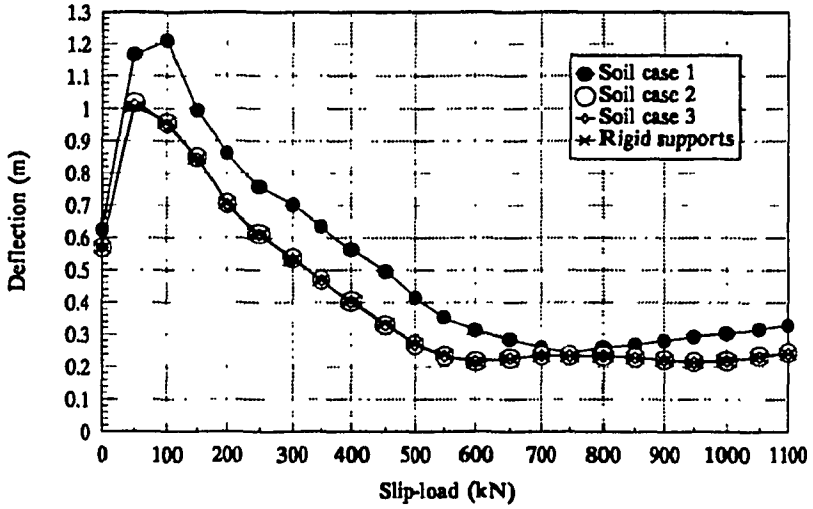

(a) Deflection at the top of the frame

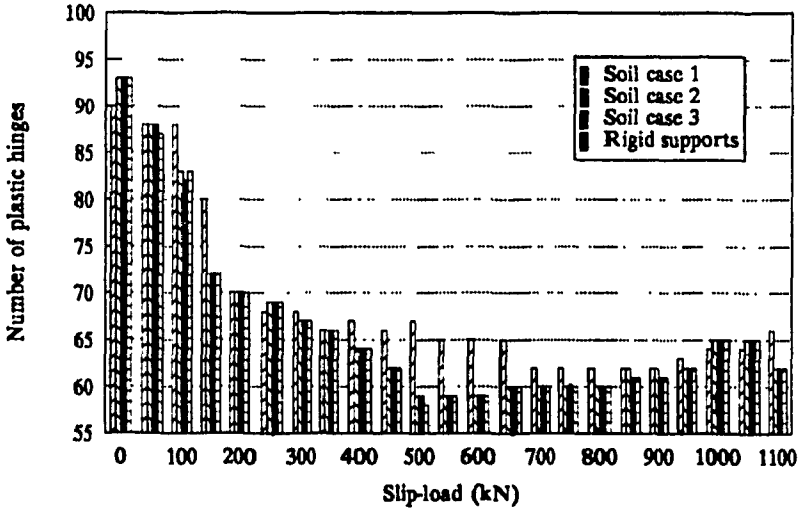

(b) Plastic hinges in beams & columns

Fig.4.11 Dynamic responses of FDBF-soil system for massless input model (NBK 0.4g)

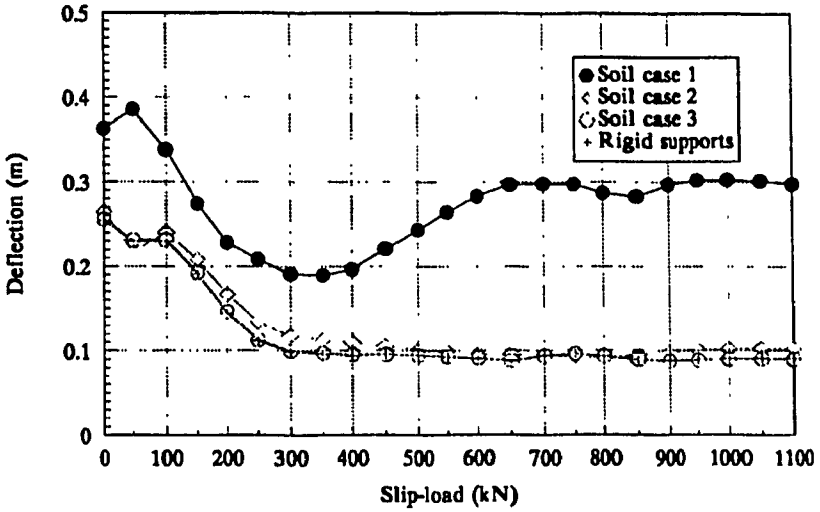

(a) Deflection at the top of the frame

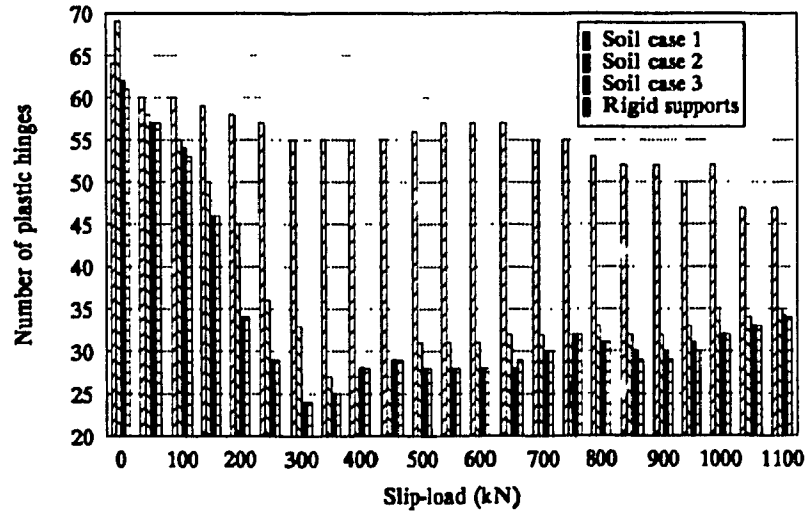

(b) Plastic hinges in beams & columns

Fig.4.12 Dynamic responses of FDBF-soil system for interface input model (El-Centro 0.2g)

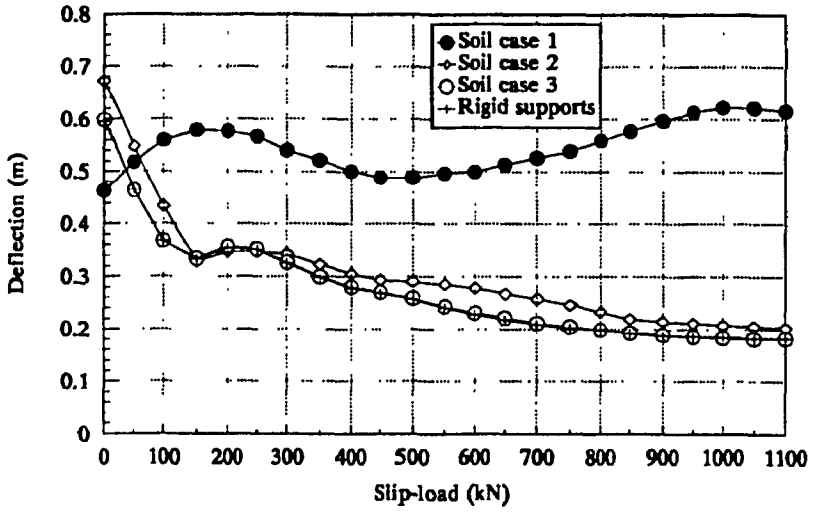

(a) Deflection at the top of the frame

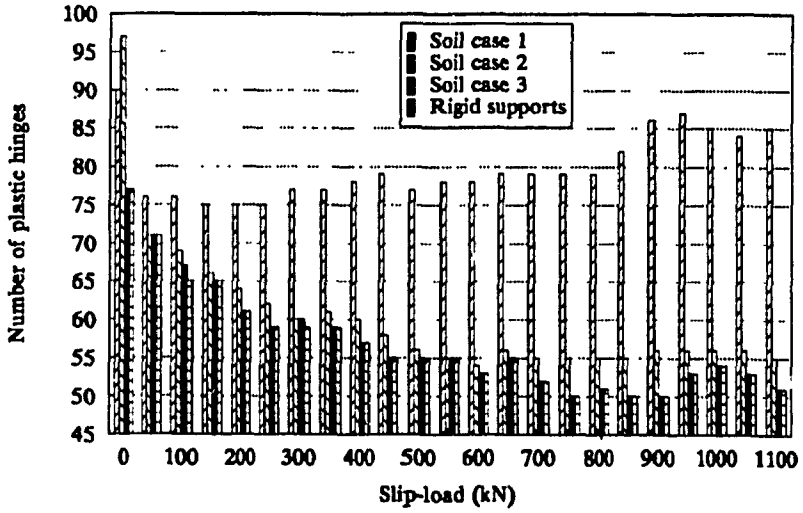

(b) Plastic hinges in beams & columns

Fig.4.13 Dynamic responses of FDBF-soil system for interface input model (El-Centro 0.4g)

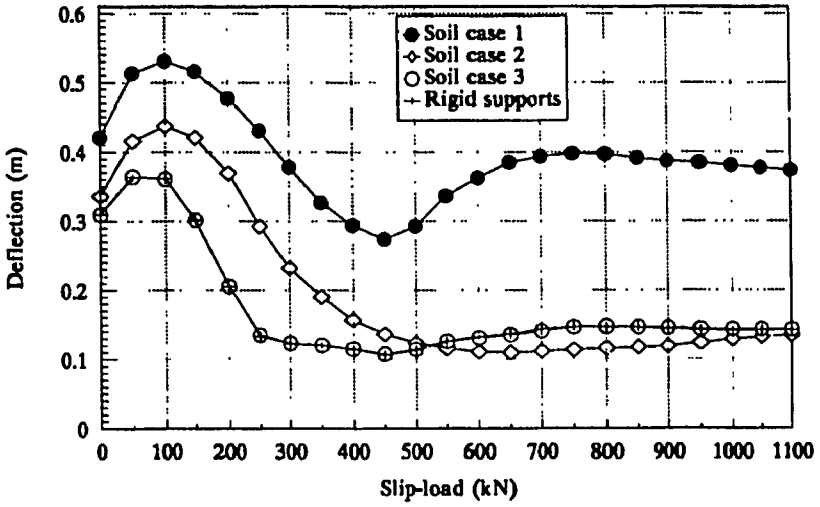

(a) Deflection at the top of the frame

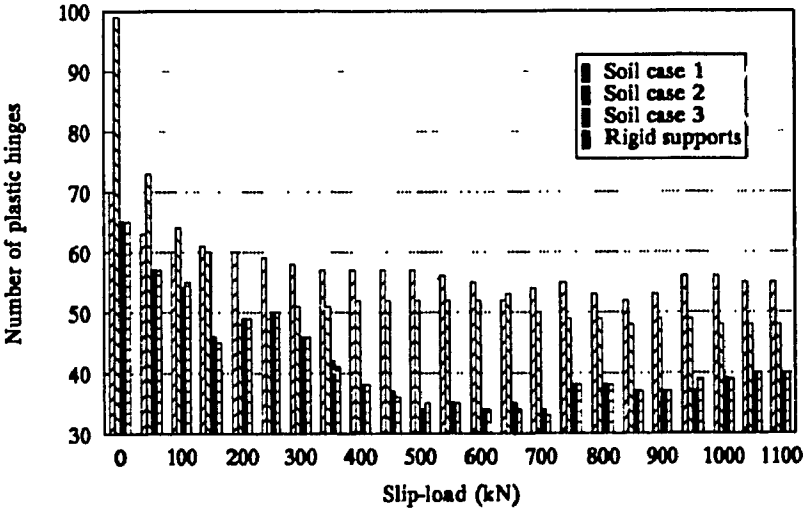

(b) Plastic hinges in beams & columns

Fig.4.14 Dynamic responses of FDBF-soil system for interface input model (NBK 0.2g)

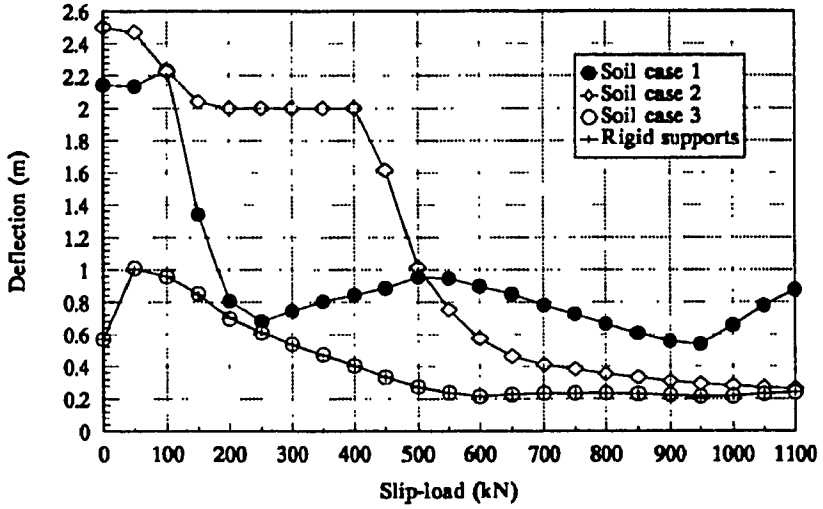

(a) Deflection at the top of the frame

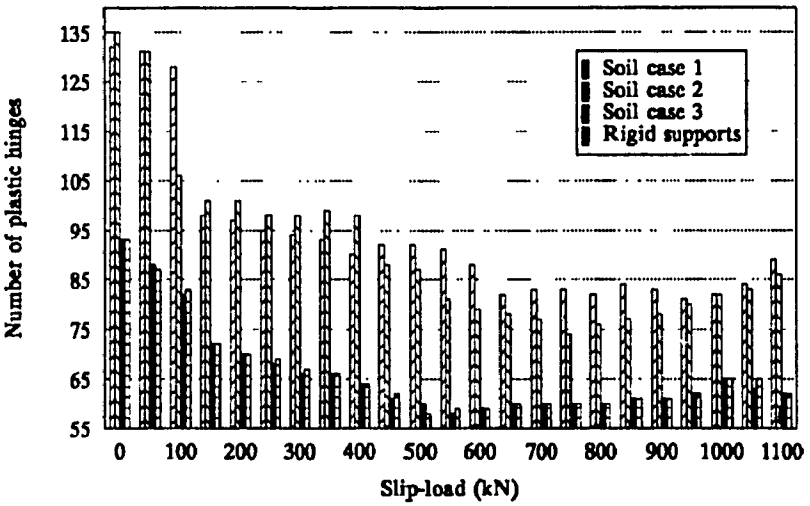

(b) Plastic hinges in beams & columns

Fig.4.15 Dynamic responses of FDBF-soil system for interface input model (NBK 0.4g)

CHAPTER 5 CONCLUSIONS

5.1 General

A computer program has been developed as a design aid for friction damped braced frames. The current design procedure, consisting of a series elastic design cycles and the non-linear dynamic analysis, is implemented and may be carried out in one run. An optimization procedure was proposed to perform an efficient search of the optimum slip-load for the friction dampers. In the determination of the optimum slip-load, the properties of the structure, the anticipated ground motion, the hysteretic behaviour of the friction devices, and the inelastic behaviour of the members in structure can all be taken into account. The proposed optimization scheme eliminates much of the tedious task of data preparation while retaining the accuracy and the flexibility in controlling the maximum deflection or the permanent damage.

Two friction damper equipped buildings were considered as application examples to evaluate the effectiveness of the developed computer aided design system. It has shown capable of providing engineers with an accurate and efficient approach to determine the optimum slip-load and to assist them in making decisions based on the dynamic responses of FDBF.

By adding a new plane-strain isoparametric quadrilateral element and rearranging the dynamic equilibrium equation which govern the time-step history analysis procedure, the computer program developed in this study can provide three alternative approaches to handle the soil-structure interaction of the FDBF system. These are the rigid-base input model, the massless-soil input model and the free-field soil-structure interface input model. The dynamic responses of FDBF-Soil system under these three different earthquake input mechanisms were evaluated, and the main conclusions are:

1) By using different earthquake input models to different soil conditions, the numerical results have demonstrated the superior performance of the FDBF-soil system as compared to MRF-soil system.

2) For stiffer soil, the dynamic responses of the coupled soil-FDBF approach those of the rigid support input model as to be expected. And thus, the effects of soil-structure interaction could be neglected for relatively hard soil condition.

3) For softer soils, the optimum slip-load may be different from that of the rigid support model.

4) The free-field interface input model provides results with an acceptable level of confidence for engineering design when the flexibility of the soil and the soil-structure interaction has to be taken into account.

5) The rigid-base input model introduced significant amplification in the dynamic response of the superstructure for the flexible soil cases. Although this model is relatively simple and easy to implement, one should be cautious of the results

especially for soft soil conditions.

5.2 Recommendations for her studies

1. The optimum slip-load obtained so far was based on the 2D-dimension analysis, 3D-dimensional analysis approach could be included in finding the optimum slip-load for the friction dampers.

2. The non-linear behaviour of soil was not included in the soil-structure interaction of coupled FDBF-Soil system in this study. Some non-linear constitutive laws and models are available for the soil media, the procedure of considering the non-linearity of soil material could be established and introduced to the computer system.

References

1. National Building Code of Canada, 1990.
2. Pall,A.S. and Marsh,C. (1982). "Response of Friction Damped Braced Frames", *Journal of the Structure Division*, ASCE, Vol.108, No. ST6, June, pp.1313-1332.
3. Pall,A.S., Verganelakis V. and Marsh,C. (1987). "Friction Dampers for Seismic Control of Concordia University Library Building", Proceedings of 5th Canadian Conference on Earthquake Engineering, Ottawa.
4. Pall,A.S., Ghorayeb Fadi and Pall Rashmi (1991). "Friction-Dampers for Rehabilitation of Ecole Polyvalente at Sorel, Quebec", Proceeding of Seminar on Innovative Techniques for Earthquake Resistant Design of Buildings, Montreal.
5. Filiatrault,A. and Cherry,A. (1986). "Seismic Tests of Friction Damped Steel Frames", Proceeding of Third Conference on Dynamic Response of Structures, ASCE, Los Angeles.
6. Aiken,Ian D., Kelly,James M., and Pall,Avtar S., (1988). "Seismic Response of a Nine-Story Steel Frame with Friction-Damped Cross-Bracings", Report No. UCB/EERC-88/17, Earthquake Engineering Research Center of the University of California, Berkeley,pp.1-7.
7. Baktash,P. (1989). "Friction Damped Braced Frames", Ph.D. Thesis, Concordia University, Montreal, Quebec.

8. Filiatrault,A and Cherry,S. (1988). "Comparative Performance of Friction Damped Systems and Base Isolation Systems for Earthquake Retrofit and Aseismic Design", Earthquake Engineering and Structural Dynamics, 16, p.389-416.

9. Filiatrault,A. and Cherry,S. (1989). "Parameters Influencing the Design of Friction Damped Structures", Canadian Journal of Civil Engineering, Vol.16, p.753-766.

10. Tan,M.H. (1990). "A Study on Friction-Damped Frames", Master Thesis, Concordia University, Montreal, Quebec.

11. Filiatrault,A. and Cherry,S. (1989). "Efficient Numerical Modelling for the Design of Friction Damped Braced Steel Plane Frames", Canadian Journal of Civil Engineering, Vol.16, p.211-218.

12. Filiatrault,A. and Cherry,S. (1990). "Seismic Design Spectra for Friction Damped Structures", ASCE, Journal of the Structural Division, p.1334-1335.

13. Wilson,E.L., Dovey,H.H., Habibullah,A., "Three Dimensional Analysis of Building Systems", Report No. UCB/EERC-72/8, Earthquake Engineering Centre, University of California, Berkeley,1972.

14. Kannan,A.E. and Powell,G.M. (1973). "DRAIN-2D, A General Purpose Computer Program for Dynamic Analysis of Inelastic Plane Structures", College of Engineering, University of California, Berkeley.

15. Sivakumaran K.S. (1988). "Seismic Response of Multi-Story Steel Buildings with Flexible Connections", Eng. Struct. 1988, Vol.10 16. Wilson,E.L., et al.

(1980). "TABS-80, Report to the US Army Engineering Waterways Experiment Station", Vicksburg, Ms, June.

17. Jeng-Fuh Ger, Franklin Y. Cheng, and Le-Wu Lu, "Collapse Behaviour of Pino Suarez Building During 1985 Mexico City" Earthquake J. Struct. Engng., ASCE 119, No. 3, 852-870 (1993).

18. Roberto Villaverde, "Explanation for the Numerous Upper Floor Collapses During the 1985 Mexico City Earthquake", Earthquake Engineering and Structural Dynamics, 20, 223-241 (1991).

19. Filiatrault,A. and Cherry,S. (1988). "Seismic Design of Friction Damped Braced Steel Plane Frames by Energy Methods", Earthquake Engrg. Res. Lab. Report, UBC-EERL-88-01, Depr. of Civ. Engrg., Univ. of British Columbia, Vancouver, Canada.

20. Arora,Jasbir S. (1989). "Introduction to Optimum Design", McGraw-Hill Book Co.

21. Canadian Standards Association, "Limit States Design of Steel Structure", CAN/CSA-S16.1-M89, Canadian Standards Association, Ontario, Canada, 1991.

22. AutoCAD Reference Manual, Autodesk Inc., 1992.

23. ICBO, Uniform Building Code, International Conference of Building Official, Whittier, CA, 1988.

24. Richart,R.E. Jr.,Hall,J.R. Jr., and Woods,R.D., "Vibrations of Soils and Foundations, Prentice-Hall, New Jersey, 1970.

25. Luco,J.E., "Impedance Functions for a Rigid Foundation on a Layered Medium", Nuclear Engineering and Design, Vol.31, No.2, December 1975.

26. Hadjian,A.H., Niehoff,D., and Guss,J., "Simplified Soil-Structure Interaction Analysis with Strain Dependent Soil Properties", Nuclear Engineering and Design, Vol.31, No.2, December 1974

27. Singh,A.K., Hsu,T.I., and Holmes,N.A., "Soil-Structure Interaction Using Substructures", presented at the ASCE Specialty Conference on Civil Engineering and Nuclear Power, Knocville, Tennessee, September 1980.

28. Chu,S.L., Agrawal,P.K., and Singh, S., "Finite Element Treatment of Soil-Structure Interaction Problem for Nuclear Power Plant Under Seismic Excitation", 2nd International Conference on Structural Mechanics in Reactor Technology, Proceedings, Vol.2, Paper K2/4, September 1973.

29. Seed,H.B. and Lysmer,J., "Soil-Structure Interaction Analysis by Finite Element Methods: State-of-the-Art", Transactions of the 4th SMiRT Conference, San Francisco, California, August 1977.

30. Seed,H.B., Lysmer,J., and Hwang,R., "Soil-Structure Interaction Analysis for Seismic Response", Journal of the Geotechnical Engineering Division, ASCE, May 1975.

31. Patel,P.N. and Spyrakos,C.C. "Time Domain BEM-FEM Seismic Analysis Including Basement Lift-Off", J. Eng. Struct. 1990, Vol.12, July

32. Stevens,D.J. and Krauthammer,T. "Combined Finite Difference/Finite Element Analysis for Soil Structure Interaction", Proc. of the sessions at

Structures Congress'87 related to Dynamics of Structures, p.485-496.

33. Borg,S.F., "The 19 September 1985 Mexican Earthquake-Rational Analysis of the Anomalous Central Mexico City Behaviour", Technical Report COE-6-1, Stevents Institute of Technology, Hoboken, NJ, April, 1986.

34. Seed,H.B., Romo,M.P., Sun,J., Jaime,A. & Lysmer, J., "Relationships Between Soil Conditions and Earthquake Ground Motions in Mexico City in the Earthquake of Sept. 19,1985". Earthquake Engineering Research Center, Report No. UCB/EERC-87/15, University of California, Berkeley, Oct. 1987.

35. Clough,R.W. and Penzien,J. "Dynamics of Structures", McGraw-Hill, Inc. 1975.

36. John P.Wolf, "Dynamic Soil-Structure Interaction", Prentice-Hall International, Inc., 1985.